

**Filamentation in Air and Water and Nonlinear
Optical Characterization of Biopolymer Using
Ultrashort Laser Pulses**

Thesis submitted to

Cochin University of Science and Technology

in partial fulfilment of the requirements

for the degree of

Doctor of Philosophy

By

Sreeja. S.

**INTERNATIONAL SCHOOL OF PHOTONICS
COCHIN UNIVERSITY OF SCIENCE AND TECHNOLOGY,
COCHIN 682022**

June 2014

Filamentation in Air and Water and Nonlinear Optical Characterization of Biopolymer Using Ultrashort Laser Pulses

Author

Sreeja. S

Research Scholar
International School of Photonics
Cochin University of Science and Technology
Kochi - 682022
Email: sreeja82nishanth@gmail.com

Research Advisor

Dr. P Radhakrishnan

Professor, International School of Photonics,
Cochin University of Science and Technology,
Cochin-682 022, Kerala, India
Email: radhak@cusat.ac.in

International School of Photonics
Cochin University of Science and Technology
Kochi - 682016

June - 2014

*Dedicated to Nishanth for
his unending support and love.....*

Certificate

*This is to certify that the thesis entitled “**Filamentation in Air and Water and Nonlinear Optical Characterization of Biopolymer Using Ultrashort Laser Pulses**” to be submitted by **Ms. Sreeja. S**, is an authentic record of research work carried out by her under my guidance and supervision in partial fulfilment of the requirement of the degree of Doctor of Philosophy of Cochin University of Science and Technology, under the Faculty of Technology and has not been included in any other thesis submitted previously for the award of any degree.*

Kochi – 682022

Prof. (Dr.) P. Radhakrishnan
(Supervising Guide)

Declaration

I, Sreeja.S, do hereby declare that the thesis entitled "Filamentation in Air and Water and Nonlinear Optical Characterization of Biopolymer Using Ultrashort Laser Pulses ". is a genuine record of research work done by me under the supervision of Dr. P Radhakrishnan, Professor, International School of Photonics, Cochin University of Science and Technology, Kochi-22, India and it has not been included in any other thesis submitted previously for the award of any degree.

Cochin 682022

Sreeja. S.

List of Publications

(a) International journals:

1. *S. Sreeja*, Ch. Leela, V. Rakesh Kumar, Suman Bagchi, T. Shuvan Prashant, P. Radhakrishnan, Surya P. Tewari, S. Venugopal Rao, and P. Prem Kiran, "Dynamics of tightly focused femtosecond laser pulses in water," *Laser Physics*, 23, 106002, 2013
2. *S. Sreeja*, B. Nityaja, Debasis Swain, V.P.N. Nampoori, P. Radhakrishnan, S. Venugopal Rao, "Nonlinear optical studies of DNA doped Rhodamine 6G PVA films using picosecond pulses," *Optics and Photonics Journal*, 2, 135-139, 2012
3. *S. Sreeja*, T. Shuvan Prashant, P. Radhakrishnan, Surya P. Tewari, S. Venugopal Rao, P. Prem Kiran, "Effect of focusing lens tilt on SCE and filamentation characteristics of fs pulses in air," in *Nonlinear Optics and Applications VI*, edited by Benjamin J. Eggleton, Alexander L. Gaeta, Neil G. Broderick, Proc. SPIE Vol. 8434 (SPIE, Bellingham, WA) 84340T, 2012.
4. *S. Sreeja*, V. Rakesh Kumar, Ch. Leela, P. Radhakrishnan, Surya P. Tewari, S. Venugopal Rao, P. Prem Kiran, "Filamentation characteristics of focused fs pulses in atmosphere," in *Nonlinear Optics and Applications VI*, edited by Benjamin J. Eggleton, Alexander L. Gaeta, Neil G. Broderick, Proc. SPIE Vol. 8434 (SPIE, Bellingham, WA), 84340U, 2012
5. *S. Sreeja*, S. Venugopal Rao, P. Radhakrishnan, Surya P. Tewari, P. Prem Kiran, "Supercontinuum emission from water using fs pulses in the external tight focusing limit," Proc. SPIE, 8247, 824718, 2012.

6. G. Sreelekha, G Vidya ,M S Ebin, K Geetha ,*S Sreeja*, Rani Joseph, S Pratapan,P Radhakrishnan, C P G Vallabhan and V P N Nampoori “Two photon fluorescence spectra from MEH-PPV/Polystyrene based film waveguides ", Journal of Optics, 101-105,OSI 2012
7. *S. Sreeja*, V. Rakesh Kumar, Ch. Leela, P. Radhakrishnan, Surya P. Tewari, S. Venugopal Rao, P. Prem Kiran, ”Peculiarities of tightly focused fs pulses in air” (Communicated)

(b) International seminar/ conference presentations

1. *S. Sreeja*, P.Radhakrishnan,S.Venugopal Rao “Effect of Temperature on Supercontinuum emission from water "; National Laser Symposium (NLS-20), January 9-12, 2012, Crystal Growth Center, Anna University, Chennai, India .
2. *S. Sreeja*, Ch. Leela, V. Rakesh Kumar, S. Venugopal Rao, P. Radhakrishnan, Surya P. Tewari, P.Prem Kiran, “Effect of external tight focusing and temperature on the Supercontinuum emission from water,” TC 2012, BRNS-ISAMP Topical conference on Interaction of lasers with atoms, molecules, and clusters, University of Hyderabad, Hyderabad, January 09-12, 2012.
3. *S. Sreeja*, S. Venugopal Rao, S. Bagchi, S. Sreedhar, T. Shuvan Prashant, P. Radhakrishnan, Surya P. Tewari, P. Prem Kiran, “Supercontinuum emission from water using femtosecond pulses in the external tight focusing limit,” UH-TIFR meeting at University of Hyderabad, August 1-3, 2011
4. *S. Sreeja*, S. Venugopal Rao, P. Radhakrishnan, Surya P. Tewari, P. Prem Kiran “ Supercontinuum emission from water soluble dyes ;

XXXVI Optical Society of India Symposium, December 3-5, 2011, IIT Delhi, India .

5. **S. Sreeja**, S. Venugopal Rao, S. Bagchi, S. Sreedhar, T. Shuvan Prashant, P. Radhakrishnan, Surya P. Tewari, P. Prem Kiran “ Supercontinuum Emission from Focused Femtosecond Laser Pulses in Air ”, AIP conf. Proc. 1391, 291-293, (2011) .
6. **S. Sreeja**, S. Venugopal Rao, Suman Bagchi, S. Sreedhar, T. Shuvan Prashant, P. Radhakrishnan, Surya. P.Tewari, P. Prem Kiran “ Supercontinuum emission from water in the tight focusing geometry using ~40 fs pulses ; Photonics 2010, 10th International Conference on Fiber optics & Photonics, December 11-15, 2010, IIT Guwahati, India. .
7. **S. Sreeja**, S. Venugopal Rao, S. Bagchi, S. Sreedhar, T. Shuvan Prashant, P. Radhakrishnan, SuryaP. Tewari, P. Prem Kiran, “Supercontinuum emission from water using 45 fs pulses in the tight focusing limit,” Photonics 2010, IIT Guwahati, December 11-15, 2010
8. M S Ebin, G Sreelekha, **S Sreeja**, P Radhakrishnan, V P N Nampoori, C P G Vallabhan, K Geetha, G Vidya, Rani Joseph and S Pratapan “ Two photon fluorescence spectra of MEH-PPV/PS blend films under femtosecond irradiation; International Conference on Recent Trends in Materials Science and Technology(ICMST) October 29-31, 2010 at Thiruvananthapuram

Acknowledgement

I would like to take the opportunity to express my sincere gratitude to Prof. P. Radhakrishnan for introducing me to the world of intense lasers. He has always been a guiding force, kept me focused during my work and motivated me to tackle the challenging issues independently. Freedom is always given to choose problems. This independence was always a boost, to him I owe the confidence in running lasers and doing experiments.

I was fortunate to be a part of collaboration between ISP and ACRHEM, Central University of Hyderabad. I am greatly indebted to Dr. Soma Venugopal Rao for his support and guidance at various fronts. The rounds of stimulating discussions with him have always been an enriching experience. His contagious enthusiasm and knowledge over broad spectra of physics has always inspired me.

I owe my thanks to Dr. P. Prem Kiran for guiding me through the highs and lows of the most important five years of my life. I learnt the art of being enthusiastic about the work that one does, from him. I was always fascinated by his courage to face the most crucial situations in the research life.

I thank Prof. V.P.N Nampoore and all teaching staff at ISP for the support they had given during my PhD days.

It has been a wonderful experience to work with Prashant, Sreedhar, Anusha, Leela, Debasis, Rakesh, and Hamad at ACRHEM. I was fortunate to be part of a team of such talented individuals. I learnt a lot from them as they have been instrumental in accomplishing the experimental part of my thesis. They have always been a strong support for me all the time.

A special word of thanks and appreciation to all my lab seniors, especially Nithyaja, Linesh and Sony for constantly encouraging and

supporting me throughout my time here, directly helping me in getting into suitable research problems .I would also like to thank all my friends at ISP for their kindness and friendship ,which makes my Ph.D life more enjoyable.

I express my heartfelt gratitude to my parents, parents-in law for the unconditional support, love and encouragement throughout these years. It is hard to imagine having made it to this point without them

My sincere thanks to Nishanth for his ample patience, love and understanding during the most difficult stage of my Ph.D venture. He deserves a major share of the credit for being with me on all account, ever since we met.

And last but not least, my little Kurinji for providing me a good company and thus assuring an ideal equilibrium in my Ph.D life.

Sreeja

CONTENTS

Chapter 1: Introduction.....	1-39
11. Overview of femtosecond lasers.....	1
12. Characteristics of ultrashort laser pulses.....	5
12.1. Relationship between pulse duration and spectral width.....	7
13. Generation of intense femtosecond laser pulses.....	10
14. Propagation of ultrashort laser pulses.....	14
14.1. Linear propagation.....	14
14.2. Nonlinear propagation.....	15
14.2.1. Nonlinear pulse propagation equation.....	15
14.2.2. Ultrashort-Pulse Propagation Effects.....	16
14.2.2.(a) Kerr self focusing.....	18
14.2.2.(b) Group velocity dispersion.....	19
14.2.2.(c) Self Phase Modulation.....	22
14.2.2.(d) Self steepening.....	24
14.2.2.(e) Space time coupling.....	25
15. Matter in intense laser fields.....	27
15.1. Interaction of light with a medium.....	27
15.2. Nonlinear response of matter in a strong radiation field.....	29
15.2.(a) Multiphoton ionisation.....	29
15.2.(b) Tunnel ionization (TI).....	30
15.2.(c) Over the barrier ionisation.....	32

1.6. Organisation of the thesis.....	33
References.....	36
Chapter 2: Laser systems	41-54
2.1. Laser systems used.....	42
2.1.1. The fs oscillator [Micra System]	43
2.1.2. Optical pump to the Regenerative Amplifier [Evolution-30].....	46
2.1.3. The Regenerative Amplifier [Legend].....	46
2.2. Pulse Measurement.....	49
2.2.1. Introduction.....	49
2.2.2. Pulse Shaper System	50
2.2.3. Measurement and manipulation of the ultrashort pulse.....	52
References.....	54
Chapter 3: Physics of filamentation and associated supercontinuum	
emission (SCE).....	55-77
3.1. Introduction.....	56
3.2. Mechanisms leading to filamentation and associated Supercontinuum	
Emission (SCE).....	58
3.2.1. Optical Kerr effect and Self-focusing in air	58
3.2.2. Self phase modulation	61
3.2.3. Multi-photon ionization and plasma defocusing.....	66
3.2.4. Conical emission.....	69
3.3. Issues of filamentation addressed in this dissertation work.....	71
3.4. Conclusions.....	72
References.....	73

Chapter 4: Characteristics of Tightly focused femtosecond

laser pulses in atmosphere 79-101

4.1. Introduction.....	80
4.2. Experimental technique.....	81
4.3. Results and discussion.....	83
4.3.1. SCE from air under tight focusing geometry-beyond intensity clamping.....	83
4.3.2. Characteristics of filamentation.....	87
4.4. Conclusions.....	96
References.....	98

Chapter 5: Effect of lens tilt on Supercontinuum Emission and

Filamentation characteristics 103-115

5.1. Introduction.....	104
5.2. Experimental technique.....	105
5.3. Results and discussion.....	106
5.4. Conclusions.....	112
References.....	113

Chapter 6: Dynamics of tightly focused femtosecond laser

pulses in water 117-141

6.1. Introduction.....	118
6.2. Experimental technique.....	119
6.3. Supercontinuum emission (SCE) studies from water.....	121
6.3.1. SCE spectral studies with linearly polarized fs laser pulses.....	122
6.3.2. Supercontinuum emission studies under different focusing geometries.....	123
6.3.3. Role of input polarization on the SCE.....	126

6.3.4. Studies on the role of minimum wavelength (λ_{\min}) and intensity clamping on SCE.....	127
6.3.5. Efficiency of Supercontinuum emission under different focusing geometries	131
6.3.6. Effect of temperature on SCE.....	132
6.3.7. Influence of Cavitation Induced Bubbles (CIB) in SCE.....	133
6.4. Conclusions.....	135
References.....	137
Chapter 7: Nonlinear optical characterization of DNA doped Rhodamine 6G-PVA films using picoseconds pulses	143-170
7.1. Introduction.....	144
7.2. Nonlinear optical measurements- Z-Scan.....	145
7.2.1. Nonlinear Absorption.....	146
7.2.2. Open Aperture Z-scan to study NLA.....	148
7.2.3. Closed-aperture Z-scan for sign and magnitude of refractive nonlinearity	150
7.3. Materials and Methods	157
7.4. Experimental techniques.....	158
7.5. Results and discussions.....	159
7.5.1. Two photon absorption with 800nm, 2ps pulses	160
7.5.2. Nonlinear refraction properties with closed aperture Z- scans	163
7.6. Conclusions.....	166
References.....	167
Chapter 8: Conclusions & Future perspectives	171-176
8.1. Conclusions.....	172
8.2. Future perspectives.....	175

Chapter - 1

INTRODUCTION

- 1.1. *Overview of femtosecond lasers*
- 1.2. *Characteristics of ultrashort laser pulses*
- 1.3. *Propagation of ultrashort linear pulses*
- 1.4. *Matter in intense laser fields*
- 1.5. *Organisation of the thesis*

Abstract

In this chapter important issues related to femtosecond (fs) pulses and its relevance to this thesis are discussed. A fundamental characteristic, like the time-bandwidth product for fs pulses is described in detail. A brief review of generation of ultrashort pulses and its propagation through an optically transparent media are presented. Interaction of strong pulses with matter and different ionization processes are also described. An overview of the thesis is presented at the end.

1.1. Overview of femtosecond lasers

Laser technology has achieved remarkable progress during the past 50 years. The progress in the field of ultrashort laser pulse generation has been rapid and continuous, and has a long lifetime ahead. This rapid development in the field of laser over the last decades enabled the scientists to move to the regime of ultrashort optics by continuously shortening the pulse duration from microsecond ($1\mu s = 10^{-6}$ seconds) range in the free running regime to the nanosecond ($1ns = 10^{-9}$ seconds) range in the regime of so-called Q-switching and finally to the picoseconds ($1ps = 10^{-12}$ seconds) and a few femtosecond ($1fs = 10^{-15}$ seconds) range in the regime of mode-locking. A laser can be referred to as a femtosecond laser if its pulse has duration from a few to hundred femtoseconds.

In the evolution of laser technology, we observe that along with the shortening of laser pulse durations, the achievable intensity of focused laser pulse is rapidly increasing as shown in figure 1.1. The increase in the available intensities has thereby often been accompanied by the discovery of new interaction processes between light and matter, whereas the reduction of the pulse duration at the same time enables to increase the resolution of time-resolved experiments. The short pulse duration provides scientists the possibility to explore physical phenomena with unprecedented time resolution. Due to this peculiarity short duration chemical reactions at the atomic level and ultrafast changes in material properties can be studied. All these processes take place on time scales of femtoseconds to picoseconds. In the realm of condensed matter physics, carrier relaxation and thermalization, wavepacket evolution, electron-hole scattering, and countless other processes also occur on these incredibly fast time scales. The increase in laser intensities achieved with

ultrashort laser pulses predetermined the discovery of major effects in nonlinear optics, such as the formation of spatio-temporal solitons [1, 2] and the generation of coherent white light. [3].

The explosive expansion of applications of these ultra short pulses range from hi- tech such as advances in the medical field (LASIK), biological imaging to more everyday applications such as inspection of packaged food. The advent of commercially available femtosecond lasers has also triggered a wealth of new technologies, such as micromachining with femtosecond pulses, multiphoton imaging techniques and femtosecond LIDAR (Light detection and ranging).

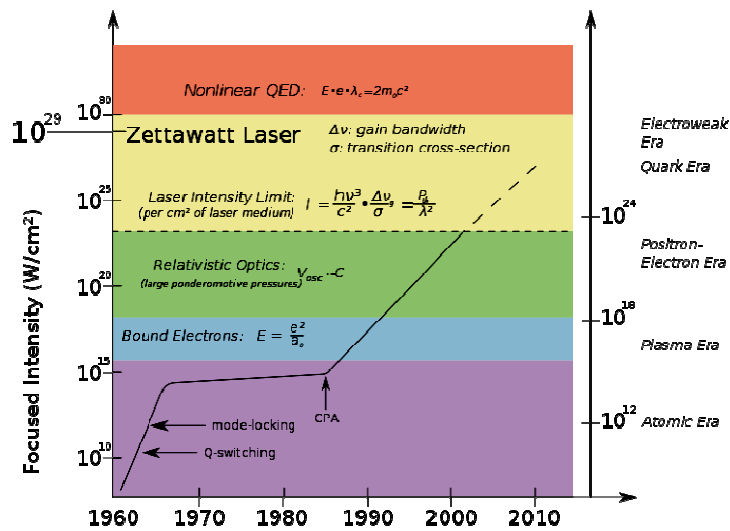


Figure: 1.1 Focused laser pulse intensity vs year
[Image courtesy: Optics and Photonics News, may 2004]

The developments in the field of ultrafast lasers are due to the introduction of four techniques such as Q-Switching, Mode-locking, Chirped Pulse Amplification, and Optical Parametric Chirped pulse amplification. Ultrafast lasers produce pulses that are millions of times faster than the strobe

flashes used for strobe photography. The first laser, was introduced by Maiman in the year of 1960 and this flash lamp pumped Ruby laser produced a burst of spikes, each several hundred nanoseconds and peak power $\sim 1\text{KW}$ [4-5]. In the year of 1962. Q -Switching technique was employed and a pulse duration of just tens of nanoseconds with a peak power $\sim 100\text{MW}$ was achieved [6-7]. The idea of Mode-locking was introduced in 1964 which enabled to reduce the pulse width to the order of $\sim 100\text{ps}$ and in 1981, with colliding pulse mode locking, the available pulse width was shortened to 100fs and peak power was increased to the order of several GW [8-12]. In 1985, G. Mourou introduced the concept of Chirped Pulse Amplification (CPA) which enabled us to achieve a pulse width $\sim 20\text{fs}$ and a peak power \sim several PW.

As these pulses shrink in length and grow in utility, the ability to measure them becomes increasingly important. But the characterisation of ultrashort pulses has always been a challenge and for many years it was possible to create them but not to measure them. A full characterisation is needed to determine experimental conditions before the pulses are used for experiments. Fortunately, in the past five years, remarkable progress has occurred in the development of techniques for the measurement of ultrashort laser pulses. It is now routine to completely characterize the time dependence of these pulses in the laboratory [13]. The work presented in this thesis is concerned with ultrashort laser at high power levels and the experiments that are presented in this work may be divided into two parts. One ensemble of experiments concern the phenomenon that is associated with the propagation of ultrashort laser pulses in air and water at high power levels, the so-called filamentation. This investigation of the propagation of fs laser pulses in these media is the main objective of the experiments described in this work. The second part focuses on the nonlinear optical characterisation of dye doped

DNA (De-oxy ribo nucleic acid) films .This part of the experiment is conducted with ultrashort laser pulses of duration $\sim 2\text{ps}$.The following sections will give a description of the characteristics, generation ,propagation and interaction of ultrashort laser pulses.

1.2. Characteristics of ultrashort laser pulses

Ultrashort laser pulses are very short burst of electro-magnetic energy and are defined by its electric field as a function of space and time. The main difference between a continuous beam and an ultrashort pulse is that the electric field of the former is sinusoidal in time whereas the electric field of latter comprises only a few cycles of a sine wave [14]. Figure1.2 shows the representation of an ultrashort laser pulse in the time domain.

The ultrashort laser pulses are fully described by the time and space dependent electric field. In the frame of a semi - classical treatment the propagation of such fields and the interaction with matter are governed by Maxwell's equations with the material response given by a macroscopic polarization. The pulse is characterized by measurable quantities that can be directly related to the electric field [15]. The complete description of the pulses can be given either in time or in the frequency domain.

Even though the measured quantities are real, it is generally more convenient to use complex representation. The real electric field corresponding to an ultrashort pulse oscillates at an angular frequency ω_0 corresponding to the central wavelength of the pulse. The complex electric field is usually represented by a product of an intensity function and a phase term. The central frequency is also explicitly written in the complex field.

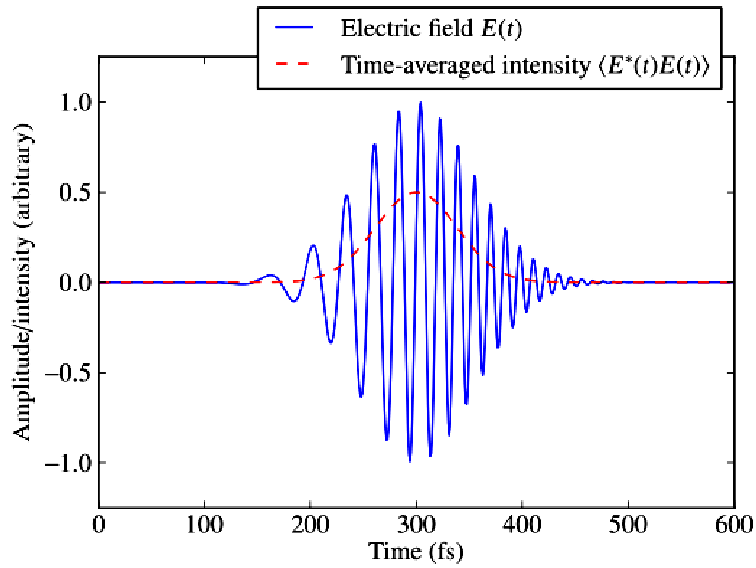


Figure1.2. An ultrashort laser pulse of light in the time domain [Image adapted from Wikipedia]

$$\tilde{E}(t) = \sqrt{I(t)} \exp(i\omega_0 t) \exp(i\phi(t)) \quad (1.1)$$

Fourier transforming the pulse electric field $\tilde{E}(t)$, we will obtain the expression for the complex electric field in the frequency domain

$$\tilde{E}(\omega) = F[\tilde{E}(t)] \quad (1.2)$$

The pulse is centered on its actual frequency, not zero. Thus, the most commonly used complex frequency-domain pulse field is

$$\tilde{E}(\omega) = \sqrt{S(\omega)} \exp(i\phi(\omega)) \quad (1.3)$$

Thus, the ω -domain electric field also has an intensity and phase. S is the spectrum, and ϕ is the spectral phase. The intensity functions $I(t)$ and $S(\omega)$ determines the time duration and the spectral bandwidth of the pulse.

1.2.1. Relationship between pulse duration and spectral width

We define the pulse duration of the ultrashort pulse Δt as the full width at half maximum (FWHM) of the intensity profile $|\tilde{E}(t)|^2$ and the spectral width $\Delta\omega$ as the FWHM of the spectral intensity $|\tilde{E}(\omega)|^2$

The general time and frequency Fourier transforms of a pulse are [16]

$$E(t) = \frac{1}{2\pi} \int_{-\infty}^{+\infty} E(\omega) e^{-i\omega t} d\omega \quad (1.4.a)$$

$$E(\omega) = \int_{-\infty}^{+\infty} E(t) e^{-i\omega t} dt \quad (1.4.b)$$

When the duration and spectral width of a pulse are calculated using the standard statistical definitions.

$$\langle \Delta t \rangle = \frac{\int_{-\infty}^{+\infty} t |E(t)|^2 dt}{\int_{-\infty}^{+\infty} |E(t)|^2 dt} \quad (1.5)$$

$$\langle \Delta \omega^2 \rangle = \frac{\int_{-\infty}^{+\infty} \omega^2 |E(\omega)|^2 d\omega}{\int_{-\infty}^{+\infty} |E(\omega)|^2 d\omega} \quad (1.6)$$

It can be shown that, these quantities can then be related by the following inequality, $\Delta t \Delta \omega \geq \frac{1}{2}$ (1.7)

Equation (1.7) is the product of pulse duration and spectral bandwidth and is known as the time-bandwidth product. The classical physical relationship eq. (1.7), which leads to the quantum-mechanical time-energy uncertainty principle, has several important consequences in the field of ultrashort light pulses:

1. In order to produce a light pulse with a given duration it is necessary to use a broad enough spectral bandwidth. A Gaussian-shaped pulse lasting for one picosecond (10^{-12} sec) has a minimum spectral bandwidth of 441 MHz ($\Delta\omega = 4.41 \times 10^{11}$ Hz). If the central frequency γ_0 of the pulse lies in the visible part of the electromagnetic spectrum, say $\gamma_0 = 4.84 \times 10^{14}$ Hz (i.e. $\lambda_0 = 620$ nm), then the relative frequency bandwidth $\frac{\Delta\gamma}{\gamma_0}$ is 10^{-3} .
3. But for a 100 times shorter pulse ($\Delta t = 10$ fs), $\frac{\Delta\gamma}{\gamma_0} = 0.1$. As $\left| \frac{\Delta\lambda}{\lambda_0} \right| = \frac{\Delta\gamma}{\gamma_0}$, the wavelength extension of this pulse is 62 nm, covering 15% of the visible window of the electromagnetic spectrum. Taking into account the wings of the spectrum, a 10 fs pulse covers most of the visible window.
2. The equality in eq. (1.7) holds for pulses without frequency modulation (unchirped) which are called “bandwidth *limited*” or “*Fourier transform limited*” pulses. Such pulses exhibit the shortest possible duration at a given spectral width and pulse shape.
3. For a given spectrum, one pulse envelope can be constructed that has the shortest possible duration. The shortest constructed pulse can only be *transform-limited* if its spectrum is symmetrical.

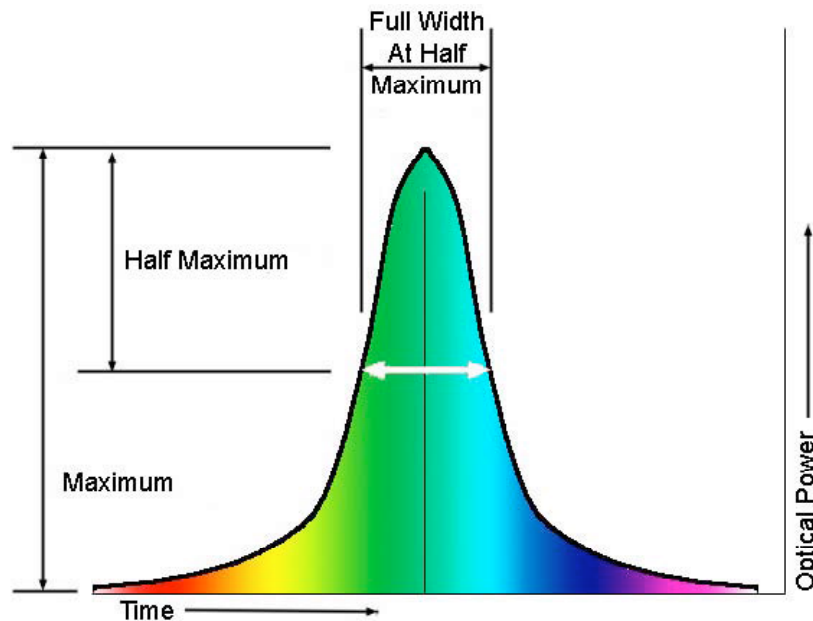


Figure 1.3. The measurement of 'full width at half maximum' of a pulse to find its duration. Image edited from <http://www.newastro.com/newastro/book/C2/images/FWHM.jpg>

The variation in phase of a Fourier transform limited pulse is beautifully uniform and so has linear time dependence; the instantaneous frequency is time independent. This can define pulse duration, though the more commonly used definition is based on the full-width at half-maximum (FWHM) principle of optical power against time, as in Figure 1.3 because experimentally it is easier to measure.

There is a **minimum duration bandwidth** given by

$$2\pi\Delta\gamma\Delta t \geq 2\pi K \quad (1.8)$$

$\Delta\gamma$ is the frequency at full-width half-maximum, Δt is the duration at full width at half maximum and K is a numerical constant of the order of 1, depending on the actual pulse shape. Some examples of the standard pulse profiles are shown in table 1.1

Shape	Intensity profile $[I(t)]$	Spectral profile $[S(\omega)]$	K
Gaussian function	$\exp - 2(t/\tau_G)^2$	$\exp - \left(\frac{\omega\tau_G}{2}\right)^2$	0.441
sech	$\text{sech}^2(t/\tau_s)$	$\text{sech}^2\left(\frac{\pi\omega\tau_s}{2}\right)$	0.315
Lorentzian function	$\left[1 + (t/\tau_L)^2\right]^{-2}$	$\exp - 2 \omega \tau_L$	0.142
Asym. sech	$\left[\exp - \left(\frac{t}{\tau_a}\right)^2 + \exp - \left(\frac{3t}{\tau_a}\right)^2\right]$	$\text{sech}^2\left(\frac{\pi\omega\tau_a}{2}\right)$	0.278
Square	1 for $\left \frac{t}{\tau_r}\right \leq$ 0 elsewhere	$\text{sinc}^2(\omega\tau_r)$	0.443

Table 1.1 Examples of standard pulse profiles: The spectral values are given for unmodulated pulses (table adapted from ref. [15])

1.3. Generation of intense femtosecond laser pulse

The production of laser pulses existing for a few nanoseconds was first suggested by Hellwarth in 1961. Laser pulses of few nanoseconds duration was produced by the switching of quality factor of a cavity from very low value to very high value. In most of the high power, short pulse lasers, generation and amplification are done in steps. The generation of short pulses are achieved with the principle of modelocking with the active and passive modes of realization. Passive modelocking was successfully employed in dye lasers for the generation of short pulses in the initial stage. Later Ti:sapphire material was proved as a suitable solid state laser gain medium having high gain bandwidth to support femtosecond pulses. The broad bandwidth, good thermal conductivity and optical quality make this material as a good pump source. Passive modelocking in the solid state lasers was found to be existed without the necessity of intracavity saturable absorber and is called “magic modelocking”. This was later theoretically understood as “Kerr Lens Modelocking (KLM)”. The ultrafast laser pulses are generated nowadays using either Kerr Lens

Modelocking (KLM) [17] or Chirped Pulse Amplification (CPA) [18]. CPA technique was employed in microwave (radar) applications.

The modelocking is a technique by which a laser can be made to produce pulses of light of extremely short duration (ps or fs). A laser cavity has several longitudinal modes (allowed frequency in a cavity) with completely different phases. In this operation, the different longitudinal modes of a cavity, which are randomly generated in time inside the laser cavity, are locked together in phase to produce a train of extremely short pulses (from ps to fs). In modelocked laser, the modes of the laser will periodically constructively interfere with one another at one point and destructively elsewhere to create an intense burst or short spike of pulse. In the laser cavity, these modes are equally spaced.

The electric field of N such modes in phase can be written as,

$$E(t) = \sum_{n=0}^{N-1} E_n e^{i\omega_0 + n\Delta\omega t} \propto \frac{e^{iN\Delta\omega t} - 1}{e^{i\Delta\omega t} - 1} e^{i\omega_0 t} \quad (1.9)$$

where ω_0 is the central frequency and $\Delta\omega$ is the mode spacing. This appears as a carrier wave with frequency ω_0 , modulated by the function with exponents, in time domain. The laser intensity is then given by,

$$I(t) = |E(t)|^2 \frac{\sin^2 N\Delta\omega t}{\sin^2 \Delta\omega t} \quad (1.9.a)$$

The modelocking was achieved by two methods a) Active modelocking b) passive modelocking. KLM is a type of passive modelocking and it is a self locking process. In Ti: sapphire laser KLM technique is employed by taking the

advantage of the non linear property of this material. When a high intense pulse passes through the amplifying medium (Ti: sapphire) it behaves like a converging lens and focuses the beam just like a lens (Kerr lens) since the refractive index is intensity dependent. By placing a variable aperture in the laser cavity, one can select short pulses because it selectively introduces losses to mode. Figure1.4 shows the Kerr lens modelocking mechanism employed in Ti:sapphire laser.

A normal fs oscillator usually produces energy of the order of only a few nanoJoules per pulse. We need to amplify these pulses by several orders of magnitude and without much temporal broadening to reach at very high peak powers .But a limitation comes into play in the process of amplification due to the tendency of bright beams to self focus destructively.

The high fluence used by the amplifiers leads ultrashort laser pulse intensities greater than the damage threshold of the amplifier which is $\sim 10 \text{ J/cm}^2$ and it causes damage to the optics. To overcome this difficulty the technique of chirped pulse amplification (CPA) is used.

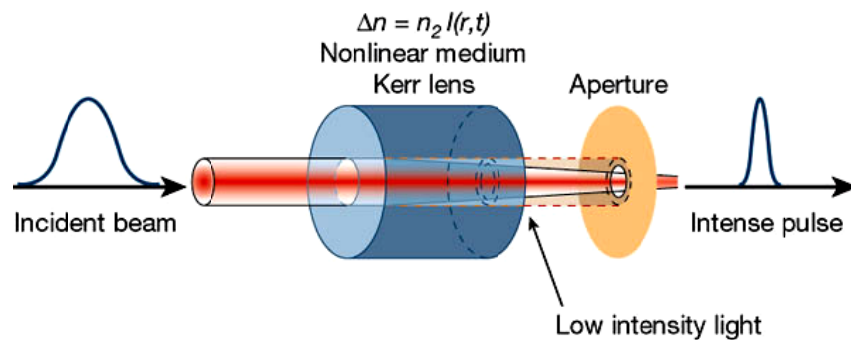


Figure1.4. Kerr lens modelocking mechanism of Ti:sapphire laser
[Recent developments in compact ultrafast lasers, Ursula Keller,
Nature 424, 831-838(14 August 2003)]

The working of CPA scheme is explained as follows: The low energy ($\sim 10^{-9}$ J) ultrashort laser pulse is generated from the oscillator at high repetition rate. These pulses are stretched using a stretcher by a large factor, usually somewhere of the order of 10^4 , so that its peak power is reduced considerably. These stretched pulses are trapped in the cavity and is amplified on each pass through the amplifier. Once the pulse saturates the gain and reaches the maximum energy, it is extracted from the amplifier and sent to the compressor where its initial duration is recovered. Figure 1.5 shows the principle of CPA.

However there are problems with chirped pulse amplification and these lie with the difficulty in recovering the initial pulse duration and quality. The compressor must compensate for the dispersion introduced not only from the stretcher but from the amplifier too, so the distance between the gratings must be set to a larger value in the compressor than the stretcher. It is possible to overall cancel out the second-order dispersion and obtain relatively short pulses, but extra care and design must be employed to keep higher-order dispersion terms, translated as wings and pre-pulses from degrading the final pulse quality.

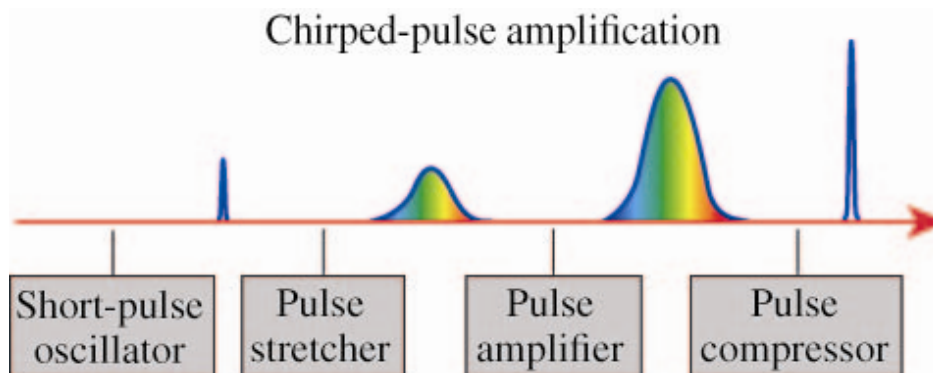


Figure 1.5. Diagrammatic representation of Chirped pulse amplification (CPA)

1.4. Propagation of ultrashort linear pulses

1.4.1. Linear propagation

The propagation of electromagnetic wave in a medium is governed by the Maxwell's four equations [19-20].

$$\nabla \cdot D = 0 \quad (1.10.a)$$

$$\mu_0 \nabla \cdot H = 0 \quad (1.10.b)$$

$$\frac{1}{\epsilon_0} \nabla \times D = -\mu_0 \frac{\partial H}{\partial t} \quad (1.10.c)$$

$$\nabla \times H = J + \frac{\partial D}{\partial t} \quad (1.10.d)$$

where the electric E and magnetic H field vectors have been expressed by the corresponding electric and magnetic flux densities D and H.

$$D = \epsilon_0 E \quad B = \mu_0 H \quad (1.11)$$

With ϵ_0 and μ_0 being the vacuum permittivity and vacuum permeability, respectively. In absence of free charges the charge density $\rho = 0$ and current density vector $J = 0$ vanish. Combining these equations and considering the dipole response of the material, the wave equation of the electric field for the of the electromagnetic wave can be obtained as:

$$\nabla \times \nabla \times E(r,t) + \frac{1}{c^2} \frac{\partial^2 E(r,t)}{\partial t^2} = \frac{1}{\epsilon_0 c^2} \frac{\partial^2 E(r,t)}{\partial t^2} \quad (1.12)$$

where E is the electric field, P is the induced dipole moment vector, c is the speed of light and ϵ_0 is the permittivity of the free space.

In the case of conventional (i.e., linear) optics, the induced polarization depends linearly on the electric field strength in a manner that can often be described by the relationship

$$P(r,t) = \epsilon_0 \chi^{(1)} E(r,t) \quad (1.13)$$

where the constant of proportionality $\chi^{(1)}$ is known as the linear susceptibility and ϵ_0 is the permittivity of free space. In an isotropic medium the susceptibility tensor is a scalar quantity and the wave equation (1.12) can be simplified into

$$\nabla^2 E(r,t) + \frac{n_0^2}{c^2} \frac{\partial^2 E(r,t)}{\partial t^2} = 0 \quad (1.14)$$

where the refractive index n_0 is given by,

$$n_0 = \sqrt{1 + \chi^{(1)}} \quad (1.15)$$

We have assumed that there are no free charges and the susceptibility is spatially dependent, so that divergence of E is zero [21]. Equation (1.14) describes the propagation of optical radiation in media and is the starting point of all the linear optics.

1.4.2. Nonlinear Propagation

1.4.2.1. Nonlinear pulse propagation equation

In this section we discuss the propagation of ultrashort laser pulses through a nonlinear media. We begin our discussion with the generalized nonlinear Schrodinger equation (NLSE).

The generalized nonlinear Schrodinger equation (NLSE) for the slowly varying field amplitude $A(r,t)$ as follows

$$\left[\left(1 + \frac{i}{\omega_0} \frac{\partial}{\partial \tau} \right)^{-1} \nabla_t^2 + 2ik_o \frac{\partial}{\partial z} + 2k_o \tilde{D} \right] \tilde{A}(r, t) = \frac{4\pi\omega_0^2}{c^2} \left(1 + \frac{i}{\omega_0} \frac{\partial}{\partial t} \right)^2 \tilde{p} \quad (1.16)$$

where the nonlinear polarization is expressed in terms of its slowly varying amplitude approximation $\tilde{p}(r, t)$. This equation includes the effects of higher-order dispersion (through the term that includes \tilde{D}), space-time coupling (through the presence of the differential operator on the left-hand side of the equation), and self-steepening (through the presence of the differential operator on the right hand side).

The nonlinear envelope equation [25] serves as a theoretical background to explain nonlinear propagation effects like self focusing, Group velocity dispersion (GVD) pulse splitting, SPM, self steepening and shock waves. Further increase of intensity bridges the way towards the strong field regime [26] which leads to the nonlinear ionization and physics of laser induced plasma filaments [27-28]. The different nonlinear effects such as self focusing, second harmonic generation, Sum frequency and Different frequency generation are also mentioned at the end of this chapter.

1.4.2.2. Ultrashort-Pulse Propagation Effects

The simplified version of NLSE equation can be obtained by ignoring the correction terms $\left(1 + \frac{i}{\omega_0} \frac{\partial}{\partial t} \right)$ by replacing $\left(1 + \frac{i}{\omega_0} \frac{\partial}{\partial t} \right)$ by unity and by including only the lowest-order contribution (known as second-order dispersion) to \tilde{D} .

For the case of material with an instantaneous third-order nonlinear response, the polarization is given by $\tilde{p}(r, t) = 3\chi^{(3)} |\tilde{A}(r, t)|^2 \tilde{A}(r, t)$.

Making use of the approximation we obtain

$$\frac{\partial \tilde{A}(r,t)}{\partial z} = \frac{i}{2k_0} \nabla_t^2 - \frac{i}{2k_0} \frac{\partial^2}{\partial t^2} + \frac{6\pi i \omega_0}{n_0 c} \chi^{(3)} \omega_0 |\tilde{A}|^2 \tilde{A} \quad (1.17)$$

the equation leads to the interpretation that the field amplitude \tilde{A} varies with propagation distance z (the left-hand side) because of three physical effects (the three terms on the right-hand side).

The first term on the r.h.s involving the transverse Laplacian describes the spreading of the beam due to diffraction, the second term involving the second time derivative describes the temporal spreading of the pulse due to group velocity dispersion, and the third term describes the nonlinear acquisition of phase

We define the distance scales where each of the three effects becomes appreciable

They are $L_{diff} = \frac{1}{2} k_0 \omega_0^2$	Diffraction length
$L_{disp} = \frac{\tau_p^2}{ k_2 }$	Dispersion length
$L_{NL} = \frac{n_0 c}{6\pi \omega_0 \chi^{(3)} A ^2} = \frac{1}{\left(\frac{\omega}{c}\right) n_2 I}$	Nonlinear length

Here ω_0 is the measure of the characteristic beam radius, and τ_p is a measure of the characteristic pulse duration. The significance of these distance scales is that for a given physical situation the process with the shortest distance scales is expected to be dominant.

1.4.2.2. (a) Kerr self focusing

The transverse Kerr effect was the first type of intensity dependent refractive index, observed in 1964 by Chiao et al. [37], as a geometrical "self-trapping of optical beams". The effect is explained as total internal reflection because of the transverse intensity dependent refractive index gradient which prevented from spatial spreading by diffraction. When a collimated beam enters a nonlinear medium, the centre of the beam containing the maximum intensity experiences the highest refractive index and is thus retarded to a larger extent as the wings. Hence the plain wave front of the collimated beam is bent as with a focusing optic. Strictly speaking, the focusing gets even tighter as the pulse propagates because the intensity depends on the square of the beam diameter. A certain threshold power value named critical power P_{cr} was found by Marburger and was defined as the starting point from where on a diffraction limited beam starts self-focusing [38]

Besides its role for self-guiding of plasma channels in air this effect is of prime importance for the operation of self-mode-locked fs oscillators [17]. Figure 1.6 shows the diagrammatic representation of Kerr self focusing when the laser beam crosses a medium with positive n_2

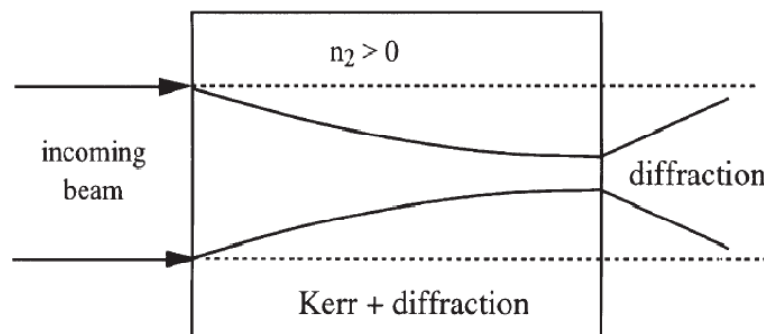


Figure 1.6: Self focusing of a laser beam crossing a medium with positive n_2 [image taken from Reference 16]

1.4.2.2. (b) Group velocity dispersion

An ultrashort pulse of light will lengthen after it has passed through glass as the index of refraction, which dictates the speed of light in the material, depends nonlinearly on the wavelength of the light. The wavelength of an ultrashort pulse of light is formed from the distribution of wavelengths either side of the centre wavelength with the width of this distribution inversely proportional to the pulse duration.

At a given wavelength, the refractive index determines the velocity of a single mode, known as the phase velocity. Figure 1.6 is a plot of refractive index, $n(\lambda)$, versus wavelength λ , and it sees $n(\lambda)$ decrease monotonically as λ increases, with a gradual upward curvature for most materials that are transparent in the optical spectrum. This is called dispersion. A material producing a downward curvature is said to have anomalous dispersion.

The slope of the curve, $\frac{dn(\lambda)}{d\lambda}$, is the group velocity, which defines the velocity of the wave packet with a central wavelength of λ . The second derivative of the slope $\frac{d^2n(\lambda)}{d\lambda^2}$, yields the group velocity dispersion (GVD), which is defined as the rate that the frequency components of the wave packet change their relative phases. Group velocity dispersion is responsible for a dispersive broadening of the pulses. Figure 1.7 shows the broadening of pulse when it propagates through a lossless, transparent medium.

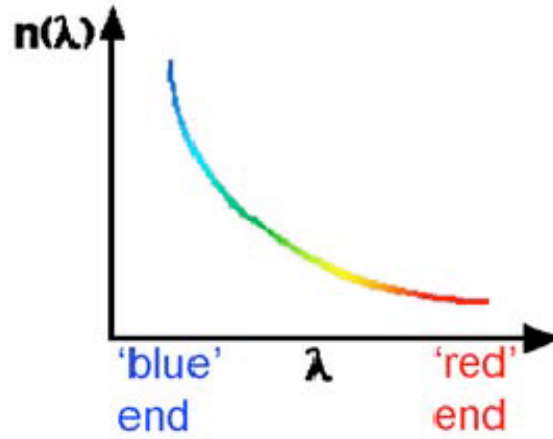


Figure1.7: Plot of refractive index, $n(\lambda)$, versus wavelength λ (image edited from Mira Seed Manual)

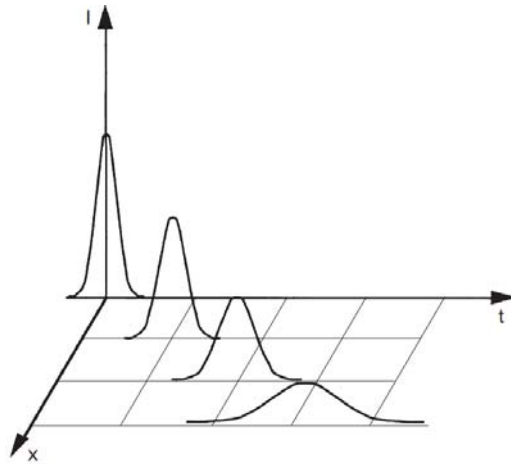


Figure 1.8: Figure showing the effect of GVD on the pulse propagating in a lossless, transparent medium along x-direction (figure adapted from ref. [16])

In the case of GVD dominated propagation, Eq. (1.17) reduces to

$$\frac{\partial \tilde{A}(r,t)}{\partial z} + \frac{i}{2k_2} \frac{\partial^2 A(z,t)}{\partial t^2} = 0 \quad (1.18)$$

Solving the equation (1.18), we obtain

$$\tilde{A}(z,\Omega) = A(0,\Omega) \exp(-ik_2\Omega^2 z) \quad (1.19)$$

where $A(z,t)$ can be obtained by taking the Fourier transform of equation (1.19). To illustrate the concepts of chirp and pulse broadening, consider a Gaussian input field having a pulse envelope given by

$$A(z,t) = A(z) \exp\left[-\left(\frac{\tau}{2\tau_0}\right)^2\right] \text{ with a pulse width } \tau_0$$

To solve the equation (1.25), we first find $\tilde{A}(z=0, \Omega)$ to be

$$\tilde{A}(0, \Omega) = 2\pi\tau_0 A(0) \exp\left[-\left(\frac{\Omega\tau_0}{\sqrt{2}}\right)^2\right] \quad (1.20)$$

Substituting equation (1.20) in equation (1.19) and taking the inverse Fourier transform, we find

$$A(z, \tau) = \frac{\tau_0}{\sqrt{2\xi}} A(0) \exp\left[-\left(\frac{\tau}{2\xi}\right)^2\right] \quad (1.21)$$

where $\xi^2 = \left(\frac{\tau_0^2 + ik_2 z}{2}\right)$

By rewriting $\xi = [\xi] \exp(-i\varphi(z))$ substituting into the solution given by Eq. (1.21), and simplifying, we can write the field amplitude as

$$A(z, \tau) = A(0) \left[1 + \left(\frac{z}{L_{dis}}\right)^2\right]^{-1/4} \exp\left[i\varphi(z) + i\psi(z, \tau) - \left(\frac{\tau}{\sqrt{2}\tau_{eff}}\right)^2\right] \quad (1.22)$$

Where $\varphi(z) = \frac{1}{2} \tan^{-1}\left(\frac{z}{L_{dis}}\right)$, $\psi(z, \tau) = \frac{\xi\tau^2}{2\tau_{eff}^2 L_{dis}}$, $\tau_{eff}^2 = \tau_0^2 \left[1 + \frac{z}{L_{dis}}\right]$

L_{dis} is a characteristic distance over which the group velocity dispersion effects become significant, sometimes referred to as the dispersive spreading length.

We see now that the temporal pulse width has now changed to τ_{eff} , as a function of the propagation distance through the material. This pulse width spreading is proportional to the GVD coefficient L_{dis}

Rewriting the equation (1.22)

$$A(z, \tau) = A(0) \left[1 + \left(\frac{z}{L_{dis}} \right)^2 \right]^{-1/4} \exp \left[i\varphi(z) + iC\tau^2 - \left(\frac{\tau}{\sqrt{2}\tau_{eff}} \right)^2 \right] \quad (1.23)$$

Equation (1.23) shows that the propagating Gaussian pulse now has a linear chirp coefficient given by $C = \frac{z}{2\tau_{eff}^2 L_{disp}}$. The chirp coefficient defines how the phase of each frequency component develops as it propagates a given length, and is dependent on k_2 and inversely proportional to initial pulse width. Shorter pulses have stronger chirp due to GVD.

1.4.2.2. (c) Self Phase Modulation

We next consider the case where GVD is negligible and only the nonlinearity on the right-hand side of Eq. (1.17) exists. This is the case where self-phase modulation is said to dominate. The optical Kerr effect is responsible for the nonlinear effect of self phase modulation (SPM). Each of the different frequency components of the pulse experiences a different phase shift, generating new frequencies and broadening the frequency spectrum of the pulse symmetrically. The leading edge of the pulse is shifted to lower frequencies (down chirp) while the trailing edge is shifted to higher frequencies (up chirp). The centre of the pulse experiences an approximate linear chirp.

In order to understand the effect of SPM, consider the propagation of the optical pulse, $\tilde{E}(z, t) = \tilde{A}(z, t) e^{i(k_0 z - \omega_0 t)} + c.c$ (1.24)

through a medium characterized by a nonlinear refractive index given by,

$$n(t) = n_0 + n_2 I(t) \quad (1.25)$$

where $I(t) = 2n_0 \varepsilon_0 c |\tilde{A}(z, t)|^2$

The length of the nonlinear medium is sufficiently small that no reshaping of the optical pulse can occur within the medium; the only effect of the medium is to change the phase of the transmitted pulse by the amount

$$\varphi_{NL}(t) = \frac{n_2 I(t) \omega_0 L}{c} \quad (1.26)$$

The instantaneous frequency, being the time derivative of the phase, can be written as

$$\omega(t) = \frac{\partial \varphi(t)}{\partial t} = \omega_0 - \omega_0 \frac{\partial n(t)}{\partial t} z \quad (1.27)$$

and the frequency variation can be written as

$$\delta\omega(t) = \omega(t) - \omega_0 = \frac{\omega_0 n_2}{2c} \frac{\partial I(t)}{\partial t} z \quad (1.28)$$

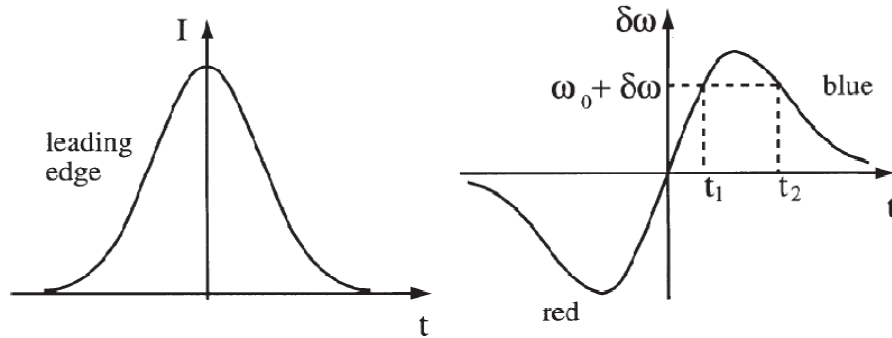


Figure 1.9: (Left) Intensity dynamics of a Gaussian pulse: the earlier times, i.e. the leading edge of the pulse. (Right): Time variation of the central pulsation which is proportional to the negative of pulse envelope derivative when the nonlinear index of refraction is positive. [Image taken from the reference 16]

Figure 1.9 shows a graphical elucidation of the above relation in case of the considered pulse of Gaussian phase variation. In the self-phase-modulation process, with n_2 positive, new low frequencies are created in the leading edge of the pulse envelope and new high frequencies are created in the trailing edge. These new frequencies are not synchronized, but are still created inside the original pulse envelope. Self phase modulation itself is not a dispersive effect, but it causes a pulse to no longer be transform-limited when crossing a transparent material, which means the pulse is then subject to dispersion,. Dispersion causes the ‘redder’ parts of the pulse to have a higher velocity than the ‘bluer’ parts, forcing the front of the pulse to move quicker than the back, temporally broadening the pulse. In anomalous dispersion the opposite is true and the pulse temporally compressed. The self phase modulation becomes stronger as the pulse becomes more intense, in turn causing more broadening. An important consequence of SPM in the fs regime is that due to the availability of high peak intensities there is enormous amount of phase modulation taking place that results in super-broadening of the initial pulse spectrally leading to a phenomenon called the ***Supercontinuum generation and Filamentation*** [29-33]

1.4.2.2.(d) Self steepening

Self steepening is due to the effect of factor $\left(1 + \frac{i}{\omega_0} \frac{\partial}{\partial t}\right)$ in the non linear source term $\tilde{p}(r,t)$ on the r.h.s of the Non Linear Schrodinger Equation (NLSE). Self-steepening has been first described by De Martini et al. [34] for Gaussian pulses in a dispersive medium and its effects on the ultrashort pulse propagation were shown by Yang, Shen and Gaeta [35]. The consequence of self steepening is the intensity dependent contribution to group velocity and the dispersive four-wave mixing contribution. The intensity dependence of the

group velocity leads to intensity dependence of the group index n_2^g . It also leads to the phenomena of self-steepening and optical shock wave formation. The incident optical pulse is assumed to have a Gaussian time evolution. After propagating through a nonlinear medium with n_2^g positive, the peak of the pulse is slowed down more than the edges of the pulse, leading to steepening of the trailing edge of the pulse. If this edge becomes infinitely steep, it is said to form an optical shock wave.

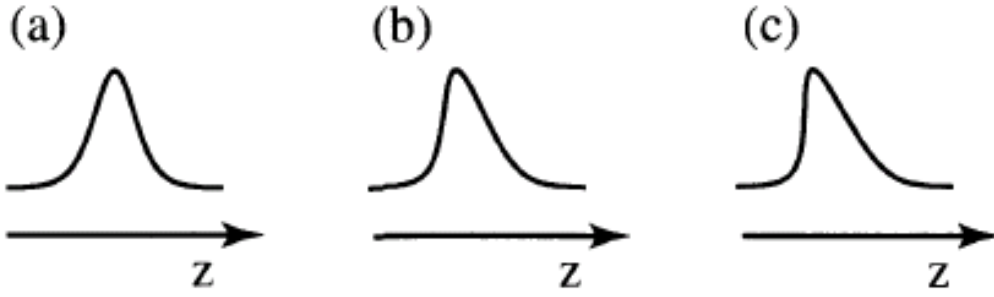


Figure1.10: Self steepening and optical shock formation
(image adapted from reference 22)

1.4.2.2.(e) Space time coupling

Space time coupling is due to the presence of the differential operator differential operator $\left(1 + \frac{i}{\omega_0} \frac{\partial}{\partial \tau}\right)^{-1}$ on the left-hand side of NLSE. To study this effect most we are considering the propagation of ultrashort pulse through a dispersionless, linear material so that the wave equation [1.15] becomes

$$\left[\left(1 + \frac{i}{\omega_0} \frac{\partial}{\partial \tau}\right)^{-1} \nabla_{\perp}^2 \tilde{A}(r, t) + 2ik_o \frac{\partial}{\partial z} \tilde{A}(r, t) \right] = 0 \quad (1.29)$$

The first term is said to represent space-time coupling because it involves both temporal and spatial derivatives of the field amplitude. To examine the significance of this mathematical form, it is convenient to rewrite this equation (1.29) as

$$\left[\nabla_{\perp}^2 \tilde{A}(r,t) + 1 + \left[\left(1 + \frac{i}{\omega_0} \frac{\partial}{\partial \tau} \right) \right] 2ik_0 \frac{\partial}{\partial z'} \tilde{A}(r,t) \right] = 0 \quad (1.30)$$

Consider the artificial example of a field of the form $\tilde{A}(r,t) = \tilde{a}(r)e^{-i\delta\omega t}$; such a field is a monochromatic field at frequency $\omega_0 + \delta\omega$. We substitute this form into Eq. (1.30) and obtain

$$\left[\nabla_{\perp}^2 \tilde{a}(r) + \left(1 + \frac{\delta\omega}{\omega_0} \right) 2ik_0 \frac{\partial}{\partial z'} a(r) \right] = 0 \quad (1.31)$$

which can be expressed as

$$\left[\nabla_{\perp}^2 \tilde{a}(r) + 2i(k_0 + \delta k) \frac{\partial}{\partial z'} a(r) \right] = 0 \quad (1.32)$$

where $\delta k = k_0 \left(\frac{\delta\omega}{\omega_0} \right)$. This wave thus diffracts as a wave of frequency $\omega_0 + \delta\omega$

rather than a wave of frequency ω_0 . More generally, for the case of an ultrashort pulse, the operator $\left(1 + \frac{i}{\omega_0} \frac{\partial}{\partial \tau} \right)$ describes the fact that different frequency components of the pulse diffract into different cone angles. Thus, after propagation different frequency components will have different radial dependences [36]

1.5. Matter in intense laser fields

1.5.1. Interaction of light with a medium

On a fundamental level optical effects like dispersion have their origin in the way the bound electrons respond on the exciting light wave. The strength of induced oscillations is determined by the resonance frequency at which the medium absorbs. After ultrashort laser pulses have been discussed within the scope of linear optics, the following section will introduce the phenomena of nonlinear optics that lead to the filamentation. In the case of optics, it is the electric field of the light wave that interacts with the atoms of the medium through which it is propagating. The light from ordinary lamps induces an electric field of about $E = \frac{1}{4} V/cm$ which is negligible compared to the Coulomb force between the electron and the nucleus of $\frac{e}{4\pi\epsilon_0 r_{bohr}^2} = 6 \times 10^{11} V/m$. However, with regard to high-power lasers this relation changes considerably, and one could even reach the field strength within the atom by focusing the high power laser beam at a distance of a few meters. Therefore, when an optical medium interacts with radiation field, the optical properties of the medium will be modified, this phenomenon is commonly called as nonlinear optics. A laser is typical source which can induce strong nonlinear effects even in weak nonlinear materials. The electric polarization plays a key role in the description of nonlinear optical phenomena as the time varying polarization acts as a source for the generation of new components of the electromagnetic field. Thus the concept of linear and nonlinear electric susceptibility [22–24] enables explanation of many light-matter interactions which are relevant for this thesis. The non linear dependence

of the polarization on the applied electric field can be expressed as a power series in E

$$P = P^{(1)} + P^{(NL)} \quad (1.33.a)$$

$$P = \epsilon_0 E \left[\chi^{(1)} + \chi^{(2)} E + \chi^{(3)} E^2 \right] \quad (1.33.b)$$

Where ϵ_0 is the vacuum permittivity. The $\chi^{(1)}$ is known as linear electric susceptibility which can be linked to the linear refractive index. The field strength in the first term of the equation describes the first nonlinear effect. The coefficient $\chi^{(2)}$ relating the polarization to the square of the field strength is called the second-order nonlinear susceptibility of the medium. Its magnitude describes the strength of second-order process. The term $\chi^{(3)}$ describes the third order processes. For most materials, the higher-order effects are extremely difficult to observe. For this reason we limit here our discussions up to and third-order effects.

Assuming linear polarization, the second order susceptibility of Eq.(1.33.b) takes the form

$$P(r,t) = \epsilon_0 \chi^{(2)} E^2 \quad (1.34)$$

Equation (1.34) denotes that three fields are coupled. Two incoming fields with their oscillation frequencies (ω_1 and ω_2) induce a polarization oscillating at frequencies equal to the linear combinations of driving fields. According to classical electrodynamics, any motion that is connected with a change of its dipole moment leads to the emission or absorption of radiation. Thus the second order polarization emits light at new frequencies [22]

$$P(2\omega_1) = \varepsilon_0 \chi^{(2)} E^2, P(2\omega_2) = \varepsilon_0 \chi^{(2)} E^2 \quad (\text{SHG}) \quad (1.35.a)$$

$$P(\omega_1 + \omega_2) = 2\varepsilon_0 \chi^{(2)} E_1 E_2 \quad (\text{SFG}) \quad (1.35.b)$$

$$(P(\omega_1 - \omega_2) = 2\varepsilon_0 \chi^{(2)} E_1 E_2^* \quad (\text{DFG}) \quad (1.35.c)$$

$$P(0) = 2\varepsilon_0 \chi^{(2)} [E_1 E_1^* + E_2 E_2^*] \quad (\text{OR}) \quad (1.35.d)$$

The abbreviations of the physical processes are second harmonic generation (SHG), sum frequency generation (SFG), difference frequency generation (DFG) and optical rectification (OR).

1.5.2. Nonlinear response of matter in a strong radiation field

The characteristic feature of all laser matter interaction is the fact that the electric field E associated with the electromagnetic wave is comparable to or larger than atomic or molecular binding field. The interaction of matter with such fields is inherently nonlinear. When the electric field is sufficiently high, the electrons do not bound and the atoms will get ionized. Experimentally, laser-induced ionization was observed shortly after the invention of the laser in the sixties already. With advances in laser technology, however, higher intensities, different wavelengths and shorter pulse durations became available. Depending on the strength of the incident electric field, there are different ionization processes such as Multi-photon ionization (MPI), Tunnel ionization (TI) and Over the Barrier (OTBI) or Barrier suppression ionization (BSI).

1.5.2.(a) Multiphoton ionization

For intensities from 10^{13} W/cm² to 10^{14} W/cm² Multiphoton ionization (MPI) becomes significant. This is an intensity regime between perturbative and strong field regime of light matter interaction. In this regime the

contribution of the free electrons becomes comparable to that of the induced atomic dipoles pertaining to the bound bound transitions. Multiphoton ionization (MPI) takes place when a single electron is insufficient to cause ionization ($h\nu < E_g$) but the intensity is sufficient for an nth order process-a combined effect of n photons to cause ionization ($n h\nu > E_g$). This effect has been predicted theoretically by Goppert-Mayer in 1931 already [39]. In MPI regime, the electron density N_e grows as:

$$\frac{dN_e}{dt} = \sigma_n I^n \quad (1.36)$$

where σ_n is the MPI coefficient for n photon absorption. The process of MPI continues until all the atoms are get ionized [40]. The physical example of this is the self channelling of fs pulses over long distances.

1.5.2.(b) Tunnel ionization (TI)

If the strength of the applied electric field is comparable or greater than that of that of the binding atomic coulomb field experienced by the valence electrons, there is a good probability of valence electrons to escape from its bound state via tunnelling or above barrier ionization. This is the strong field regime and in this regime, ionization dominates over atomic polarization. In the intensity regime of 10^{14} W/cm² to 10^{15} W/cm² tunnel ionization (TI) dominates whereas for intensities greater than 10^{15} W/cm², above the barrier ionization takes place.

If more photons are absorbed by the electron than required for overcoming the binding energy of the atom, the electron spectra show characteristic maxima separated by the energy $n\hbar\omega$ (with an integer $n > 0$). Hence the kinetic energy of the electron is larger than the photon energy, E_{kin}

$> \hbar\omega$. In the extended version of the Einstein equation, photo-ionization is given by[40]

$$E_{kin} = (n + s) \hbar\omega - E_{ion} \quad (1.37)$$

where n is the number of photons required for multiphoton process to occur and s is the excess number of photons absorbed. This ionization process was termed Above Threshold Ionisation (ATI) [41-42].

At higher intensities, the distortion of the Coulomb potential is so large that the barrier between a bound state and the continuum does not remain infinite. The potential is lowered such that the electrons can tunnel through, as shown in figure(1.11) where the distortion in the frequency atomic potential at a particular instant is shown in figure. [43-45]. Tunnel ionization of gas atoms or molecules is similar to multiphoton ionization in the sense that both are high intensity effects. Depending on the combined condition of the laser and the ionization of the material to be ionized we can distinguish MPI and TI. The popular parameter that separates MPI and TI is the Keldysh (adiabatic) parameter γ [43] which is given by

$$\gamma = \sqrt{\frac{I_p}{2U_p}} \propto \frac{\omega}{E} \sqrt{I_p} \quad (1.38)$$

where U_p is the ponderomotive energy and I_p is the ionization energy. Tunnelling applies for strong fields and long wavelengths; i. e. for $\gamma < 1$ and for MPI $\gamma > 1$.

1.5.2.(c) Over the barrier ionisation (OTBI)

At very high laser intensities the Coulomb barrier suppression is so large and lower than the bound electron's energy. The modified Coulomb potential because of the application of an external electric field of amplitude E can be written as

$$V(x) = -\frac{Ze^2}{x} - eEx \quad (1.39)$$

with Z being the charge of the ion which will be produced and E the external electric field strength.

If this barrier falls below E_{ion} , the binding energy of the electrons then the electrons can escape spontaneously. This process is known as Over the Barrier (OTBI) or Barrier Suppression Ionization (BSI) mechanism.

The position of the barrier, x_{max} , can be derived by setting $\frac{\partial V(x)}{\partial x} = 0$ yielding $x_{max} = \frac{Ze}{E}$ (1.40)

Setting the height of the barrier as $V(x_{max}) = E_{ion}$ to find out the threshold field strength at which OTBI can occur, we get the threshold field strength, E_{Th}

$$E_{Th} = \frac{E_{ion}^2}{4Ze^3} \quad (1.41)$$

The minimum laser intensity required for the ions with charged state Z is given by

$$I_{BSI} = \frac{\pi^2 c \epsilon_0^3 E_{ion}^4}{2Z^2 c^6} \approx 4.10^{19} \left[\frac{E_{ion}}{ev} \right]^4 Z^{-2} \frac{W}{cm^2} \quad (1.42)$$

This relation has been confirmed experimentally over several orders of magnitude using noble gases [46]. For the example, in the case of a hydrogen atom ($Z = 1$, $E_{\text{ion}} = 13.6 \text{ eV}$), one finds,

$$I_{\text{BSI}} = \frac{I_a}{256} \approx 1.37 \times 10^{14} \frac{W}{\text{cm}^2}$$

Schematic representation of different ionization schemes is shown in figure 1.11

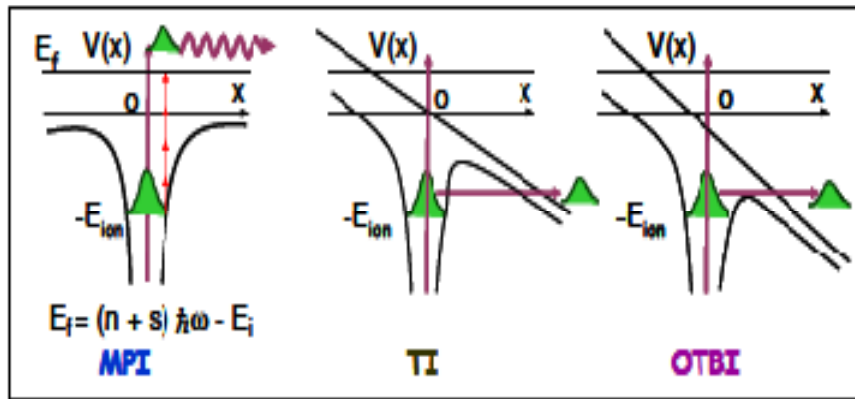


Figure 1.11: Schematic representation of ionization mechanisms

1.6. Organisation of the thesis

Chapter 2:- This chapter is devoted to the discussion of the details of laser system used for the experiments carried out in this thesis. The characterisation of the pulse using “Silhouette” based on Multiphoton Intrapulse Interference Phase Scan (MIIPS)” is also discussed in this chapter.

Chapter 3:- This chapter serves as the introductory material to the complex phenomena of filamentation and associated Supercontinuum Emission (SCE). The detailed description of the underlying

physics behind the filamentation and the various nonlinear processes occurring in the filamentation process are addressed here.

Chapter 4:- In this chapter, we present the experimental investigations of the filament characteristics of sharply focused fs pulses in air. The measurements of Supercontinuum Emission (SCE) generated by ultrashort Ti: Sapphire laser, filamentation in air under different focusing geometries and the dynamics of filaments via direct imaging are detailed here. We demonstrate the variations in the length and width of the filament as a function of focal geometry, input power and polarization of the laser pulse. The presence of coherently interacting multiple filaments either resulting in a fusion or exchange of power is also observed

Chapter 5:- This is dedicated to the investigation of the evolution of Supercontinuum Emission (SCE) associated with filaments and the filament characteristics due to the tilt of focusing lens under tight focusing geometries.

Chapter 6:- This chapter involves the study of evolution of plasma dynamics via supercontinuum emission (SCE) resulting from propagation of tightly focused femtosecond (fs) laser pulses propagating in water. We studied the effect of input polarization of laser pulses on SCE in different external focal geometries. SCE with higher efficiency and a considerable spectral blue shift is observed under tight focusing conditions ($f/6$) compared to loose focusing conditions of ($f/7.5$) and ($f/10$).

Chapter 7:- We present our results on the non linear optical properties (NLO) of PVA- Rhodamine 6G matrix doped with DNA, using ps pulses. The addition of DNA enhanced the NLO properties of thin films .We conclude that PVA is a good matrix for fluorescent dyes incorporated into the double helix of DNA molecule enabling them suitable for practical applications in optical devices

Chapter 8 :- This chapter summarizes the results obtained in this thesis. Future implications and directions are discussed in brief.

References

- [1] J. P. Gordon, "Interaction forces among solitons in optical fibers", *Optics Letters* 8, 596 -598, (1983).
- [2] G. I. Stegeman and M. Segev, "Optical Spatial Solitons and Their Interactions: Universality and Diversity", *Science* 286, 1518 - 1523,(1999).
- [3] R. L. Fork, C. V. Shank, C. Hirshman, R. Yen, and W. J. Tomlinson," Femtosecond white-light continuum pulses" *Optics Letters* 8, 1 - 3,(1983).
- [4] T. H. Maiman, "Stimulated Optical Radiation in Ruby" *Nature* 187, 493 -494,(1960),
- [5] A. E. Siegman, "Laser Spectroscopy for Sensing: Fundamentals, Techniques and Applications "Lasers, University Science Books, California (1986)
- [6] R.W. Hellwarth, "Control of fluorescent pulsations" in *Advances in Quantum Electronics*, edited by J.R.Singer., Columbia University Press, New York 334-341,(1961)
- [7] J. McClung and R.W. Hellwarth, "Giant optical pulse from ruby" *J. Appl. Phys.* 33, 828-829, (1968).
- [8] M. DiDomenica, "Small signal analysis of internal modulations of lasers" *J.Appl. Phys.* 35, 2870-2876, (1964)
- [9] L.E. Hanngrove, R.L. Fork, and M.A. Pollack, ""Locking of He Ne laser modes by synchronous intracavity modulation" *Appl.Phys.Lett.* 5, 4-5, (1964)
- [10] A. Yariv," Internal modulation in multimode laser oscillators" *J. Appl. Phys.* 36, 388 -391,(1965)

- [11] R.L. Fork, B.I. Green and C.V. Shank, "Generation of optical pulses shorter than 0.1 psec by colliding pulse mode locking," *Appl. Phys. Lett.* 38, 671-672 (1981)
- [12] R.L. Fork, C.V. Shank, R. Yen, and C.A. Hirlimann,"Femtosecond optical pulses" *IEEE J. Quantum. Electron.* QE-19, 500-506, (1983).
- [13] Rick Trebino, Kenneth W. DeLong, David N. Fittinghoff, John N. Sweetser, Marco A. Krumbu" gel, and Bruce A. Richman "Measuring ultrashort laser pulses in the time-frequency domain using frequency-resolved optical gating" *Rev. Sci. Instrum.*, 68, 3277-3295,(1997)
- [14] <http://frog.gatech.edu/talks.html>
- [15] Jean-Claude Diels, Wolfgang Rudolph, Paul F. Liao, Paul Kelley, "Ultrashort laser pulse phenomena: Fundamentals, Techniques, and Applications on a Femtosecond Time Scale", Academic Press,(2006)
- [16] Rullière, C.; *Femtosecond Laser Pulses: Principles and Experiments*, Springer, 2005,
- [17] D.E Spence , P.N.Kean, and W.Sibbett, 60-fsec pulse generation from a self-mode- locked Ti:sapphire laser. *Opt. Lett.*, 16,42-44,(1991).
- [18] D. Strickland, G. Mourou,"Compression of amplified chirped optical pulses" *Opt. Commun.* 56, 219 -221,(1985)
- [19] J. D. Jackson, "Classical Electrodynamics", Wiley New York, (1975)
- [20] M. Born and E.Wolf, "Principles of optics", Peragamon,Oxford, (1980)
- [21] R.W. Boyd, "Nonlinear optics", Academic Press, Boston,(1992)
- [22] Robert W. Boyd. "Nonlinear Optics". Academic Press, London, (2003)
- [23] G. P. Agrawal. "Nonlinear fiber optics". Academic Press, San Diego, (2001).
- [24] Y. R. Shen. "Principles of nonlinear optics". Wiley, New York, (1984).

- [25] T. Brabec and F. Krausz. “Nonlinear optical pulse propagation in the single-cycle regime”. *Phys. Rev. Lett.*, (17):3282–3285, (1997).
- [26] T. Brabec and F. Krausz. “Intense few-cycle laser fields: Frontiers of nonlinear optics.” *Rev. Mod. Phys.*, 72 (2):545–591, (2000).
- [27] L. Bergé, S. Skupin, R. Nuter, J. Kasparian, and J.-P. Wolf. “Ultrashort filaments of light in weakly-ionized, optically-transparent media. *Rep. Prog. Phys.*, 70:1633-1713,(2007).
- [28] A. Mysyrowicz A. Couairon. “Femtosecond filamentation in transparent media”. *Physics Reports*, 441:47–189, (2007).
- [29] R. R. Alfano, “The Supercontinuum laser source”, Springer, Berlin (1989).
- [30] J. M. Dudley, G. Genty, and S. Coen,” Supercontinuum generation in photonic crystal fiber” , *Rev. Mod. Phys.* 78, 1135 - 1184 (2006)
- [31] R. R. Alfano, and S. L. Shapiro, “Emission in the Region 4000 to 7000 Å Via Four-Photon Coupling in Glass” *Phys. Rev. Lett.* 24, 584–587 (1970)
- [32] P. B. Corkum, C. Rolland, and T. Srinivasan-Rao, "Supercontinuum Generation in Gases”*Phys. Rev. Lett.* 57, 2268 -2271, (1986)
- [33] R. L. Fork, C. V. Shank, C. Hirlimann, R. Yen, and W. J. Tomlinson, “Femtosecond white light continuum pulses” *Opt. Lett* 8, 1-3,(1983).
- [34] F. DeMartini, C. H. Townes, T. K. Gustafson, and P. L. Kelley, “Self steepening of light pulses”*Phys. Rev.* 164, 312 -322,(1967).
- [35] G. Yang, Y. R. Shen: *Opt. Lett.*,”Spectral broadening of ultrashort pulses in a nonlinear medium” 1 9, 510-512 (1984)
- [36] J. E. Rothenberg, *Opt. Lett.* “Space–time focusing: breakdown of the slowly varying envelope approximation in the self-focusing of femtosecond pulses 17, 1340-1342, (1992).

- [37] R. Y. Chiao, E. Garmire, and C. H. Townes. “Self-trapping of optical beams”. *Phys. Rev. Lett.*,13, 479–482, (1964).
- [38] J.H. Marburger. “Self-focusing: Theory”. *Prog. Quant. Electr.*, 4:35-110, (1975).
- [39] M. G^oppert-Mayer, “Elementary processes with two-quantum transitions”, *Annalen der Physik* 9, 273-294, (1931).
- [40] P. Lambropoulos, “Mechanisms for Multiple Ionization of Atoms by Strong Pulsed Lasers” *Phys.Rev.Lett.*55,2141-2144,(1985)
- [41] Y. Gontier, M. Poirier and M. Trahin, “Multiphoton absorption above the ionization threshold”, *J. Phys. B-At. Mol. Opt.* 13, 1381-1387, (1980).
- [42] P. Agostini, F. Fabre, G. Mainfray, G. Petite and N. K. Rahman, “Free-Free Transitions Following Six-Photon Ionization of Xenon Atoms”, *Phys. Rev. Lett.* 42, 1127-1130, (1979).
- [43] L. V. Kleldysh, “Ionization in the field of a strong electromagnetic wave”, *Sov. Phys. JETP Lett.* 20, 1307 -1309, (1965).
- [44] A. M. Perelomov, V. S. Popov and M. V. Terentev, “Ionization of atoms in an alternating electric field”, I, *Sov. Phys. JETP Lett.* 23, 924 -934, (1966).
- [45] A. M. Perelomov, V. S. Popov and M. V. Terentev, Ionization of atoms in an alternating electric field, II, *Sov. Phys. JETP Lett.* 24, 207 - 217,(1967).
- [46] T. Auguste, P. Monot, L. A. Lompr^e, G. Mainfray and C. Manus, Multiplycharged ions produced in noble gases by a 1 ps laser pulse at $\lambda = 1053$ nm, *J. Phys. B - At. Mol. Opt. Phys.* 25, 4181-4194, (1992).

Chapter - 2

LASER SYSTEMS

- 2.1 Laser system used:
- 2.2 Pulse Measurement
- 2.3 Conclusions

Abstract

This chapter deals with the important aspects of the laser systems employed in this thesis for various studies. The amplified femtosecond (fs) laser system used throughout the thesis is introduced here. The Multiphoton Intrapulse Interference Phase Scan (MIIPS) based pulse shaper for measuring and manipulating the fs pulse is also explained in detail.

2.1. Laser system used:

The laser system used in this dissertation is a commercially available diode-pumped mode-locked Ti: sapphire laser purchased from Coherent. The main components of the laser system for generating the ultrashort pulses in the laboratory are

1. Femtosecond mode-locked Ti: sapphire laser [Coherent Mira Seed].
2. Pump laser for the regenerative amplifier [Coherent Evolution 30].
3. High Energy femtosecond regenerative amplifier [Coherent Legend USP].

The seed laser system (MICRA) produces high repetition rate, nJ, fs pulses, and regenerative amplifier (LEGEND) produces amplified fs pulse [1]. The pictorial overview of the fs laser facility present is as shown in figure 2.1.

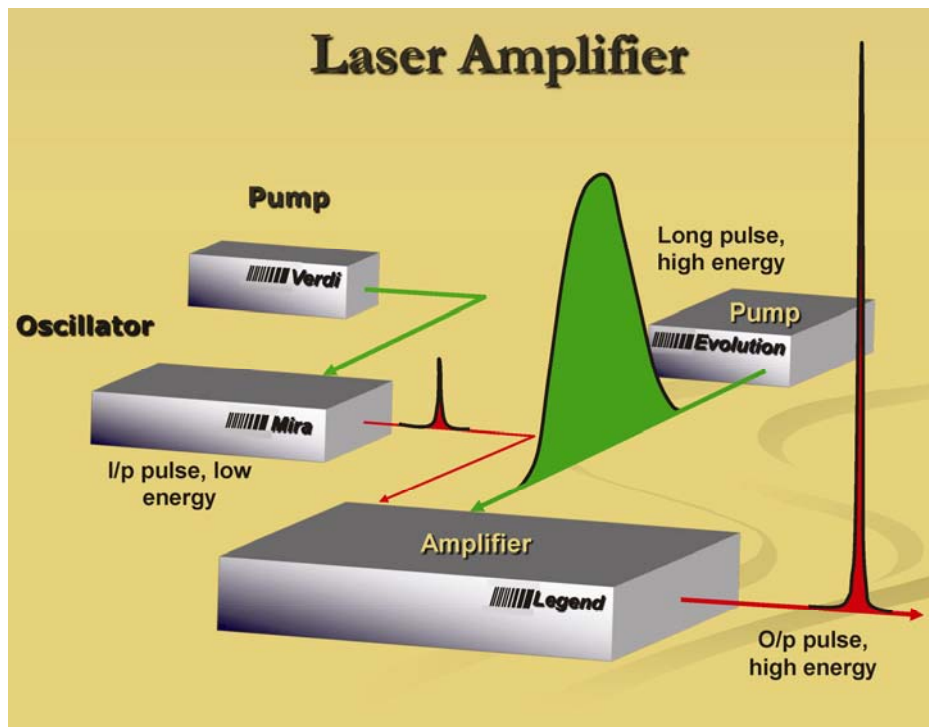
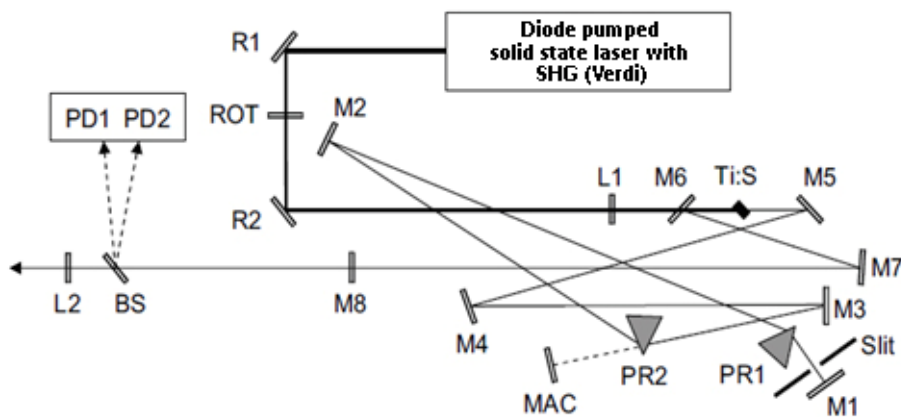


Figure 2.1 Overview of the fs laser facility (Image courtesy: Coherent)

2.1.1. The fs oscillator [Micra System]

The oscillator is a Titanium: sapphire laser system [Micra] capable of producing mode locked pulses with bandwidths exceeding 100 nano meters. A key feature of the oscillator is the incorporation of the cw diode pumped laser into the oscillator cavity. Ti: sapphire which serves as the gain medium requires a pump in the blue-green region of the spectrum. Although there are a wide range of pump wavelengths available, no laser diodes are powerful enough to pump this spectral region. An optical pump at the correct wavelength is required to provide energy to the gain medium in the oscillator. The pump power should be of several watts because the upper-state lifetime of Ti: sapphire is very short (3.2 μ s) and the saturation power which is the incident optical power required to achieve significant saturation of an absorber [2] ,is very high. Originally Ti: sapphire lasers were pumped using argon-ion lasers at 514 nm, which were powerful but bulky, inefficient and expensive to run [3]. The cw pump chamber contains intracavity, frequency doubled solid state Nd: YVO₄ laser giving 532 nm laser output. The pump laser employs Nd: YVO₄ as the gain medium which is commonly called as “vandate”. The high absorption coefficient of vandate at 808nm wavelength and large stimulated emission cross section at 1064nm makes it an ideal choice for pump laser. The frequency-doubling in the pump laser occurs within a lithium triborate (LBO) nonlinear crystal and produces green light at 532 nm, allowing efficient absorption by the Ti: sapphire crystal. The absorption band of Ti: sapphire extends from 400nm to 600nm (in the blue and green region) which makes 532 nm output of cw laser, an ideal pump source for Ti: sapphire laser [Verdi]. The fluorescence band of Ti: sapphire medium extends from 600 nm to wavelength greater than 1000 nm making it possible for wide broadband tunable laser emission. The femtosecond oscillator (Micra) adopts passive mode-locking technique i.e Kerr

lens modelocking in combination with an intra cavity prism pair to generate low-noise, large-bandwidth, and high peak power ultrafast pulses to produce pulses around 15 fs in pulse duration and 1 Watt average power. The repetition rate of the fs oscillator is 80 MHz and the central wavelength is 800 nm, which is most efficient for Ti: sapphire. Figure 2.2 gives the schematic representation of the fs seed laser (MICRA)



**Figure 2.2 Schematic diagram of Micra seed optical laser
(Picture taken from the MICRA manual)**

R1 - Pump beam routing optic with Power Track beam steering actuators, M1- M8 Oscillator cavity mirrors, MAC- Auxiliary cavity end mirror, ROT- Polarizer, PR1, PR2 -Prism pair, R2 - Pump beam routing optic, BS – Beamsplitter, L1- Pump beam focusing lens, PD1, PD2- Fast and slow photodiodes Ti: S- Titanium :sapphire laser crystal, L2 -Collimating lens.

The fs pulse laser can be wavelength tuned by a pair of compensating prisms. As the wavelength is changed, the pulse width and spectral width of the fs laser will also be changed. The characteristics of pulse width tuning in a Ti: sapphire fs laser is greatly influenced by the dispersive elements within a laser cavity. An oscillating pulse will receive a total round trip chirp due to self phase

modulation (SPM) in the Ti: sapphire rod, which results from the interaction of the short optical pulse with the nonlinear refractive index and the positive material Group velocity dispersion(GVD) from the optical components and negative GVD caused by the prism pairs. The cumulative effect from a lack of compensation for both GVD and SPM effects would see a temporal broadening for the pulse. In order to obtain stable, short pulses the chirping caused by SPM plus positive material GVD should compensate the negative GVD. The overall system GVD of zero is achieved by orientating the prisms so that the light travels through either more or less of the glass. Under these conditions, the red and blue wavelength components of the pulse do not change their relative positions within the pulse over one complete round trip through the cavity.

The fs oscillator Ti: sapphire laser system (MICRA) delivers ~ 40 fs, 80 MHz pulse train with pulse energy of 1 nJ. The output spectrum with its peak at 800 nm is as shown in figure 2.3

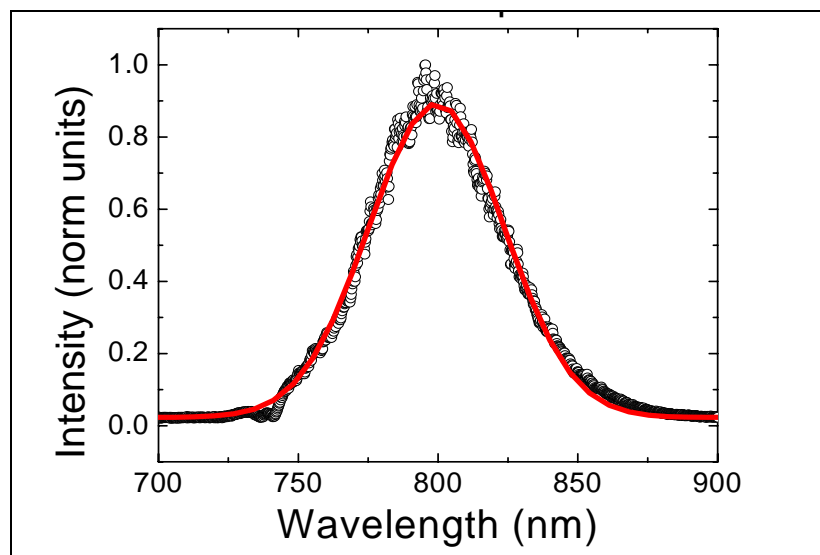


Figure 2.3 Output spectrum of Ti: sapphire Oscillator (MICRA)

2.1.2. Optical pump to the Regenerative Amplifier [Evolution-30]

To pump the amplifier, a Q-switched, frequency doubled, neodymium-doped yttrium lithium fluoride (Nd: YLF) laser [Coherent Evolution-30], is used. The amplifier produces pulses of duration 250 ns at 527 nm with a repetition rate of 1 kHz. The power output is 20 W giving each pulse 20 mJ of energy. Nd: YLF lasers have good beam quality due to their low noise, are compact, stable and very reliable. The range of power levels that are available make them ideal for pumping ultrafast Ti: sapphire amplifiers.

2.1.3. The Regenerative Amplifier [Legend]

The regenerative amplifier [Coherent Legend USP], is used to convert the (optimised) 15 fs, 1nJ pulses from the oscillator to 40 fs, 2.5 mJ pulses, increasing the energy by 6 orders of magnitude. The energy for the Ti: sapphire gain medium comes from the pump laser in the form of 20 mJ pulses at 250 ns duration. The amplifier possess a pre pulse contrast ratio of $>1000 :1$ and a post pulse contrast ratio of $>100:1$. The repetition rate of the pump is 1 kHz, which differs greatly from the repetition rate of 80 MHz for the femtosecond pulses from the oscillator. To solve this problem only 1 pulse (in every 80,000) is selected from the oscillator pulse train each time and the energy in the Ti: sapphire gain medium is maximised by the pump beam (1,000 times every second). The selected pulse is injected into the cavity and allowed to oscillate by the regenerative amplifier until it has the maximum possible energy.

The regenerative Ti: sapphire amplifier laser system (Legend) used for the studies contains three essential elements to amplify ultra short pulses to the mJ. These elements include (a) an optical pulse stretcher (b) regenerative amplifier (RGA) and (c) an optical pulse compressor The regenerative amplifier

(RGA) system employs conventional chirped pulse amplification (CPA) technique for the amplification. Figure 2.4 shows the diagrammatic representation of CPA technique employed in the fs amplifier [3].

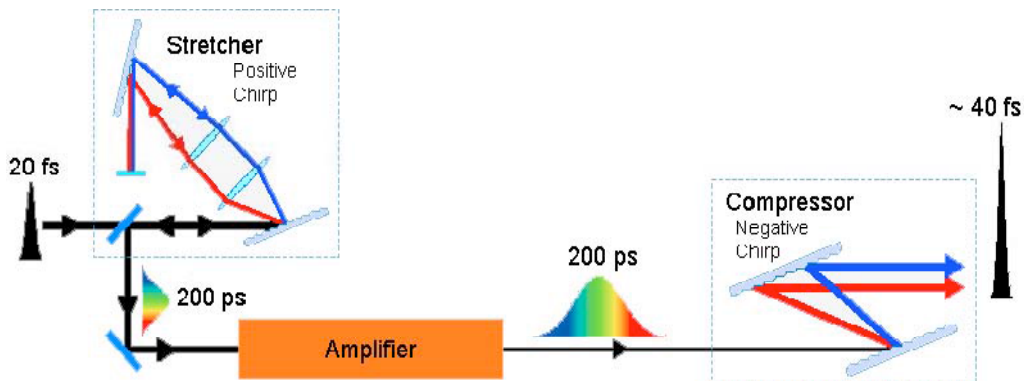


Figure 2.4 Diagram of chirped pulse amplification in the Legend regenerative amplifier [3]

In the amplifier the seed pulses are first stretched to about 200 ps in a diffraction-grating stretcher to reduce nonlinear effects and avoid damage to the optical elements in the amplifier and, at the same time, to allow efficient energy extraction from the amplifier. These temporally expanded pulses are trapped into a regenerative amplifier cavity and are amplified on each pass through the gain medium. Once the pulse saturates in gain and reaches the maximum energy, it is extracted from the amplifier and sent to the compressor to obtain amplified pulses of ~ 40fs of 2.5mJ maximum energy at a repetition rate of 1 KHz. The output of the Ti: sapphire amplifier (Legend) is of 15mm beam diameter with a spectral bandwidth of ~23 fs at 800nm central wavelength is shown in the figure 2.5

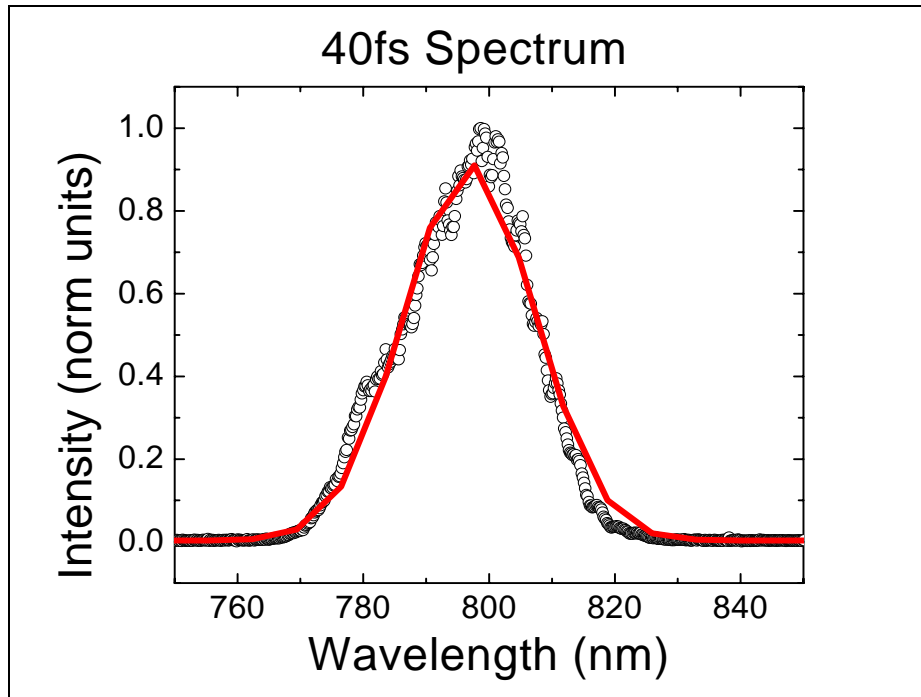


Figure 2.5 Output spectrum of Ti: sapphire amplifier [Legend]

Table 2.1 summarises the general and most important characteristics of the fs laser system used throughout the studies in the thesis.

Table 2.1 Summary of the laser output characteristics of the fs laser system used

	Femtosecond Oscillator (MICRA)	Femtosecond Amplifier (LEGEND)
Central wavelength	800nm	800nm
Pulse width	15fs	40fs
Average power	1Watt	2.5Watt
Pulse Energy	1nJ	2.5mJ
Rep.Rate	80MHz	1KHz
Polarization	Horizontal	Horizontal

2.2. Pulse Measurement

2.2.1. Introduction

The characterisation of ultrashort pulses has always been a challenge and for many years it was possible to create them but not to measure them. A full characterisation is needed to fully determine the experimental conditions before the pulses are used for experiments. Measurements can be made to find the energy (or power), shape, duration and spectrum of the pulse. Characterising ultrashort laser pulses has proved difficult, as the photo detectors used to detect longer pulses are not fast enough to use with ultrashort pulses. Moreover, these detectors, which are wavelength sensitive, respond to intensity which is proportional to $|E^2|$ and while measuring intensity the phase information is lost.

To measure a pulse, it is sufficient to measure the intensity and phase of the pulse either in time or frequency domain. The electric field of a pulse can be specified as a function dependent on time or dependent on spatial position and a product of the two functions can give the whole spatiotemporal profile of the electric field of a pulse [3]. However, a pulse produced from Kerr lens mode-locking show signs of significant coupling of both spatial and temporal properties (it has a time-dependent beam radius), making a complete pulse characterisation very tricky.

Although the pulse energy can be measured directly or calculated from the average power and repetition rate, and the pulse power can be found using a photodiode, a complete pulse characterisation in one step is much more beneficial. A complete characterisation will reveal the variation of the electric field with time or the complex spectrum, which includes the spectral shape and phase.

The problems addressed in the thesis use ultrashort laser pulses with very high peak intensities. The shorter the pulse, the more difficult it is to handle due to the accumulation of phase distortions. Due to the dispersion effects, the short pulses lose their shapes when they pass through the optical components so that they are temporally dilated when they reach the sample under investigation. Accurate measurement and spectral phase correction of amplified femtosecond pulses are crucial to achieve the highest peak intensities, and delivery of amplified arbitrary phase-shaped intense pulses is critical for reproducible laser control applications. Unfortunately, pulse shaping of amplified pulses results in losses ($> 50\%$) and the possibility of damaging the pulse shaper optics. These problems can be avoided by placing an external pulse shaper capable of performing Multi photon Intrapulse Interference Phase Scan (MIIPS) [5-7] in between the oscillator and regenerative amplifier.

2.2.2. Pulse Shaper System

The pulse shaper used in this dissertation uses a device (SILHOUTTE from Coherent), that employs MIIPS technology for measuring and manipulating the ultrashort pulses. The pulse shaper box consists of a zero dispersion pulse stretcher (4f-set up) [9], a liquid crystal spatial light modulator(SLM) as well as a spectrometer. This is fiber coupled to the sampling head that primarily consists of a thin doubling crystal that enables the broad band phase matching. The spectrometer is connected to a laptop and using the installed software, the system automatically measures the spectrum, controls the SLM and gives an output of the pulse data. Figure 2.6 shows the schematic sketch of MIIPS components.

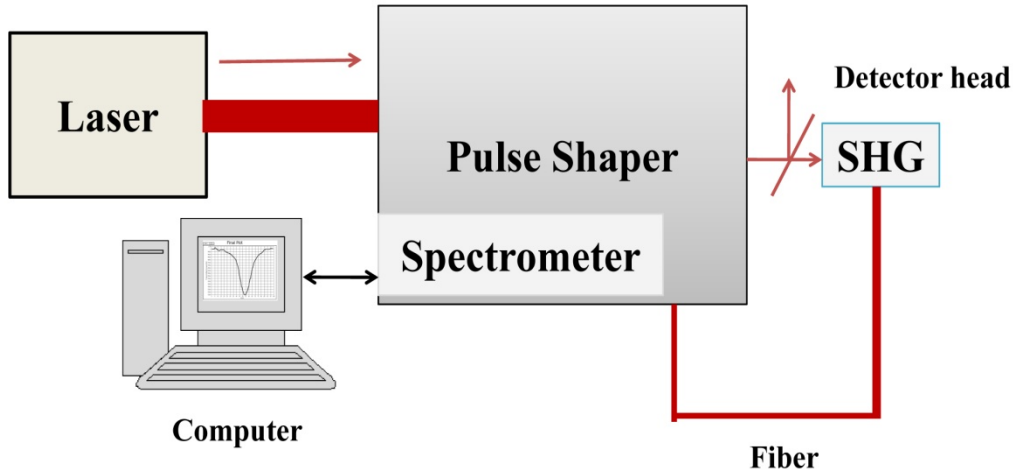


Figure 2.6. MIIPS Components

The pulse in the frequency domain is modulated by spectrally resolving the pulse such that its constituent spectral components are spatially separated. In order to spatially resolve the spectral components, a so-called 'zero dispersion' or '4f' stretcher [9] is utilized (Figure 2.7). At this point, the input beam is linearly and spectrally resolved at the SLM by the first grating and lens combination. Then the components pass through the SLM. The SLM is controlled by a computer. After the SLM, the beam goes through an identical combination of optics to re-combine the components into the desired transform limited pulse [4]. So, in summary, the steps involved in the pulse shaper (Silhouette) design based on a spatial light modulator are:

1. Spatially separate (disperse) spectral components
2. Modulate them individually in phase and amplitude
3. Recombine the modulated spectral components to reconstruct the pulse in time domain

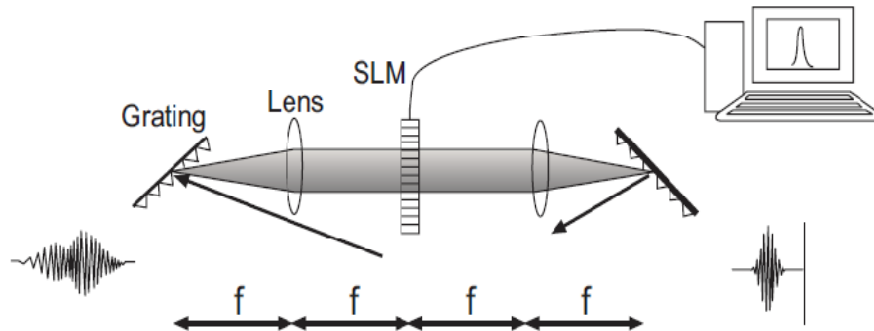


Figure 2.7 Schematic diagram showing the principle of zero dispersion (4-f configuration) pulse shaper (Image taken from the Coherent Silhouette manual)

2.2.3. Measurement and manipulation of the ultrashort pulse

The MIIPS method for femtosecond pulse characterization and dispersion correction is very different from all other methods commonly used. The MIIPS, measures the phase distortions in the frequency domain directly, without the need for time correlation. Because it is a single-beam method, MIIPS requires no interferometer and no overlapping beams. MIIPS measures the phase distortions in the pulses and cancels them through the use of an adaptive pulse shaper. The pulse shaper introduces a series of calibrated reference phase function to measure spectral phase distortions. The phase dependence of nonlinear optical processes such as second-harmonic generation (SHG) is used by the algorithm to directly measure the second derivative of the phase, without the need for inversion algorithms. As the reference phase is scanned across the pulse, the spectral phase deformation is obtained. The resulting MIIPS trace, which is a three dimensional plot of second harmonic intensity as a function of wavelength phase mask position, contains all the information required to analytically obtain the second derivative of the spectral phase distortions. Double integration of this results in the spectral phase. Once the spectral phase of the pulses is measured, the same pulse shaper is used to

introduce their complement to compensate the distortions to obtain transform limited pulses. A small number of iterations (usually 2-3) are required to obtain the pulse compression and this process lasts for a few seconds. When a sinusoidal reference phase function is used the MIIPS trace shows straight parallel lines separated by π for transform limited pulses [8]. Linear chirp changes the relative distance between these lines, quadratic chirp changes their angle, and higher order distortions lead to changes in their curvature [5]. MIIPS data obtained for femtosecond amplified pulses using the MIIPS technique and Silhouette (Coherent) is shown in figure 2.8.

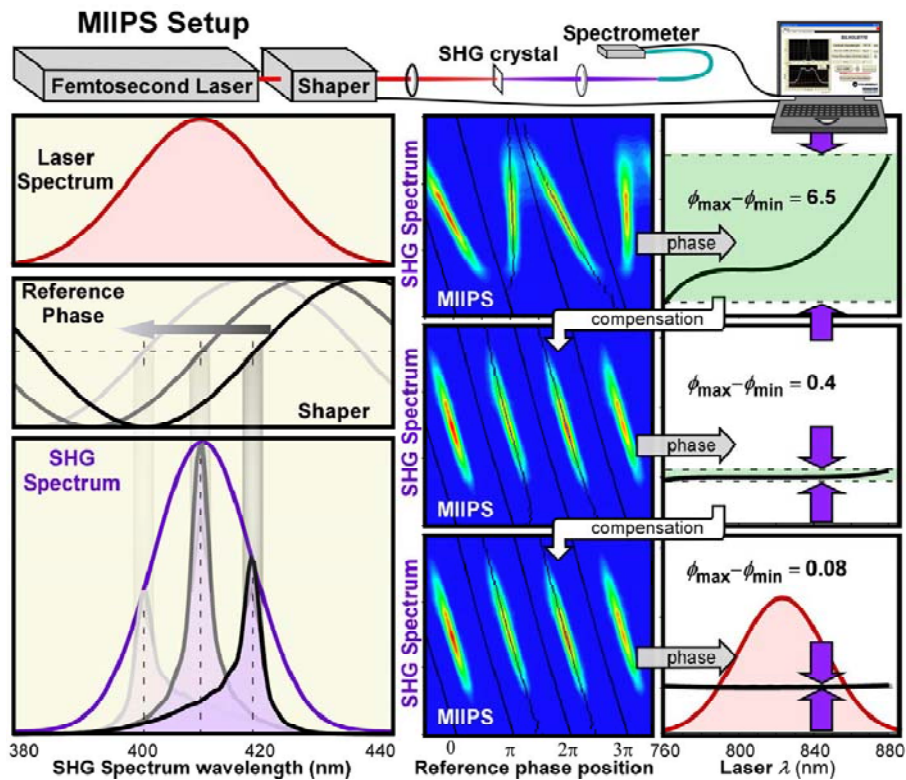


Figure 2.8. The heart of the MIIPS measurement is a programmable pulse shaper capable of introducing a well-calibrated phase function across the laser spectrum (top). The reference phase function (left) is one that causes a local correction to the second derivative of the phase. As it scans across the spectrum of the laser, the maximum intensity in the second-harmonic signal scans as well (shaded region). (Image courtesy: Biophotonics Solution)

References

- [1] Coherent operation manuals for *MICRA*, *EVOLUTION* and *LEGEND*
- [2] http://www.rp-photonics.com/saturation_power.html
- [3] www.ull.rdg.ac.uk/documents/ULL_Antoncini.pdf
- [4] *Coherent Operation manual for the pulse shaper SILHOUTTE.*
- [5] V.V. Lozovoy, I.Pastirk, M. Dantus, "Multiphoton intrapulse interference. 4. Characterization of the phas of ultrashort laser pulses," *Opt. Lett.* 29, 775-777 (2004).
- [6] M. Comstock, V.V. Lozovoy, I. Pastirk, M. Dantus, "Multiphoton intrapulse interference 6; binary Phase shaping," *Opt. Express* 12, 1061 - 1066 (2004).
- [7] B.Xu, J.M Gunn, J.M. Dela Cruz, V.V. Lozovoy, M. Dantus, "Quantitative investigation of the multiphoton intrapulse interference phase scan method for simultaneous phase measurement and compensation of femtosecond laser pulses," *J. Opt. Soc. Am. B* 23, 750-759 (2006).
- [8] I. Pastirk, Bojan Resan, Alan Fry and John MacKay, M. Dantus, "No loss spectral phase correction and arbitrary phase shaping of regeneratively amplified femtosecond pulses using MIIPS" *Optics Express*,14, 9537-9543, (2006).
- [9] A. M. Weiner, J. P. Heritage and E. M. Kirschner, "High Resolution femtosecond pulse shaping". *J. Opt. Sot. Am. B* 5, 1563-1572 (1988)

**PHYSICS OF FILAMENTATION AND
ASSOCIATED SUPER CONTINUUM
EMISSION (SCE)**

- 3.1. Introduction
- 3.2. Mechanisms leading to filamentation and associated Supercontinuum Emission (SCE)
- 3.3. Issues of filamentation addressed in this dissertation work
- 3.4. Conclusions

Abstract

In this chapter, the phenomenon of filamentation and associated Super continuum Emission (SCE) is introduced. The various nonlinear mechanisms such as optical Kerr effect, Self phase modulation (SPM), multiphoton ionosation (MPI) and plasma defocusing leading to filamentation and SCE are discussed in detail. The conical emission and the factors leading to this are also addressed

3.1 Introduction

The propagation of intense fs pulses in transparent condensed media or gases is characterized by strong modification of its spatial and temporal profile due to the dynamic interplay between the self-collapse of the laser pulse and the associated spectral broadening due to self-phase modulation (SPM) [1,2]. The spectral manifestation of the spatio-temporal modifications of focused laser beam in a medium results in a broad frequency sweep known as supercontinuum emission (SCE) extending, typically, from ultraviolet to the near infrared range. The SCE is manifested as a white light disk surrounded by a distinct, concentric, rainbow like pattern referred to as conical emission and the low divergence central part of the output beam is called “Supercontinuum” or “White-light – continuum”. Although the main mechanisms responsible for SCE is believed to be self-focusing followed by SPM, the evolution of SCE under different situations is not understood completely. Different mechanisms generate diverse components of the SCE/white light spectrum at certain positions along the propagation pathway of pulse [1]. Self-steepening, space time focusing, plasma generated by multi-photon ionization, four wave mixing are also believed to play a significant role [1]. Whenever an intense laser pulse propagates through a medium, it changes the refractive index, which in turn changes the phase, amplitude, and frequency of the incident laser pulse. A phase change can cause a frequency sweep within the pulse envelope. This process is called self-phase modulation (SPM) [3]. Self Phase modulation (SPM) enhances the SCE spectrum symmetrically to some extent till the plasma generation comes. The generated plasma induces ionisation and thus causes the depletion of the trailing edge of the pulse whereas the leading edge of the pulse remains unaffected. This creates a red shift in the spectrum of the pulse which can be explained by the occurrence of a steep leading edge of the pulse

temporal profile [4-6]. The repeated focusing and defocusing events favours multi peaked temporal profiles which spans the SCE spectra. Also, there exists a significant broadening of the angular spectrum dictated by the spatial variations of the pulse phase. These variations are responsible for conical emission (CE) [7-8] through which the beam diverges as a concentric rainbow with colours ranging from red to green.

The first study of the generation of Supercontinuum dates back to the years 1968 to 1972. Alfano and Shapiro first observed the “white” picoseconds continuum in solids and liquids and the observed spectra extended from ~ 6000 cm^{-1} in the visible to the infrared wavelength region [9]. Bondarnko et.al published similar results independently [9]. Supercontinuum generation (SCG) in gases was first investigated by Corkum et al [10] Gases are the ideal media to study the nonlinear phenomena such as Filamentation and associated Supercontinuum Emission (SCE). The low density of gases makes them the best material for this purpose[1]. The advent of Chirped pulse amplification[11] and Kerr-Lens mode locked laser cavities resulted in the phenomenon of atmospheric filamentation which was first demonstrated at the University of Michigan by Braun et al. in 1995 [12]. Braun et al. used a laser pulse with center wavelength 775 nm, duration 200 fs, and energy as high as 50 mJ in their experiment. This pulse was allowed to propagate in atmosphere over a distance 20 m. They found that pulses with energy greater than 2 mJ would slightly focus over that distance, and that pulses with energy greater than 5 mJ would collapse into a single or multiple high-intensity filaments after 10 m of propagation and then continue propagating at a filamentary diameter near ~ 100 microns over the next 10 m. Following this attempt, many research groups have studied the science and applications of ultrafast atmospheric filamentation [1].

3.2 Mechanisms leading to filamentation and associated Supercontinuum Emission (SCE)

3.2.1 Optical Kerr effect and Self-focusing in air

In the case of conventional (linear optics) optics, when light is propagated through an isotropic medium, the induced macroscopic polarisation P , depends linearly on the electric field strength E :

$$P = \varepsilon_0 \chi^{(1)} E \quad (3.1)$$

where $\chi^{(1)}$ is the first order susceptibility and ε_0 is the permittivity of free space. The resulting linear refractive index of the medium is

$$n_0 = \sqrt{1 + \chi^{(1)}} \quad (3.2)$$

But in the non linear optics the eqn (3.1) does not hold good indeed, the displacement of bound electrons in the atoms of the medium becomes so large that the resulting dipole moment and hence the macroscopic polarization, cannot be considered a linear function of the applied field. This is the optical Kerr effect. The nonlinear optical response can be mathematically expressed as a power series in the Electric field strength $E(t)$.

$$P = \varepsilon_0 E \left[\chi^{(1)} + \chi^{(2)} E + \chi^{(3)} E^2 \right] \quad (3.3)$$

The quantities $\chi^{(2)}$ and $\chi^{(3)}$ are known as the second- and third-order nonlinear optical susceptibilities, respectively. All the even orders susceptibilities $\chi^{(2)}$ vanish in centrosymmetric materials, such as gaseous media, and Eq.(3.3) can be rewritten as follows: The higher order susceptibility contribution remains negligible unless high intensities are at play.

$$P = \varepsilon_0 E [\chi^{(1)} + \chi^{(3)} E^2] \quad (3.4)$$

where the series has been truncated to the third order. The refractive index thus reads:

$$n = \sqrt{1 + \chi^{(1)} + \chi^{(3)} E^2} \approx n_0 + n_2 I \quad (3.5)$$

where the product EE is identified as $I = |E|^2$. Hence the refractive index of air n in the presence of an intense electromagnetic field depend on its frequency and the space and time dependent intensity $I(r, t)$ of the laser according to the equation (3.5). Therefore the strong electric field can locally modulate the refractive index of the medium by superimposing to the constant linear term n_0 , an additional term $n_2 I$ where n_2 is determined by the equation

$$n_2 = \frac{3\chi^{(3)}}{4\varepsilon_0 c n_0} \quad (3.6)$$

where c is the velocity of light, ε_0 denotes the permittivity of vacuum and $\chi^{(3)}$ the nonlinear susceptibility of the medium. In most of the non resonant optical materials, the non linear coefficient n_2 is usually positive, leading to an increase of the refractive index in the presence of intense radiation [1]. Figure 3.1 shows the principle of self-focusing when a collimated beam enters a $\chi^{(3)}$ medium. The spatial profile of a laser beam can be described by a Gaussian distribution, and according to the equation (3.5), n_2 reaches its maximum at the centre of the beam and rapidly decays towards the edges. Hence the total refractive index increases from the edges of the beam to its axis. As a result a plain wave front of the collimated beam bents with a focusing optics. Strictly speaking, the focusing gets even tighter as the pulse propagates because the intensity depends

on the square of the beam diameter. The beam itself, therefore, acts as a convex lens, constricting its own diameter during propagation and is called self focusing which is essential requirement for the filamentation regime.

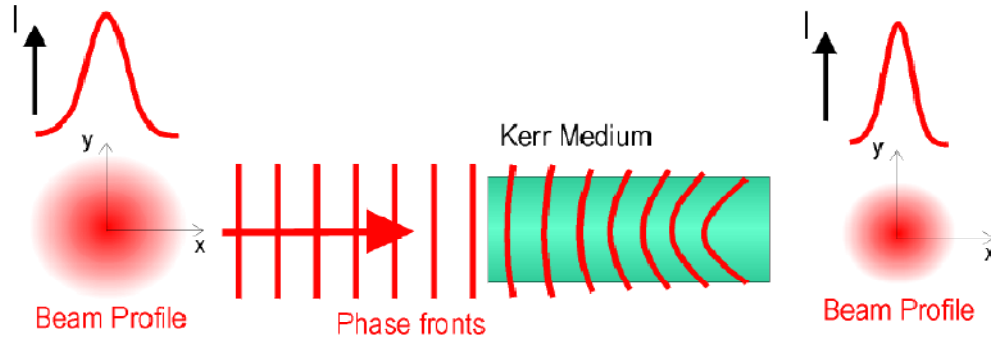


Figure 3.1 Schematic illustration of Self-focusing or Kerr lensing, due to the intensity dependent refractive index in a nonlinear optical medium.

Self-focusing is a threshold process. At low intensities, ie, in the linear regime diffraction the transverse spread of the beam occurs during the propagation a. As the intensity increases the self focusing sufficiently counteracts with the diffraction and finally overcomes it. A certain threshold power value named critical power P_{cr} was found by Marburger and was defined as the starting point from where a diffraction limited beam starts self-focusing [44]

$$P_{cr} = \frac{3.77\lambda^2}{8\pi n_0 n_2} \quad (3.7)$$

where λ_0 is the central wavelength, n_0 and n_2 are the linear and non linear refractive indices. It also defines the unstable equilibrium point that separate the linear diffractive regime from the catastrophic collapse of the beam.

If the peak power of a Gaussian laser beam is higher than the critical power P_{cr} , the beam undergoes self-focusing [13]. This is the so-called whole beam steady state Kerr self-focusing. For $\lambda_0 = 800$ nm, the critical power in air is $P_{cr} = 3$ GW. However during the propagation of powerful femtosecond lasers, it is not the whole beam self focusing, but the moving focus model ‘slice by slice’ self focusing takes place. In the moving focus model [14-16] the laser pulse is stacked into time slices that are considered to be independent of each other. Each time slice contains a specific power and all the central slices of a pulse with peak power above critical are self-focused at distances that become larger as the corresponding power is closer to critical value. The slices with power below P_{cr} diffract. It is easy to obtain a high peak power that can readily overcome the linear diffraction and GVD in the case of femtosecond laser pulses.

3.2.2 Self phase modulation

The influence of $\chi^{(3)}$ on powerful short pulses propagating in air does not limit to Kerr self-focusing. In the temporal domain, the pulse intensity is not constant (e.g. Gaussian) such that the intensity dependent index of refraction modulates the pulse phase $\varphi(t)$. Like in the spatial coordinates, the typical temporal profile of a laser pulse features a Gaussian-like intensity envelope. Therefore, the central slice will ‘see’ a higher refractive index and will be delayed with respect to its wings. This results in a spectral broadening of the pulse towards both red and blue sides and the phenomenon is called self-phase modulation. [3,17,18].

In the plane wave approximation, the plane wave front at the self-focus is given by the function

$$F(z, t) = \exp \left\{ i \left[\omega_0 t - kz \right] \right\} = \exp \left\{ i \left[\omega_0 t - \frac{\omega_0 n}{c} z \right] \right\} \quad (3.8)$$

where z is the propagation distance, and ω_0 is the central angular frequency of the laser.

The variation in the refractive index with laser intensity is given by,

$$n \approx n_0 + \Delta n(t) \quad (3.9)$$

where

$$\Delta n(t) = n_2 I(t) - \frac{4\pi e^2 N_e(t)}{2m_e \omega_0^2} \quad (3.10)$$

where, $n_2 I(t)$ is the Kerr nonlinear refractive index of the neutral gas, $I(t)$ being the intensity. The last term is the plasma contribution where $N_e(t)$ is the electron density generated through tunnel ionization of the molecules; e and m_e are the charge and mass of an electron, respectively. Since the electron –ion recombination time is of the order of many nanoseconds, which is pretty much higher than the femtosecond time scale, the generated plasma could be considered as static during the interaction with the pulse. The wave enters the optical medium at $(z=0, t=0)$. At the position z , equation (3.8) becomes

$$= \exp \left\{ i \left[\omega_0 t - \frac{\omega_0 n_0}{c} z - \frac{\omega_0 \Delta n(t)}{c} z \right] \right\} \quad (3.11)$$

$$= \exp \left\{ i \left[\left(\omega_0 t - \frac{\omega_0 n_0}{c} z \right) + \int_0^t \frac{\partial}{\partial t} \left(-\frac{\omega_0 \Delta n(t)}{c} z \right) dt \right] \right\} \quad (3.12)$$

$$= \exp \left\{ i \left[\left(\omega_0 t - \frac{\omega_0 n_0}{c} z \right) + \int_0^t (\Delta \omega) dt \right] \right\} \quad (3.13)$$

where

$$\Delta\omega = \frac{\partial}{\partial t} \left(-\frac{\omega_0 \Delta n(t)}{c} z \right) = -\frac{\omega_0}{c} z \frac{\partial [\Delta n(t)]}{\partial t} \quad (3.14)$$

SPM is the modulation (variation) of the phase of the wave due to the self-

generated extra phase $-\frac{\omega_0 \Delta n(t)}{c} z$ (see Eq. (3.11)). It is manifested by the frequency shift $\Delta\omega$ of Eq. (3.13) and (3.14). Since the front part of the pulse always sees the neutral gas, from Eq. (3.14) and (3.10), without the plasma contribution,

$$\Delta\omega = -\frac{\omega_0 z}{c} \frac{\partial [\Delta n(t)]}{\partial t} = -\frac{\omega_0 z}{c} n_2 \frac{\partial I(\text{front part})}{\partial t} < 0 \quad (3.15)$$

The last inequality of Eq. (3.15) occurs because the front part of the pulse has a positive temporal slope for which the value ranges continuously between zero and a maximum value. Hence, the front part of the pulse contributes principally to red (Stokes) shift/ broadening. But the trailing part of the pulse should also see the neutral gas since the gas is only partially ionized. This would lead to a blue shift/broadening but it is masked by the strong blue shift/broadening due to SPM in the plasma together with eventual SPM, due to the very steep descent of the back part of the pulse (i.e. self-steepening). The contributions of the plasma term in Eq. (3.10) to frequency shift/broadening starts soon after the plasma is generated. The plasma interacts at the self-focal zone with the self-focusing slice of the pulse and with the slices coming from behind (i.e. from the back part of the pulse). Using Eq. (3.10) and (3.15), the frequency shift/broadening due to the plasma term is

$$\Delta\omega = + \frac{2\pi z e^2}{cm_e \omega_0} \frac{\partial N_e}{\partial t} \quad (3.16)$$

The electrons are generated through tunnel ionization of the air molecules. For simplicity, we can use the experimental results to empirically state that the effective tunnel ionization rate of oxygen (and nitrogen) molecules is proportional to the intensity raised to the power of m where m is the empirical slope of the experimental ion yield vs. intensity curve in the log-log scale [19]. Thus the electron density can be expressed as

$$N_e \cong N_0 w \int_{-\infty}^t I^m(t) dt \quad (3.17)$$

In Eq. (3.17), N_0 is the density of the neutral air, w is the effective empirical tunnel ionization rate of oxygen (and nitrogen) and I^m is the empirical power law of ionization. Substituting Eq. (3.17) into Eq. (3.16), we obtain

$$\Delta\omega = + \frac{2\pi z e^2 N_0 w}{cm_e \omega_0} I^m \quad (3.18)$$

This positive blue shift/broadening of the frequency is large partially because of the highly nonlinear dependence on the high intensity inside the self-focal region. Besides SPM, towards the end of propagation; i.e. towards the end of the diffraction length given by ka^2 , (k and a are the wave number and the radius of the beam profile at $1/e^2$ level of intensity, respectively), the back part of the intensity distribution of the pulse becomes very steep and the slope is negative. This temporal variation happens mostly in the neutral gas because it is at the end of filamentation where ionization is negligible. It would give rise to a large blue shift of the frequency given by equation (3.15).

$$\Delta\omega = -\frac{\omega_0 z}{c} n_2 \frac{\partial I(\text{very steep back part with negative slope})}{\partial t} \quad (3.19)$$

This is a major source of the large broadening towards the blue side of the pump frequency and it is induced by the Kerr nonlinearity. This so-called self-steepening in the case of the propagation of a powerful femtosecond pulse is the consequence of a continuous spatio-temporal self transformation process of the pulse during propagation. This can be qualitatively understood as follows. The central part of the pulse with the highest intensity would propagate with a velocity $\frac{c}{n}$ where $n = n_0 + \Delta n_{\text{kerr}} + \Delta n_p$, where n is the total index of refraction, $n_0, \Delta n_{\text{kerr}}, \Delta n_p$, are the indices of refraction of the neutral air, the non linear Kerr index and the index of plasma respectively. The peak of the pulse sees an increase of the index of refraction due to the nonlinear contribution (Kerr nonlinear index) which is proportional to the intensity. Its velocity is thus slowed down. The back part of the pulse has a lower intensity and sees weak plasma. The index of refraction in plasma is less than unity. Hence, the back part of the pulse would propagate faster than the peak of the pulse. Soon the back part would almost catch up with the peak resulting in a steep rise in intensity at the back part. SPM is proportional to the derivative of this part of the pulse; hence, a very large blue shift will occur according to Eq. (3.19). SPM therefore yields a broadening of the initial spectrum of the laser pulse, a phenomenon commonly known as whitelight generation (WL) or supercontinuum generation.

The propagation distance z also plays a role in both the red and blue broadening (see Eq. (3.15) and (3.18)). Thus, during experimental observations, the spectral broadening of the pulse develops progressively as the propagation distance increases. Theoretically, the Maxwell's equations are first transformed

to a nonlinear wave equation and the latter is solved numerically. By taking the Fourier transform of the electric field associated with the deformed pulse during the propagation, the spectral content of the pulse is obtained.

Both experiment and numerical simulation shows similar broadening [20-21]. A strong broadening in air towards the red up to 4 microns was recently reported [22]. The central part of the pattern of Fig. 3.2b is an example of such a frequency broadening from the pump 800nm towards the blue side across the whole visible frequency range; hence, it appears white. This is what we call by the self transformed white light laser pulse.

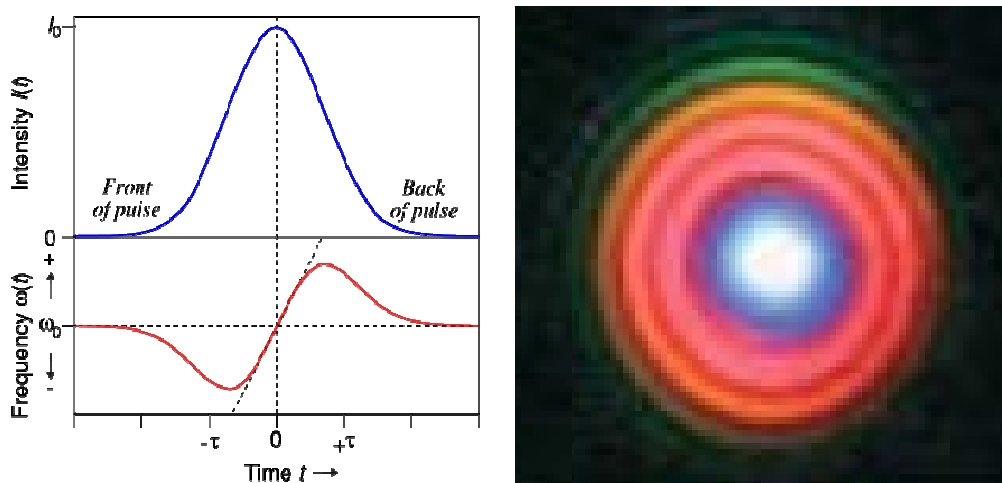


Figure 3.2(a) Schematic of Self phase modulation (b) single filamentation

3.2.3 Multi-photon ionization and plasma defocusing

The high laser intensities that are the necessary starting point for the filamentation are initiated by the self focusing collapse of the incident optical pulse within the medium. Such collapse has to be accompanied by a mechanism like multi photon ionisation (MPI) that arrests an intensity catastrophe within the medium. Due to the availability of high-power lasers emitting in this spectral region, the filamentation regime is generally investigated in the near-

infrared, at 800 nm. At this wavelength, the ionization potential of major air constituents (oxygen and nitrogen) largely exceeds the energy borne by a single photon. Indeed, the simultaneous absorption of 8 photons is required for the ionization of oxygen, which features the lowest ionization barrier. This process is highly improbable at low intensities, that is, before self-focusing. Thus the beam propagates lossless conveying the whole beam power towards the onset of filamentation. However, when the beam approaches collapse, the pulse intensity increases enormously and ionization becomes possible. Ionization takes place abruptly since its probability strongly depends on the light intensity. At the optical intensities typically featured by the filament core, i.e. 50 TW/cm², Multi-photon ionization (MPI) dominates over the tunnel ionization, which becomes relevant above 10¹⁴ W/cm², according to the Keldysh theory [23]. The enormously increased intensity at the self focusing zone will become sufficient to partially tunnel ionize the air molecules, resulting in the generation of weak plasma. The generated plasma creates a negative refractive index according to the relation $\Delta n = \rho / 2\rho_c$, where ρ is the generated plasma density and $\rho_c = \frac{\epsilon_0 m_e \omega_0^2}{e^2}$ is the critical plasma density above which the plasma becomes opaque (m_e and e are the electron mass and charge, ω_0 the pulse frequency, and $\rho_c \sim 1.7 \times 10^{21}$ cm⁻³ at 800 nm). Therefore, the negative index variation induced by the free electrons provides a mechanism which counteracts the third-order Kerr -self-focusing, as it is depicted in Fig3.3. Indeed, the refractive index spatial profiles induces an opposite curvature of the wave front, resulting in a negative lens which would be sufficient to de-focus the focusing slice back to the main body of the pulse or background reservoir.[17]. As it defocuses, the intensity decreases and, consequently, no more plasma is formed.

The highest intensity that this self-focusing slice would reach is thus limited due to the balance between self-focusing in the neutral and self-defocusing in the self-generated weak plasma. It is a constant that depends on the material property; i.e., it depends on how easy or difficult it is to generate free electrons in the self focal zone. Thus the defocusing nature of the plasma limits and stabilizes the light intensity in each of the filament. Thus, filamentation is the result of dynamical balance between the two effects: Kerr focusing and Plasma defocusing. Since the energy loss in ionization is very small, the pulse could repeat the whole process again and leads to several beam refocusing cycles that maintains the filament size approximately constant over several Rayleigh distances. The filament has a diameter of 100-200 μm and keeps an almost fixed energy (few mJ) and intensity ($50 \text{ TW}/\text{cm}^2$) [24-25] in this phenomenon known as intensity clamping. In air, for 800 nm laser pulses, the clamped intensity is of the order of $5 \times 10^{13} \text{ W}/\text{cm}^2$ [22,27-28]

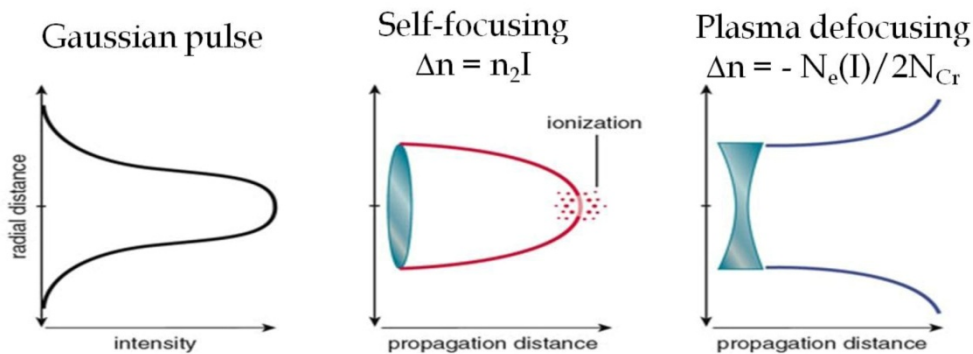


Figure 3.3 First figure shows a Gaussian Pulse. Second figure shows self-focusing of a beam by optical Kerr effect. The refractive index of the medium depends on the intensity of the laser and acts as a lens by making convergent an initially collimated beam. Self-focusing prevails over diffraction when the power of the beam exceeds a critical power P_{cr} ($P_{cr} = 3\text{GW}$ for air at the wavelength of 800 nm) and leads, in the absence of other nonlinear effects, to the collapse of the beam on itself. Third figure shows defocusing of the beam by the presence of a plasma. The ionization of the medium initially takes place in the center of the beam, where the intensity is most significant. The creation of an under-dense plasma decreases the local index of the medium, which causes beam defocusing.

3.2.4 Conical Emission (CE)

The filament regime is enriched by peculiar phenomena such as pulse splitting, self-steepening, shock formation, supercontinuum generation, and conical emission (CE)[29-30]. Conical emission is a visually spectacular effect associated with filamentation [7,31]. The conical emission which is considered as a signature of filamentation creates a wide variety of coloured rings around the beam in the forward direction, for which peak wavelength decreases from infrared to ultraviolet with increasing distance from the propagation axis. The radial order of the spectral components is inverse of diffraction with bluer frequencies appearing on the outside rings. Thus the spectrum of the pulse is transformed not only in the frequency domain but also in the domain of the spatial wave numbers. In media with normal group velocity dispersion (GVD), no matter if of solid, liquid, or gaseous nature, CE accompanies filamentation, producing radiation at angles that increase with detuning from the carrier frequency [7,30]. The mechanism at the root of conical emission is still debated. It may imply Cerenkov radiation [7,32] self-phase modulation (SPM) [8], four-wave mixing (FWM)[33-34] or X-Waves modelling [30,35-36].

All the different interpretations of the conical emission present a different facet of the problem and should combine into a unified description. Luther et al[34] explained that the minimal model which is proposed to demonstrate the arrest of collapse by normal GVD leading to pulse splitting induces a four wave interaction that promotes a transport of energy from the band of wave trains (k, ω) to sidebands $(k + k_{\perp}, \omega + \omega_{\perp})$ closely related to those of the modulational instability of the uniform plane-wave solutions [38-39].

The balance of linear diffraction and dispersion results in the cancelling of signal and idler terms given by the equation

$$k_{\perp}^2 = k k' \omega^2 \quad (3.20)$$

where ω here denotes the frequency detuning from the central frequency. As a result, the phase matching for maximum stability rate is occurred. The appearance of frequency-shifted off-axis radiation in the far-field of the pulse which appears as a colored ring is the consequence of the growth of these new spectral features. Thus, this four-wave mixing process was shown to be responsible for the pulse splitting due to GVD and to induce a spatio-temporal dynamics resulting in conical emission. According to Golub [32], the phase matching conditions of the four wave mixing process $2k(\omega) = k_{blue} + k_{red}$ predict an inverse spatial order of the emitted photons in the observed conical emission. Golub,[32] interpreted conical emission using Cherenkov type process. In this case, the polarization generated by the filament in the medium, propagating at the laser pulse group velocity v_{gr} , results in an emission at frequencies fulfilling a Cherenkov condition at conical angle θ given by $\cos \theta = \frac{v_{ph}}{v_{gr}}$, where $v_{ph} = \frac{c}{n(\omega)}$ is the phase velocity of the emitted light.

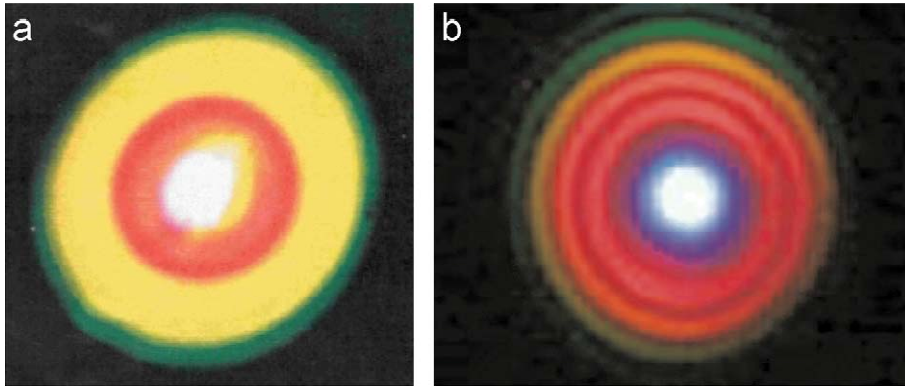


Figure 3.4 Conical emission accompanying a self-guided pulse. (a) A central white core (the filament) is surrounded by Newton's rings having a divergence of the order of the mrad (Nibbering et al., 1996). (b) Conical emission measured at 25m from a 5 mJ, 45 fs, 800 nm pulse (Chin, 2004). [taken from Couairon-Physics reports 441]

The dispersive properties of the medium select each Fourier component of the nonlinear polarization to emit at a specific angle. In fact, a similarity exist between the condition for Cherenkov emission by a source moving along the interface between the plasma channel and the gas and the refraction laws of light at this boundary. This is the origin of the proposition of a leaky waveguide by Nibbering et al.[7] to explain simultaneously the self-guiding and the conical emission phenomena associated with filamentation. Finally, the phenomenon of conical emission was revisited and reinterpreted using the paradigm of X-waves. The claim of the connection between conical emission and Nonlinear X-waves was proposed for the first time by Contiet al.[39]. The angular dispersion of colored conical emission associated with filamentation was measured for different media (water, lithium-triborate and air) by Faccio et al [40]. The chromatic dispersion of the material was shown to play a key role in the determination of the cone angle of CE that follows Eq(3.20). These measurements are in complete agreement with the interpretation of CE as a manifestation of the spontaneous generation of nonlinear X-waves [39,41-42]. In addition, this interpretation supported by the results of numerical simulations [35,43] , was shown to be consistent with the interpretation in terms of Cherenkov like process, i. e. leading to the same prediction for the frequency dependence of the cone angle [40].

3.3 Issues on Filamentation addressed in this dissertation work

- Very few studies exist on the propagation of ultrashort pulses in tight focusing condition. In this thesis we address the issue of filamentation and associated SCE under tight focusing geometry.
- Earlier attempts in the field of filamentation in air revealed that there is a limit to the spectral extent of the attainable SCE with a high-

frequency cutoff irrespective of the pulse energy. In a loose focusing geometry, the highest intensity in a filament is clamped by nonlinear effects including multiphoton absorption and plasma defocusing and this intensity clamping was shown to limit the plasma enhanced self phase modulation, resulting in a constant frequency upshift of the SCE of an ultrashort pulse undergoing filamentation when the pulse energy is increased [22,45]. Strategies to overcome this will be of great scientific importance.

- We have performed an analysis of the filament characteristics such as filament length, width, intensity under different input power, polarization and external focusing condition to understand the effect of laser parameters on filamentation under loose & tight focusing regimes completely. We have also made attempt to control the number, pattern and emission from the filaments in this dissertation.

3.4 Conclusions

- The temporal, spatial, and spectral properties of an ultrashort pulse experience modification when it propagates through nonlinear media resulting in the generation of a spectrally broad white light termed as Supercontinuum Emission (SCE).
- Filamentation and associated SCE is a consequence of the interplay of several dynamical processes such as self-focusing, group velocity dispersion, Self-steepening, space time focusing, plasma generated by multi-photon ionization, intensity clamping, anti- Stokes spectral broadening, filament fusion, filament breakup and competition between multiple filaments

References

- [1] Couairon and A. Mysyrowicz, "Femtosecond filamentation in transparent media", *Phys. Rep.* 441, 47-189, (2007).
- [2] R.W. Boyd, S.G. Lukishova, and Y.R. Shen, Eds. "Self-focusing: Past and Present: Fundamentals and Prospects" Chapter 1, Springer Science+Business Media, Inc., New York, USA, (2009).
- [3] R.R. Alfano, "The Supercontinuum Laser Source", Chapter 2, Springer-Verlag, Berlin (1989)
- [4] A. Couairon, S. Tzortzakis, L. Bergé, M. Franco, B. Prade, and A. Mysyrowicz, "Infrared femtosecond light filaments in air: simulations and experiments" *J. Opt. Soc. Am. B* 19, 1117-1131 (2002),
- [5] Th. Lehner and N. Aubry, "Stabilization of the Kerr effect by self induced ionization: Formation of optical light spatially localized structures" *Phys. Rev. E* 61, 1996-2005 (2000),.
- [6] G. P. Agrawal, *Nonlinear Fiber Optics*, 3rd ed. (Academic, New York, 2001), pp. 274
- [7] E. T. J. Nibbering, P. F. Curley, G. Grillon, B. S. Prade, M. A. Franco, F. Salin, and A. Mysyrowicz, "Conical emission from self-guided femtosecond pulses in air" *Opt. Lett.* 21, 62-64 (1996),
- [8] O. Kosareva, V. P. Kandidov, A. Brodeur, C. Y. Chien, and S.L. Chin, "Conical emission from laser-plasma interactions in the filamentation of powerful ultrashort laser pulses in air" *Opt. Lett.* 22, 1332-1334 (1997)
- [9] N.G. Bondarenko, I. V. Eremina and V.I. Talanov, "Broadening of spectrum in self-focusing of light in crystals," *Pis'ma Zh. Eksp. Teor. Fiz.* 12, 125-128 (1970), [*JETP Lett.* 12, 85-87, (1970)].
- [10] P. B. Corkum, C. Rolland, and T. Srinivasanrao, "Supercontinuum Generation in gases" *Phys. Rev. Lett.* 57, 2268-2272 (1986).

- [11] D. Strickland and G. Mourou, “Compression of amplified chirped optical pulses, *Optics Communications* “56, 219 -221(1985).
- [12] A. Braun, G. Korn, X. Liu, D. Du, J. Squier, and G. Mourou, Self-channeling of high- peak-power femtosecond laser pulses in air, *Optics Letters* 20, 73-75 (1995).
- [13] E. L. Dawes and J. H. Marburger. “Computer studies in self-focusing. *Physical Review*”, 179:862-868, (1969).
- [14] Lugovoi, V.N., Prokhorov, A.M.,” A possible explanation of the small-scale self-focusing filaments.” *JETP Lett.* 7, 117–119(1968).
- [15] Shen,Y.R., “The Principles of Nonlinear Optics.” Wiley-Interscience, New York (1984)
- [16] Brodeur, A., Chien, C.Y., Ilkov, F.A., Chin, S.L., Kosareva, O.G., Kandidov, V.P., “Moving focus in the propagation of ultrashort laser pulses in air.” *Opt. Lett.* 22 ,304–306,(1997)
- [17] A. Brodeur and S. L. Chin. “Ultrafast white-light continuum generation and self- focusing in transparent condensed media”. *J. Opt. Soc. Am. B*, 16,637-650, (1999)
- [18] X. Xie, J. Dai, and X.-C. Zhang. “Coherent control of THz wave generation in ambient air.” *Phys. Rev.Lett*, 96, 075005-07005-4, (2006).
- [19] A. Talebpour, J. Yang and S. L. Chin,” Semi-empirical model for the rate of tunnel ionization of N_2 and O_2 molecule in an intense Ti: sapphire laser pulse” *Opt. Commun.* 163, 29-32 (1999)
- [20] G. Méjean, J. Kasparian, J. Yu, S. Frey, E. Salmon, R. Ackermann, J.P. Wolf, Supercontinuum generated by femtosecond pulse filamentation in air: Meter-range experiments versus numerical simulations," *Appl. Phys. B* 82, 341-345 (2006)

- [21] L. Bergé, S. Skupin, G. Méjean, J. Kasparian, J. Yu, S. Frey, E. Salmon, and J.-P. Wolf, "Supercontinuum emission and enhanced self-guiding of infrared femtosecond filaments sustained by third-harmonic generation in air," *Phys. Rev. E.* 71, 016602-016602-13, (2005)
- [22] W. Liu, S. Petit, A. Becker, N. Aközbek, C. M. Bowden, S. L. Chin, "Intensity clamping of a femtosecond laser pulse in condensed matter" *Opt. Commun.* 202, 189-197 (2002).
- [23] V.P. Kandidov, O.G. Kosareva, I.S. Golubtsov, W. Liu, A. Becker, N. Akozbek, C.M. Bowden and S.L. Chin , "Self-transformation of a powerful femtosecond laser pulse into a white-light laser pulse in bulk optical media (or supercontinuum generation) *Appl. Phys. B* 77, 149-165 (2003).
- [24] N. Aközbek and C. M. Bowden and S. L. Chin, "Propagation dynamics of ultra-short high- power laser pulses in air: supercontinuum generation and transverse ring formation," *J. Mod. Opt.* 49, 475-486 (2002).
- [25] J. Kasparian, R. Sauerbrey, D. Mondelain, S. Niedermeier, J. Yu, J-P Wolf Y-B. André, M. Franco, B. Prade, S. Tzortzakis, A. Mysyrowicz, M. Rodriguez, H. Wille, L. Wöste "Infrared extension of the super continuum generated by femtosecond terawatt laser pulses propagating in the atmosphere," *Opt. Lett.* 25(18), 1397–1399 (2000).
- [26] L. Keldysh, "Ionization in the field of a strong electromagnetic wave," *Soviet Physics JETP*,. 20, 1307–1314, (1965).
- [27] J. Kasparian, R. Sauerbrey, and S. Chin, "The critical laser intensity of self-guided light filaments in air," *App. Phys. B*,. 71877–879, 2000.
- [28] A. Becker, N. Aközbek, K. Vijayalakshmi, E. Oral, C.M. Bowden and S.L. Chin, "Intensity clamping and re-focusing of intense femtosecond laser pulses in nitrogen molecular gas," *Appl. Phys B: Lasers Opt.* 73, 287–290 (2001).
- [29] A. Gaeta, "Collapsing light really shines" *Science* 301, 54-55 (2003).

- [30] Daniele Faccio, Miguel A. Porras, Audrius Dubietis, Francesca Bragheri, Arnaud Couairon, and Paolo Di Trapani” Conical Emission, Pulse Splitting, and X-Wave Parametric Amplification in Nonlinear Dynamics of Ultrashort Light Pulses PRL 96, 193901-193901-4, (2006)
- [31] O. G. Kosareva, V. P. Kandidov, A. Brodeur, and S. L. Chin, "Conical emission from laser plasma interactions in the filamentation of powerful ultrashort laser pulses in air," Opt. Lett. 22, 1332-1334 (1997).
- [32] I. Golub, "Optical characteristics of supercontinuum generation," Opt. Lett. 15, 305-307 (1990).
- [33] Q. Xing, K. M. Yoo, and R. R. Alfano, "Conical emission by four-photon parametric generation by using femtosecond laser pulses," Appl. Opt. 32, 2087-2089 (1993).
- [34] G. G. Luther, A. C. Newell, J. V. Moloney, and E. M. Wright, "Short-pulse conical emission and spectral broadening in normally dispersive media," Opt. Lett. 19, 789-791 (1994)
- [35] M. Kolesik, E. M. Wright, and J. V. Moloney, "Dynamic Nonlinear X Waves for Femtosecond Pulse Propagation in Water," Phys. Rev. Lett. 92, 253901-253901-4, (2004).
- [36] D. Faccio, A. Averchi, A. Lotti, P. Di Trapani, A. Couairon, D. Papazoglou, and S. Tzortzakis, "Ultrashort laser pulse filamentation from spontaneous XWave formation in air," Opt. Express 16, 1565-1570 (2008).
- [37] Liou, L.W., Cao, X.D., Kinstrie, C.J.M., Agrawal, G.P.,". Spatiotemporal instabilities in dispersive nonlinear media". Phys. Rev. A 62, 4202-4208, (2000)
- [38] Couairon, A., Berge, L." Modeling the filamentation of ultra-short pulses in ionizing media. Phys. Plasmas" 7, 193–209 (2000).
- [39] Conti, C., Trillo, S., Di Trapani, P., Valiulis, G., Piskarskas, A., Jedrkiewicz, O., Trull, J." Nonlinear electromagnetic X-waves". Phys. Rev. Lett. 90, 170406-170406-3, (2003)

- [40] Faccio, D., Porras, M.A., Dubietis, A., Tamošauskas, G., Kučinskas, E., Couairon, A., Di Trapani, “Angular and chromatic dispersion in Kerr-driven conical emission.” *Opt. Commun.* 265, 672-677,(2006).
- [41] Faccio, D., Di Trapani, P., Minardi, S., Bramati, A., Bragheri, F., Liberale, C., Degiorgio, V., Dubietis, A., Matijosius, A.,” Far-field spectral characterization of conical emission and filamentation in Kerr media.” *J. Opt. Soc. Am. B* 22 (4), 862–869, (2005).
- [42] Faccio, D., Matijosius, A., Dubietis, A., Piskarskas, R., Varanavičius, A., Gaižauskas, E., Piskarskas, A., Couairon, A., Di Trapani, P.,” Near and far-field evolution of laser pulse filaments in Kerr media.” *Phys. Rev. E* 72, 037601-037601-4,(2005).
- [43] Couairon, A., Gaižauskas, E., Faccio, D., Dubietis, A., Di Trapani, P.,”Nonlinear X-wave formation by femtosecond filamentation in Kerr media”. *Phys. Rev. E* 73, 016608-016608-13,(2006)
- [44] J.H. Marburger.” Self-focusing: Theory”. *Prog. Quant. Electr.*, 4:35-110, (1975).
- [45] A. Couairon, H. S. Chakraborty, and M. B. Gaarde, “From single-cycle self-compressed filaments to isolated attosecond pulses in noble gases,” *Phys. Rev. A* 77, 053814-053814-10, (2008).

CHARACTERISTICS OF TIGHTLY FOCUSED FEMTOSECOND LASER PULSES IN ATMOSPHERE

- 4.1. Introduction
- 4.2. Experimental technique
- 4.3. Results and discussion
- 4.4. Conclusions

Abstract

In this chapter, we present the experimental investigations of the filament characteristics of sharply focused fs pulses in air. The dynamics of filaments were observed via direct imaging of the entire reaction zone. The measurements of Supercontinuum Emission (SCE) generated by ultrashort Ti:sapphire laser and characteristics of filaments in air for different tight focusing geometries are presented here. The variations in the length and width of the filament for different focal geometry, input powers and polarization of the laser pulse is also addressed. The presence of coherently interacting multiple filaments either resulting in a fusion or exchange of power is also observed.

4.1. Introduction

From the initial observations of self-channelling of high-peak power femtosecond (fs) laser pulses in air by Braun et.al. [1], studies on the propagation of intense ultra-short laser pulses in different media has been one of the most exciting fields of nonlinear optics. The observation of long-distance self-guiding of ultrashort pulses in air has attracted considerable attention. The remarkable features of filamentation include Supercontinuum Emission (SCE) which spans from the visible spectral region to the infrared wavelengths. Filamentation studies traditionally start from letting a beam focus in air and it refers to a phenomenon by which self-focusing [2] of an intense pulse in air is followed by an extended region where the light remains concentrated in a diameter of the order of 100 μm . The region of propagation of femtosecond laser pulse in air can be classified into three such as preparation, filamentation and diffraction [3]. Nonlinear interaction between the pulse and the air in the preparation phase is supported by the theory of the moving focus model of Shen [4] in which the temporal intensity distribution of a large beam creates a moving focal point. But this interpretation can't successfully explained this phenomena as it predicts that only a small amount of energy can be found in a single filamentary mode. The second phase which is a stable filamentation region is the result of balance between two competing nonlinear effects: Kerr effect leading to self-focusing and defocusing effect of the electron plasma created by multiphoton ionization. The self-guiding model [5] explained this regime. The third region is used for observation of far field diffraction of the surviving optical beam and conical emissions [6,7]. All these theories and interpretations are based on one common concept of nonlinear interaction of light and matter, in a regime where light intensity is sufficiently high to ionize matter, and the matter is dense enough to affect the light [8]. Filamentation has

found many applications to detect hazardous molecules [9] LIDAR for atmospheric applications [10], HHG [11] generation of single cycle pulses, [12] Supercontinuum generation, [13] THz emission, [14] acoustic emission, [15] laser based propulsion [16] etc. amongst many others. We have also studied and presented the effect of tight focusing on the evolution of SCE from fs laser pulses propagating in air and the effect of polarization on SCE under tight focusing geometry. But the measurement of intensity inside the filament has been quite a challenge and is of importance for many applications. Though most of the efforts in estimating the filament intensity are based on theoretical modelling [17-18] few methods have successfully measured the filament intensity [19]. These methods rely on the spectroscopic emission from the excited states of the atoms of constituent medium. Though the filament intensity is observed to be clamped to a fixed intensity [20], recent work clearly demonstrated the presence of intensities of the order of 10^{14} W/cm². This exceeds the clamping value of a few 10^{13} W/cm² obtained for filamentation in a loose focusing geometry by at least one order of magnitude and has opened up interesting avenues [21-22].

However, the presence of multiple filaments and the interaction of the propagating filaments at higher input powers have made the measurements more challenging. In this chapter, we look at the multiple filament characteristics under different external focusing conditions making it possible to measure the filament diameter accurately.

4.2. Experimental technique

Figure 4.1 shows the experimental set up used for the study of characteristics of filaments formed in air. Transform limited linearly polarized laser pulses of 2mJ energy with duration of 40 fs, 800nm, with a repetition rate

of 1 KHz (Coherent-Legend UPS) were focused into air. The amplifier was seeded with 15 fs pulses from an oscillator (MICRA, Coherent, 1W average power, 80 MHz rep rate and 800 nm central wavelength). The pulse characteristics were measured using “Silhouette” (Coherent USA) based on the Mutiphoton Intrapulse Interefernce Phase Scan(MIIPS) technique. The input diameter ($1/e^2$) before the focusing element was 10 ± 0.1 mm. The self emission from the filament was captured using a calibrated digital camera. A set of neutral density filters (NDFs) were used in front of the camera to avoid the saturation of the image. An attenuator, combination of a half wave plate (HWP) and a Brewster polarizer(BP) was used to vary the input pulse energy into the medium.

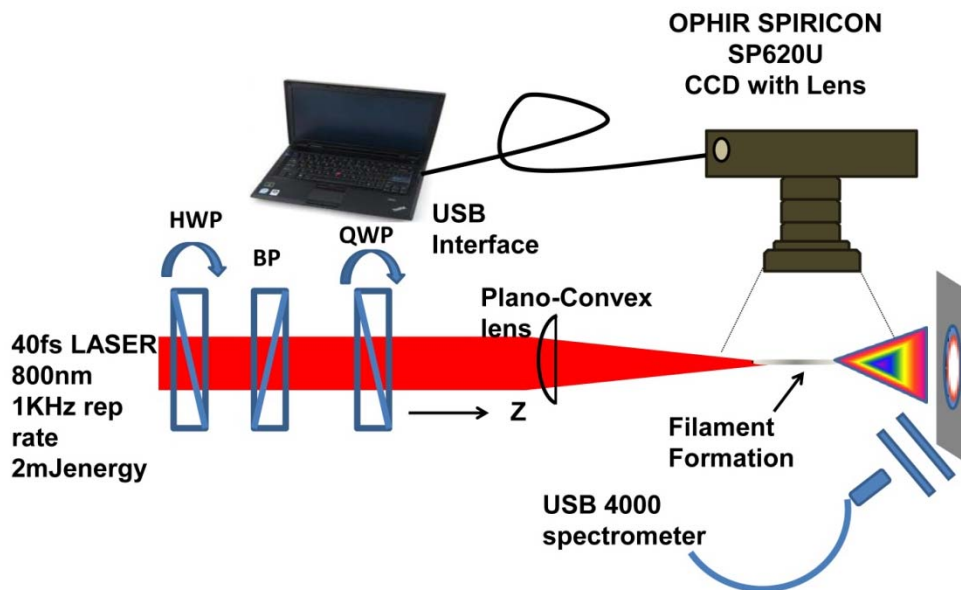


Figure 4.1: Experimental Schematic for measuring the characteristics of filaments formed in air

The sharply focused fs laser pulses were focused into air using plano convex lens of focal length 6, 15 and 20cm respectively. Inside the filament, because of self phase modulation and self steepening the 800 nm laser pulse self transforms into a chirped white light laser (Super continuum). The SCE

associated with filaments was scattered and collected using a fiber coupled spectrometer (USB 4000, Ocean Optics Spectrometer). A set of calibrated neutral density filters were placed in front of the spectrometer to avoid saturation of the CCD pixels.

To characterise the filaments we used different plano convex lens of focal lengths 10, 15 and 20 cm corresponding to numerical apertures (NA) of 0.05, 0.033 and 0.025, respectively. These plano convex lenses were used to focus fs pulses. The laser pulse power was varied between 0.5-1.8W corresponding to a peak power of 3-12.2 P_{Cr}. A Quarter Wave Plate (QWP) was placed in order to produce both Linearly Polarized (LP) and Circularly Polarized (CP) Light. The self-emission from filament was captured using a triggerable CCD camera (OPHIR SPIRICON SP620U). The images were captured under same experimental conditions for all the three different numerical apertures. CCD Camera was connected to laptop using an USB interface.

In house developed MATLAB Code was executed for extracting the length, width and intensity profile along the propagation axis of laser beam [I (z) vs z] and transverse directions [I(r) vs. r] from the captured self-emission images. The presence of multiple filamentation was observed by extracting and analyzing the transverse profiles [I (r) vs. r] at different positions (z₁, z₂, z₃...) along the propagation direction.

4.3. Results and discussions

4.3.1. SCE from air under tight focusing geometry-beyond intensity clamping

The critical power for self focusing can be calculated from the equation $P_{Cr} = 3.77\lambda^2/8\pi n_0 n_2$ where λ is the central wavelength, n_0 and n_2 are the linear

and nonlinear refractive indices, respectively. The P_{Cr} for air is calculated to be 3GW with a nonlinear index coefficient of $n_2 = 3.2 \times 10^{-19} \text{ cm}^2/\text{W}$ [18]. The SCE from tightly focused 40 fs laser pulses propagating in air have shown a central white disk surrounded by coloured rings. At a given input power, the SCE spectrum from both LP and CP pulses for the $f/6$ focusing geometry is more compared to $f/15$ and $f/20$ focusing geometries which indicates the conversion of laser energy to SCE spectrum is higher for tight focusing geometry compared to loose focusing geometries. A strong blue pedestal wing for the $f/6$ focusing geometry indicates stronger plasma enhanced self-phase modulation. As the polarization of the laser is changed from linear to circular the SCE intensity is considerably reduced for all focusing geometries as reported earlier [23-24].

Figures 4. 2(a) and 4.2.(b) show the variation of SCE with LP and CP pulses under $f/6$ and $f/15$ and $f/20$ focusing geometries. In comparison to linearly polarized (LP) light pulses, the onset of filamentation in the case of circular polarization (CP) is delayed due to the ratio of 1.5 on the critical power for self-focusing. This results in a difference in the nonlinear focus for LP and CP with the same input power. The ratio of 1.5 of the critical powers for self focusing with LP and CP pulses explains the reason for MPE being less efficient for CP pulses [17]. The blue edge of the SCE spectrum i.e., the minimum cutoff wavelength (λ_{min}) or maximum positive frequency shift (ω_{max}) as a function of the input laser power from the collected SCE spectra is found to decrease continuously with increasing input power for different focusing geometries. The λ_{min} is found to be blue shifted for tight focusing conditions compared to loose focusing geometry. A similar behaviour is observed in CP pulses also.

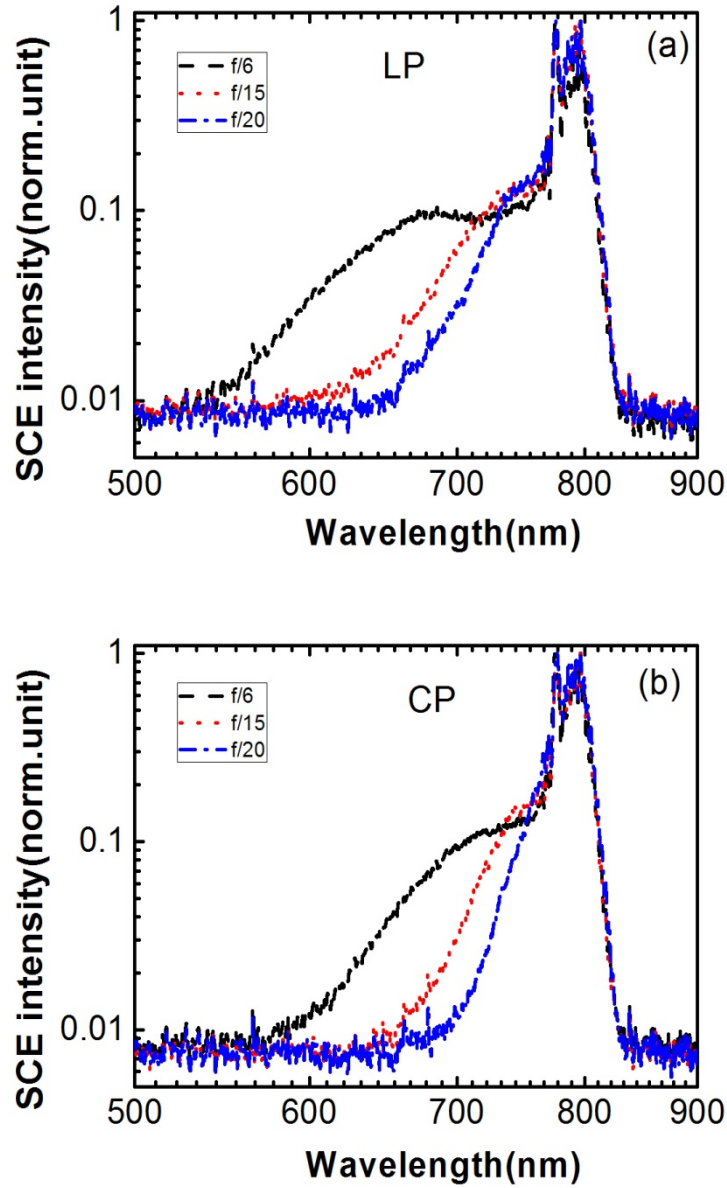


Figure 4.2(a): SCE spectra with LP pulses and Figure 4.2(b) SCE spectra with CP pulses obtained using f/6, f/15 and f/20 geometries at an input power of 1.8W

Figure 4.3 shows the variation of λ_{\min} for f/6, f/15 and f/20 focusing geometries for LP & CP pulses. In the tight focusing geometry, the initial high beam curvature, due to external focusing, leads to complete

ionization of the medium, which in turn prevents the plasma defocusing to play an important role in the intensity clamping [22]. In a loose focusing geometry, the highest intensity in a filament is clamped by nonlinear effects including multiphoton absorption and plasma defocusing [12,20]. A criterion characterizing intensity clamping was proposed by Liu et al. from measurements of the supercontinuum spectrum of an intense femtosecond laser pulse propagating in condensed optical media: intensity clamping was limited by plasma-enhanced self-phase-modulation, resulting in a constant frequency upshift bounding the supercontinuum spectrum of an ultrashort laser pulse undergoing filamentation when the pulse energy is increased [20]. Recent studies indicated that third harmonic generation within filamentation permit refocusing processes with intensity spikes exceeding the clamping value by a factor of three [25].

We have also estimated laser clamped intensity inside the filament using recent technique followed by Shengqi et. al. [19]. Though the filament intensity is observed to be clamped to a fixed value, recent work demonstrating the presence of intensities of the order of 10^{14} W/cm² has opened up interesting avenues [26]. The recent numerical and experimental studies in the tight focusing regime opens a new regime in which initial focusing plays the main role in the determination of the highest intensity during interaction with the gas. Intensities exceeding 10^{15} W/cm² were numerically demonstrated for large numerical apertures (NA > 0.1) [18]. Therefore, according to the criterion proposed by Liu et al. [20] which links intensity clamping to a constant cut off of SCE, we conclude that no intensity clamping was observed up to input powers of $15 P_{Cr}$ with a $f/6$, $f/15$ and $f/20$ focusing geometries, where the critical power for self-focusing $P_{Cr} = 3$ GW denotes a reference value calculated with the nonlinear index coefficient $n_2 = 3.2 \times 10^{-19}$ cm²/W [18].

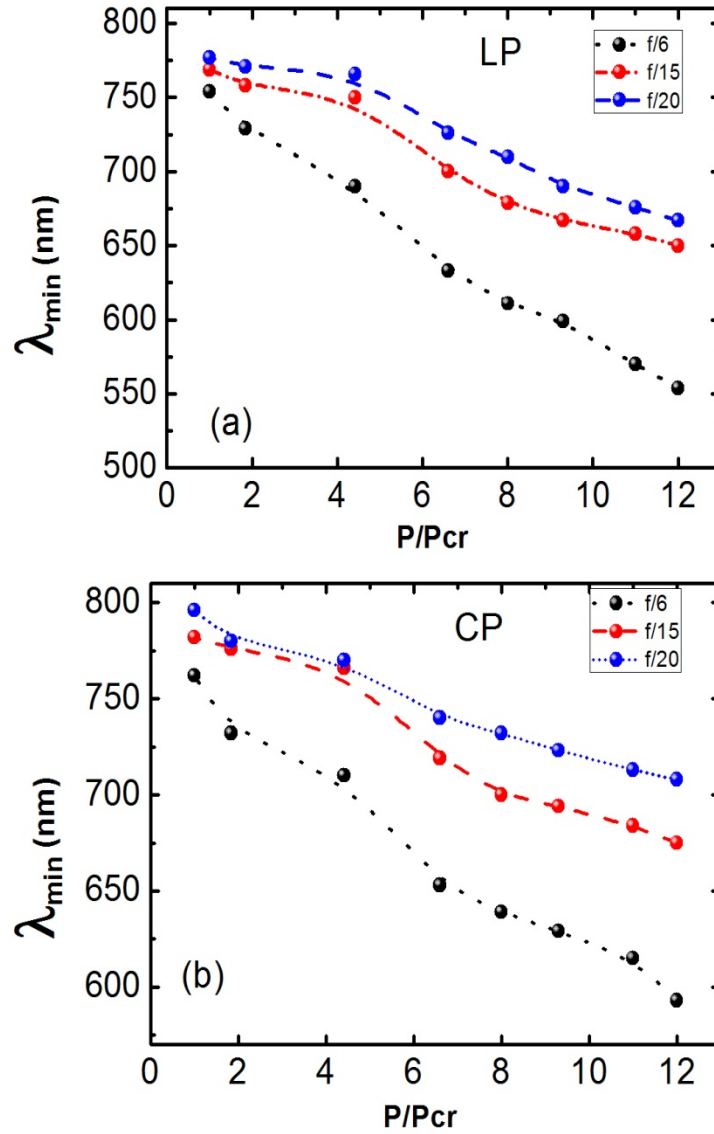


Figure 4.3: Variation of minimum wavelength (λ_{\min}) with P/P_{cr} for (a) LP pulses under $f/6$, $f/15$ and $f/20$ focusing geometries (b) CP pulses under $f/6$, $f/15$ and $f/20$ focusing geometries

4.3.2. Characteristics of filamentation

The investigation of the filamentation in air under different focusing geometries is of special interest due to the numerous potential application of it in different fields.

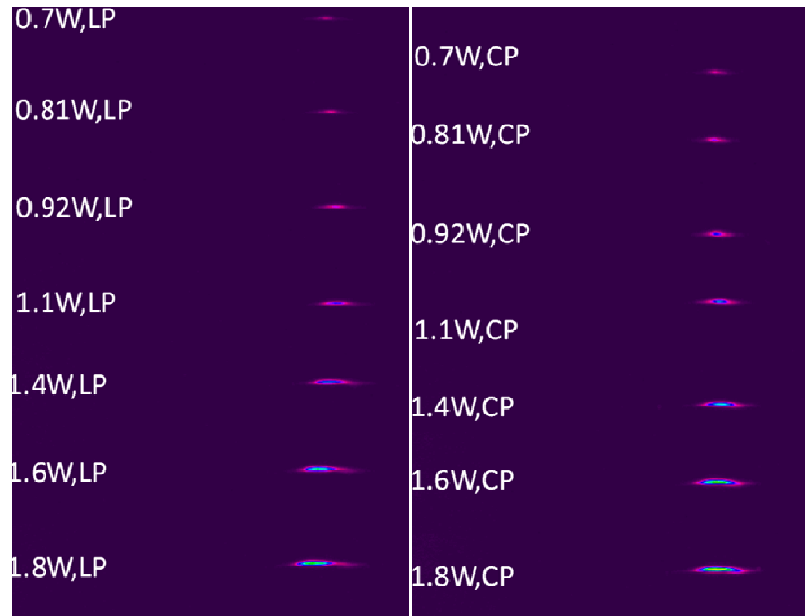


Figure 4.4(a): Self-emission from the filaments produced using $f/10$ for LP and CP pulses

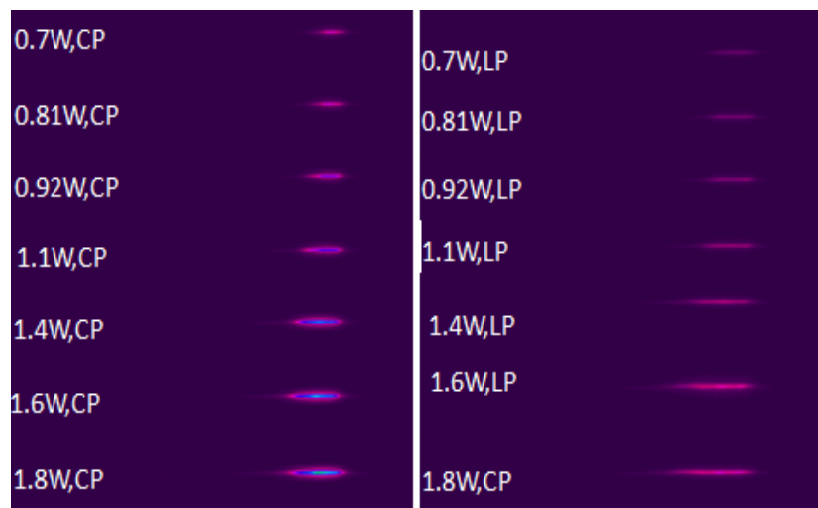


Figure 4.4(b): Self-emission from the filaments produced using $f/15$ for LP and CP pulses

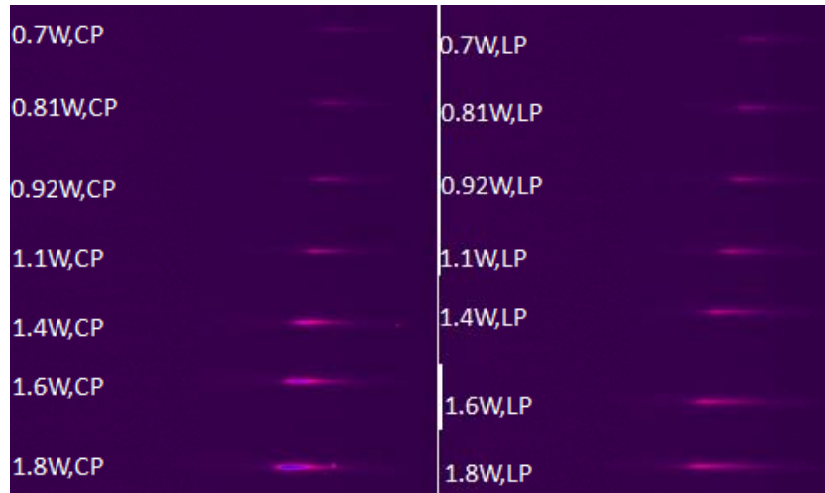


Figure 4.4(c): Self-emission from the filaments produced using f/20 for LP & CP pulses

The complete characterisation of the filaments was performed under f/10 (NA=0.05), f/15(NA=0.033) and f/20(0.025) respectively. Filaments were observed to propagate distances over few tens of Z_R , Z_R being Rayleigh length of the focused pulses in vacuum. The CCD captured images of the filaments give us more information as how the length, width and intensity change under different focal geometry and power. The pulse propagates from left to right. Figure 4.4 (a) to (c) show the self-emission from the filaments produced using f/10 (NA=0.05), f/15(NA=0.033) and f/20(0.025) for linearly and circularly polarized (CP) pulses at different input powers.

For a given NA and polarization of pulses, the length and intensity of self emission increased with increasing input power. For smaller NA, filamentation occurred before the geometrical focus while the intensity at the geometrical focus was low. In such cases filament length is the distance between transformed self focus and geometrical focus of the filament. For higher NA, the filament was more localized near the geometrical focus. A

similar behaviour was observed earlier [27]. The length of the filament was observed to be longer for LP pulses. In general the filament was observed to propagate over 2-5 Z_R . However, the width was observed to spread over 2-40 ω_0 ; ω_0 being the spot size of the laser beam at the focus in vacuum. The width of the filament also increases with increased input power for any given NA. But the intensity of self-emission is observed to be higher with CP pulses compared to LP pulses. These observations are in tune with the recent results reported in literature [19]. Filament length and width as a function of input powers and polarisation for different NA are shown in figures 4.5(a) to (h). Comparison of filament length as a function of power for different NA's confirm that with higher NA length was almost saturated for all input powers but in lower NA length increases with increase in power.

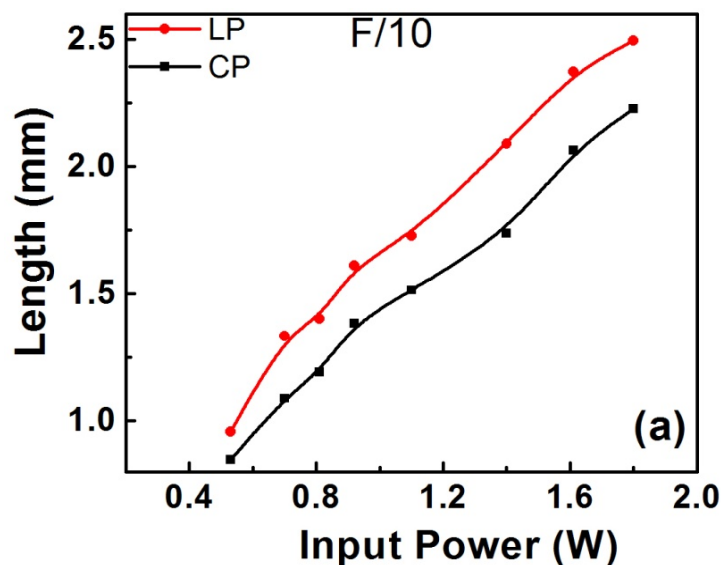


Figure 4.5(a): Comparison of Length for LP & CP pulses in f/10 focusing geometry

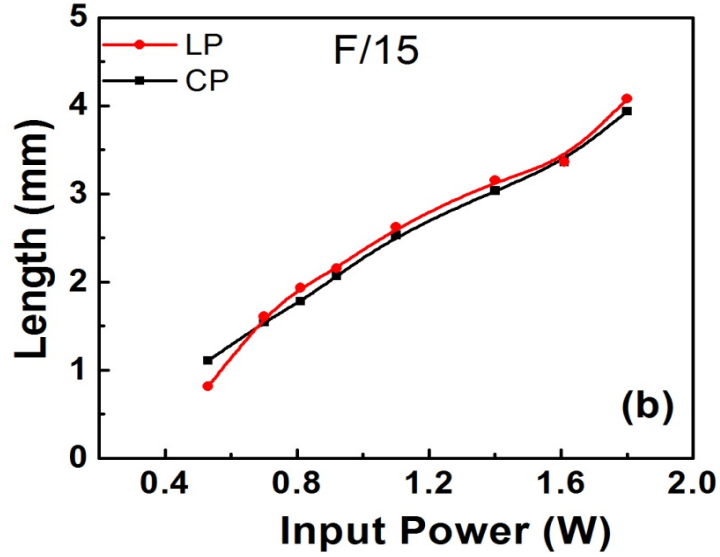


Figure 4.5(b): Comparison of Length for LP & CP pulses in f/15 focusing geometry

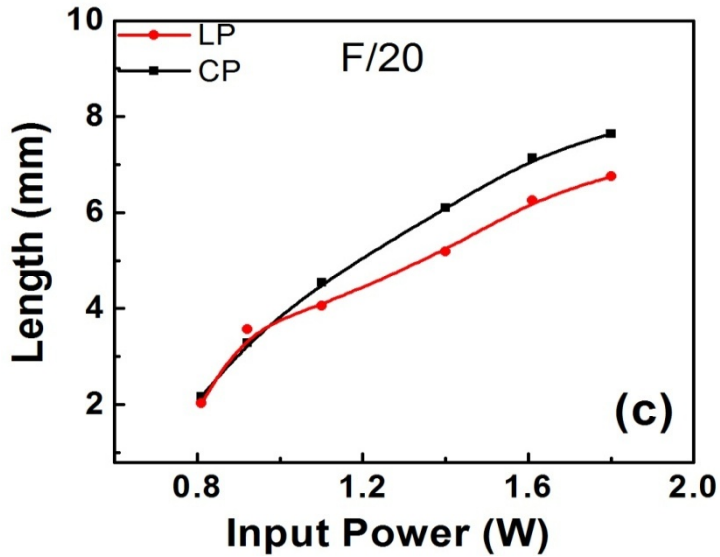


Figure 4.5(c): Comparison of Length for LP & CP pulses in f/20 focusing geometry

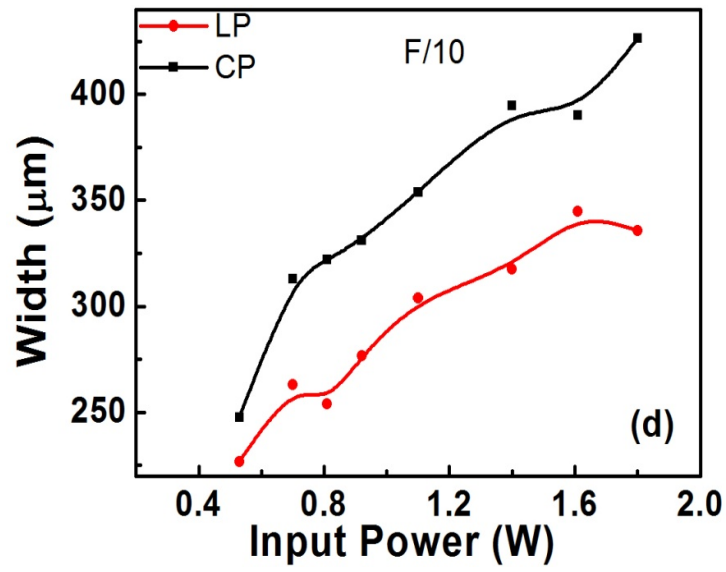


Figure 4.5(d): Comparison of width for LP &CP pulses in f/10 focusing geometry

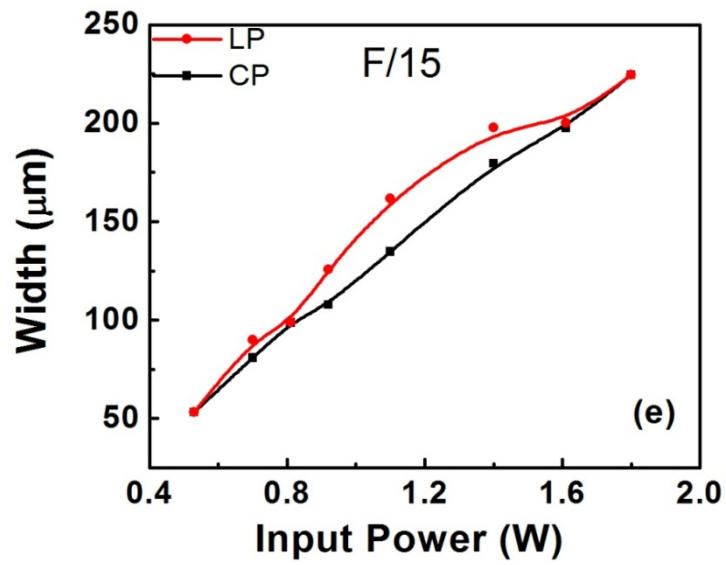


Figure 4.5(e): Comparison of width for LP &CP pulses in f/15 focusing geometry

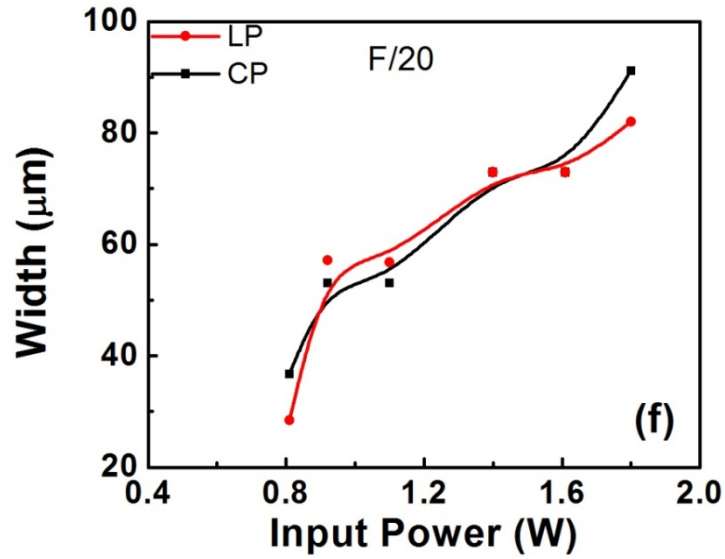


Figure 4.5(f): Comparison of width for LP & CP pulses in f/20 focusing geometry

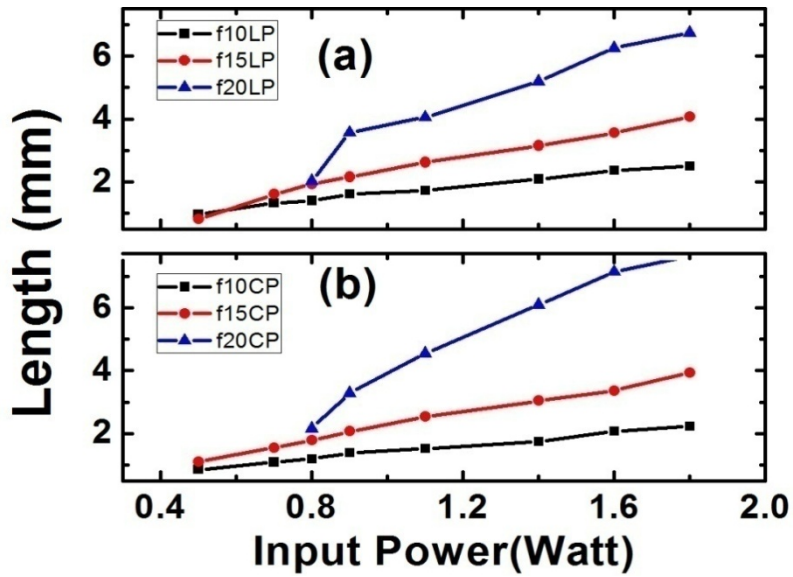


Figure 4.5 (g) Comparison of length for (a) LP and (b) CP pulses in different focusing geometry

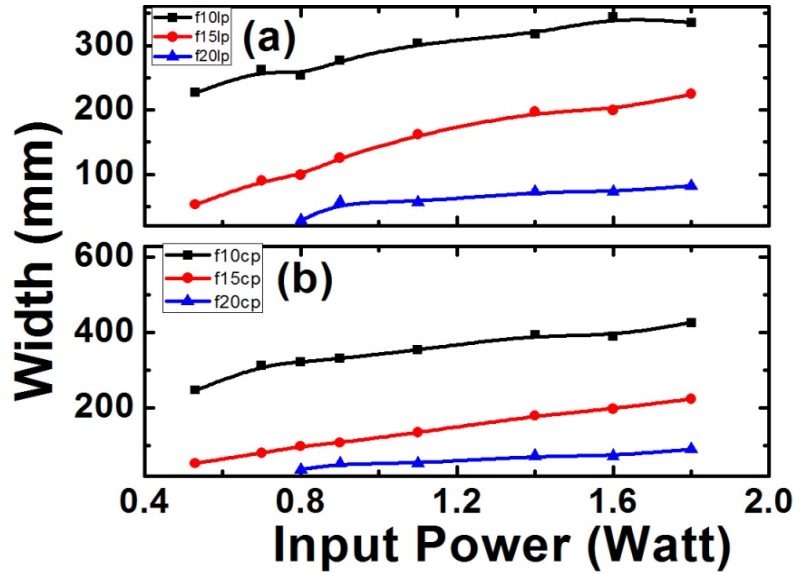


Figure 4.5 (h) Comparison of width for (a) LP and (b) CP pulses in different focusing geometry

The filament width was measured to be $\sim 40\text{-}200\ \mu\text{m}$ with NA's of 0.025, 0.033 and with these NA, multiple filaments were not observed. As the NA was increased to 0.05 the width increased to $250\text{-}440\ \mu\text{m}$. This indicates the presence of multiple filaments at higher NA (tighter focusing geometries) as observed by the self-emission. The filament diameter observed is in tune with the earlier measurements [18,29]. The filament width measured is used to estimate the intensity within the single filament following the methodology proposed by Shengqi et. al.[19]. From the transverse line profiles along a fixed Z the width of the self-emission d_{sf} is measured which in turn was used to estimate the width of the plasma filament d_{laser} (laser beam diameter). The intensity for $12.2\ P_{\text{Cr}}$, LP under NA 0.05 is calculated to be $3.8 \times 10^{12}\ \text{W}/\text{cm}^2$. However the appearance of multiple filaments makes these measurements more challenging.

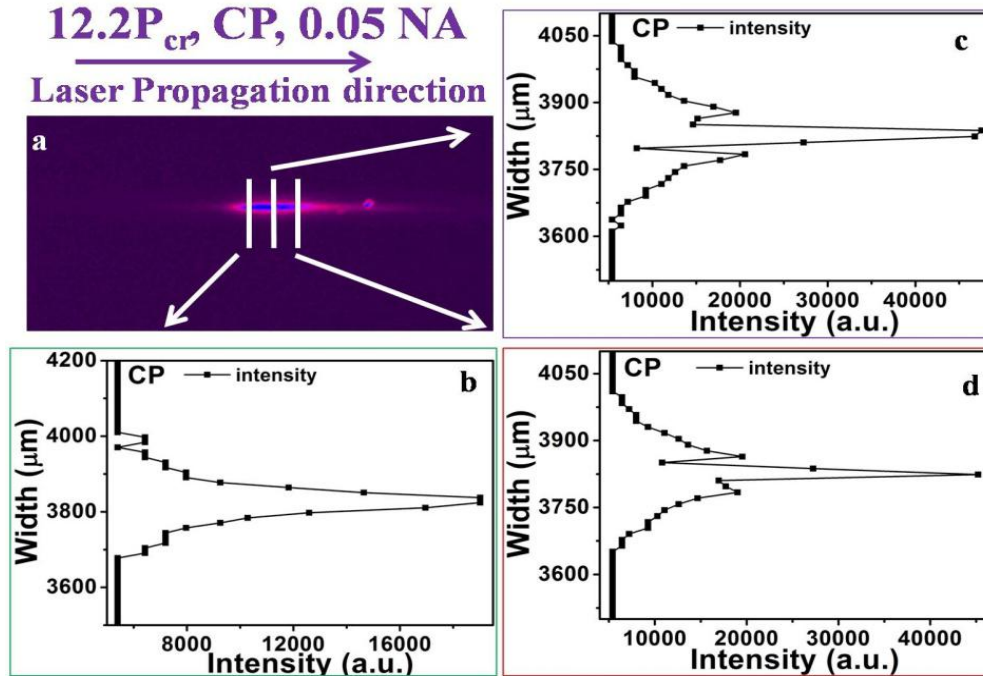


Figure 4.6: Filamentation image for 12.2 P_{Cr} for CP and line cut intensity profile at three different Z positions showing multiple filamentation.

Figure 4.6 shows the filament observed at tighter focusing geometry (NA of 0.05) at an input peak power of 12.2 P_{Cr}. Multiple filamentation was observed only for NA 0.05 and maximum of 3 filaments have been observed with input power in the range of 6.2-12.2 P/P_{Cr} which can be clearly visible from the the vertical profile of the filaments. Comparison of the vertical profile of the filaments is shown in figure. The self-emission profiles at three different positions along the propagation direction clearly indicate the presence of multiple filaments and interaction between the propagating filaments around geometrical focus in cognizance with the phenomena observed with unfocused or loosely pre -focused fs pulses propagating in air [28]. From figure 4.6(b), at Z₁ position, filament was single and had a width of 69.4 μm. From figure 4.6(c), at Z₂ position, filament had been split into three having individual

widths of 91.7 μm , 21.8 μm and 73 μm . From figure 4.6(d), at Z_3 position, second and third filaments are almost in a stage of recombination and these three filaments had widths of 101.2 μm , 7.4 μm and 72.2 μm . The presence of breakup and fusion of multiple filaments along Z clearly indicates that the intensity is not constant throughout the propagation of filament at higher NA (tight focusing geometries).

With shorter focal lengths (higher NA) the presence of multiple filaments was observed only at higher input powers for circular polarization. Multiple filaments are well-known to grow randomly due to slightest noise in the beam intensity profile [17,30,31], modulational instability [32-33] over large range of input powers and vectorial effects [34]. Each of the multiple filament is known to take power of P_{Cr} and interact among themselves during propagation before coalescing into a single filament making the measurement of filament intensity more challenging and erroneous.

4.4 Conclusions

- Filament characteristics resulting from the propagation of kHz repetition rate fs laser pulses were studied under different external focusing conditions. The effect of polarization of the input pulses on filamentation was also studied.
- For a given focusing geometry, the filament length and width increased with increasing input peak power; however, at higher NA, the length and width were observed to saturate.
- Breakup of a single filament into multiple filaments and fusion along the propagation direction was observed with higher NA of 0.05 for CP pulses.

- Filament intensity inside a single filament estimated from the self-emission was found to be of the order of 10^{12} W/cm². However, the same method may not be extended to estimate the filament intensity in the presence of multiple filaments, as the effects like break up and fusion of the propagating filaments indicate varying intensity along the direction of propagation.

References

- [1] Braun, A., Korn, G., Liu, X., Du, d., Squier, J. and Mourou, G., “Self-channeling of high-peak-power femtosecond laser pulses in air,” *Opt. Lett.* 20, 73-75 (1995)
- [2] G. A. Askar’yan, “Effects of gradients of a strong electromagnetic beam on electrons and atoms,” *Sov. Phys. JETP* 15, 1088–1090, (1962).
- [3] A. Dubietis and A. Piskarskas, R. Danielius, D. Mikalauskas “Self-Guided Intense Laser Pulse Propagation in Air”, *Nonlinear Analysis: Modelling and Control*, 6, 21-26,(2000).
- [4] A. Brodeur, C. Y. Chien, F. A. Ilkov, S. L. Chin, O. G. Kosareva, and V. P. Kandidov, "Moving focus in the propagation of ultrashort laser pulses in air", *Opt. Lett.* 22, 304-306 (1997).
- [5] H. R. Lange, G. Grillon, J. F. Ripoche, M. A. Franco, B. Lamouroux, B. S. Prade, A. Mysyrowicz, E. T. J. Nibbering, and A. Chiron, "Anomalous long-range propagation of femtosecond laser pulses through air: movingfocus or pulse self-guiding?", *Opt. Lett.* 23, 120-122 (1998).
- [6] D. Faccio, A. Averchi, A. Lotti, P. Di Trapani, A. Couairon, D. Papazoglou, and S. Tzortzakis, “Ultrashort laser pulse filamentation from spontaneous X-Wave formation in air,” *Opt. Express* 16, 1565–1570 (2008).
- [7] F. Th’eberge, M. Ch’ateaneuf, V. Ross, P. Mathieu, and J. Dubois, “Ultrabroadband conical emission generated from the ultraviolet up to the far-infrared during the optical filamentation in air,” *Opt. Lett.* 33, 2515–2517 (2008).
- [8] Ladan Arissian, Daniel Mirell, Sherminéh Rostami, Aaron Bernstein, Daniele Faccio, and Jean- Claude Diels, “The effect of propagation in air on the filament spectrum,” *Optics Express* 20,8337-8343(2012)
- [9] Me’jean, G., Kasparian, J., Yu, J., Frey, S., Salmon, E., and Wolf, J.-P., “Remote detection and identification of biological aerosols using a femtosecond terawatt lidar system”, *Appl. Phys. B* 78, 535-537 (2004).

- [10] Kasparian, J., Rodriguez, M., Me'jean, G., Yu, J., Salmon, E., Wille, H., Bourayou, R., Frey, S., André, Y.-B., Mysyrowicz, A., Sauerbrey, R., Wolf, J.-P., and Wöste, L., "White light filaments for atmospheric analysis," *Science*, 301, 61-64, (2003).
- [11] Suntsov, S., Abdollahpour, D., Papazoglou, D. G., and Tzortzakis, S., "Efficient third-harmonic generation through tailored IR femtosecond laser pulse filamentation in air," *Opt. Express* 17, 3190 -3195, (2009).
- [12] Couairon, A., Chakraborty, H.S., and Gaarde, M.B., "From single-cycle self-compressed filaments to isolated attosecond pulses in noble gases," *Phys. Rev. A* 77, 053814-053814-10, (2008).
- [13] Alfano R.R., "The Supercontinuum Laser Source: Fundamentals with Updated References, Springer Science + Business Media, Inc., New York, USA, (2006).
- [14] D'Amico, C., Houard, A., Akturk, S., Liu, Y., Le Bloas, J., Franco, M., Prade, B., Couairon, A, Tikhonchuk, V., T. and Mysyrowicz, A., "Forward THz radiation emission by femtosecond filamentation in gases: theory and experiment," *N. J. Phys.* 10, 013015,013015-18, (2008).
- [15] Yu, J., Mondelain, D., Kasparian, J., Salmon, E., Geffroy, S., Favre, C., Boutou, V., Wolf, J.-P., "Sonographic probing of laser filaments in air", *Appl. Opt.* 42, 7117–7120 (2003).
- [16] Zheng, Z.-Y., Zhang, J., Hao, Z.-Q., Zhang, Z., Chen, M., Lu, X., Wang, Z.-H., Wei, Z.-Y., "Paper airplane propelled by laser plasma channels generated by femtosecond laser pulses in air", *Opt. Express* 13, 10616-10621, (2005).
- [17] Couairon, A. and Mysyrowicz, A., "Femtosecond filamentation in transparent media," *Phys. Rep.* 441, 47-189 (2007).
- [18] Kiran, P. P., Bagchi, S., Krishnan, S., R., Arnold, C., L., Kumar, G., R. and Couairon, A., "Focal dynamics of multiple filaments: Microscopic Imaging and Reconstruction," *Phys. Rev. A* 82, 013805-013805-8, (2010).

- [19] Shengqi, X., Xiaodong, S., Zeng, B., Chu, W., Zhao, J., Liu, W., Cheng, Y., Zhizhan, X. and Chin, S., L., "Simple method of measuring laser peak intensity inside femtosecond laser filament in air," *Opt. Express* 20, 299-307 (2012).
- [20] Liu, W., Petit, S., Becker, A., Akozbek, N., Bowden, C., M. and Chin, S., L., "Intensity clamping of a femtosecond laser pulse in condensed matter," *Opt. Commun.* 202, 189-197 (2002).
- [21] Shengqi, X., Xiaodong, S., Zeng, B., Chu, W., Zhao, J., Liu, W., Cheng, Y., Zhizhan, X. And Chin, S., L., "Simple method of measuring laser peak intensity inside femtosecond laser filament in air," *Opt. Express* 20, 299-307 (2012).
- [22] Kiran, P. P., Bagchi, S., Krishnan, S., R., Arnold, C., L., Kumar, G., R. and Couairon, A., "Filamentation without intensity clamping," *Opt. Express.*, 18(20), 21504-21510 (2010).
- [23] C. Santhosh, A.K. Dharmadhikari, J.A. Dharmadhikari, K. Alti, D.Mathur,"Supercontinuum generation in macromolecular media" *Appl. Phys.B.* 99, 427-432 (2010).
- [24] S. Sandhu, S. Banerjee, D. Goswami," "Suppression of supercontinuum generation with circularly polarized light", *Opt. Comm.*181,101-107 (2000).
- [25] M. B. Gaarde and A. Couairon, "Intensity Spikes in Laser Filamentation: Diagnostics and Application,"*Phys. Rev. Lett.* 103, 043901 (2009)
- [26] H. S. Chakraborty, M. B. Gaarde, and A. Couairon, "Single attosecond pulses from high harmonics driven by self-compressed filaments," *Opt. Lett.* 31, 3662–3664 (2006).
- [27] Chin, S. L., [Femtosecond laser filamentation], *Springer Series on Atomic, Optical, and Plasma Physics*, 1st ed., 55 (2010).
- [28] Tzortzakis, S., Bergé, L., Couairon, A., Franco, M., Prade, B. and Mysyrowicz, A., "Breakup and Fusion of Self-Guided Femtosecond Light Pulses in Air", *Phys. Rev. Lett.* 86, 5470–5473 (2001).

- [29] La Fontaine, B., Vidal, F., Jiang, Z., Chien, C.Y., Comtois, D., Desparois, A., Johnston, T.W., Kieffer, J.-C., Pepin, H., “Filamentation of ultrashort pulse laser beams resulting from their propagation over long distances in air”, *Phys. Plasmas* 6, 1615-1621, (1999).
- [30] M'echain, G., Couairon, A., Franco, M., Prade, B. and Mysyrowicz, A., “Organizing multiple Femtosecond filamentation in air”, *Phys. Rev. Lett.* 93, 035003-035003-4, (2004).
- [31] Mlejnek, M., Kolesik, M., Moloney, J.V., Wright, E.M., “Optically turbulent femtosecond light guide in air”, *Phys. Rev. Lett.* 83, 2938–2941 (1999).
- [32] Vidal, F., Johnston, T.W., “Electromagnetic beam breakup: multiple filaments, single beam equilibria, and radiation”, *Phys. Rev. Lett.* 77, 1282–1285 (1996).
- [33] Fibich, G., Eisenmann, S., Ilan, B., Erlich, Y., Fraenkel, M., Henis, Z., Gaeta, A.L., Zigler, A., “Self-focusing distance of very high power laser pulses”, *Opt. Express* 13, 5897-5903, (2005).
- [34] Fibich, G. and Ilan, B., "Deterministic vectorial effects lead to multiple filamentation," *Opt. Lett.* 26, 840- 842(2001).

**EFFECT OF LENS TILT ON
SUPERCONTINUUM EMISSION AND
FILAMENTATION CHARACTERISTICS**

5.1	Introduction
5.2	Experiment
5.3	Results and Discussions
5.4	Conclusion

Abstract

The evolution of Supercontinuum Emission (SCE) associated with filaments and the characteristics of filaments due to the tilt of focusing lens under tight focusing geometries are presented in detail

5.1 Introduction

Intense ultra-short laser pulses are well suited for long range propagation in many transparent media. This long range filamentary propagation is due to the dynamic balance between nonlinear self focusing of an intense optical pulse and laser plasma induced defocusing¹. These long propagating filaments in air have received significant attention over the last decade due to impending applications in the fields of remote sensing^{2,3}, lightning guiding⁴⁻⁶, supercontinuum generation (SCG)⁷⁻⁹, pulse compression¹⁰ and THz generation.¹¹ During the propagation of filament the pulse undergoes temporal and spectral changes due to the linear and nonlinear effects within the medium such as self-phase modulation and Raman scattering amongst others^{1,12,13}. Filamentation of fs pulse comes into play when a high intense laser pulse having transverse power (P) greater than critical power for self-focusing (P_{Cr}), propagates through air. For very low powers, generally, a single filament is observed. As the power of the beam increases unavoidable spatial irregularity across the wave front would be induced either due to imperfection of the beam quality or due to propagation through a non-homogeneous medium in the real environment and the pulse exhibits splitting, multiple collapse, and repeated filamentation over large distances. This results in the breaking up of single filament into many, termed as multiple filamentation¹⁴⁻¹⁶. Understanding and controlling multiple filaments¹⁷⁻¹⁹ during the long range propagation of high power fs pulses has been a major challenge for various applications²⁰.

Lens tilting has been used for the control of filaments in managing multiple filaments over long distances^{17, 20}. It has been demonstrated that it is possible to control the number, pattern, and spatial stability of filaments by changing the tilt angle of the focusing lens¹⁹. Moreover, the effect of spherical

aberration on femtosecond filamentation has been reported²¹, where a single filament was observed to split into two along the propagation direction. However, to date attention has been mainly focused on the effect of lens tilting on the filament properties under a long focusing geometry. In this chapter, we present a systematic study of the tilting of focusing lens on filamentation characteristics and Supercontinuum emission (SCE) for both tight and loose focusing geometries.

5.2 Experimental Technique

Figure 5.1 shows the experimental set up used for the study. Transform limited linearly polarized pulses with duration of 40 fs, 800 nm, with a repetition rate of 1 kHz (Coherent; Legend-USP) were focused into air. The amplifier was seeded with ~15 fs pulses from an oscillator (MICRA, Coherent, 1W average power, 80 MHz repetition rate, and 800nm wavelength). The pulse characteristics were measured using ‘Silhouette’ (Coherent, USA) based on the Intrapulse Interference Phase Scan (MIIPS) technique. The input beam diameter ($1/e^2$) before the focusing element was 10 ± 0.01 mm. BK-7 lenses of focal length 60 mm, 75 mm, and 120 mm were used to attain the focal geometries of $f/6$, $f/7.5$ and $f/12$. The corresponding numerical apertures (NA) were 0.04, 0.06 and 0.08. The focusing lens was placed on a rotation stage with a precision of $1/60$ degree and was tilted from 0 to 20 degrees. The self-emission from the filament was captured using a calibrated digital camera. A set of neutral density filters (NDFs) were used in front of the camera to avoid the saturation of image. An attenuator, combination of a half wave plate (HWP) and a Brewster polarizer (BP) was used to vary the input pulse energy into the medium. Inside the filament, because of self phase modulation and self steepening, the 800nm laser pulse self transforms into a chirped white light

laser (Supercontinuum). The SCE associated with the filaments was scattered and collected using a fibre optic coupled spectrometer (USB 4000, Ocean Optics Spectrometer).

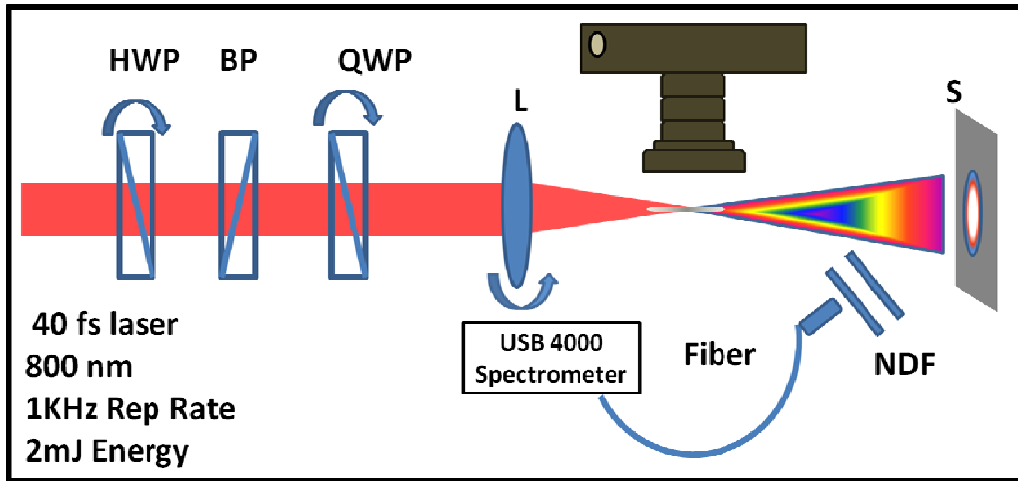


Figure 5.1: Experimental Schematic showing filament formation at the geometrical focus captured through CCD and SCE collected through fibre optic coupled spectrometer.

5.3 Results and Discussions

The critical power for self focusing can be calculated from the equation $P_{Cr} = 3.77\lambda^2/8\pi n_0 n_2$ where λ is the central wavelength, n_0 and n_2 are the linear and nonlinear refractive indices, respectively. The P_{Cr} for air is calculated to be 3GW with a nonlinear index coefficient of $n_2 = 3.2 \times 10^{-19} \text{ cm}^2/\text{W}$. The self-emission from the filaments was recorded for different tilt angles from 0 to 20 degrees for all the three focusing geometries. Figure 5.2 shows the evolution of the filaments with the tilt of focusing lens in $f/12$ geometry. In all these focusing geometries ($f/6$, $f/7.5$, $f/12$) only one filament was observed when the lens was tilted from 0° up to 8° . At a tilt angle of 8° , the single filament was observed to break up into two shorter filaments along the propagation direction, with the filament towards the focusing lens having weak intensity looking

almost like a comet. Beyond a rotation of 8° , the separation between the filaments was observed to increase continuously with increasing tilt of the lens. For all the angles greater than 8° , the intensity of the filament towards the focusing lens is smaller compared to that of the farther filament. This is attributed to the astigmatism coming into play because of the lens tilt²¹.

The separation between the filaments can be estimated from the formula^{21,22}

$$X = f \sin \varphi \tan \varphi \quad (5.1)$$

where f and φ are the focal length and the tilting angle of the lens.



Figure 5.2: Filaments for different tilt angles under f/12 focusing geometry.

Figures 5.3(a) to 5.3(c) show measured separation between the filaments and the calculated separation using equation 5.1. All of these matched very well for longer focusing geometry of f/12 in our measurements in tune with the earlier reports²¹. However at tighter focusing geometry of f/6, the mismatch between the estimated and the observed separation increases as we move to larger tilt angles.

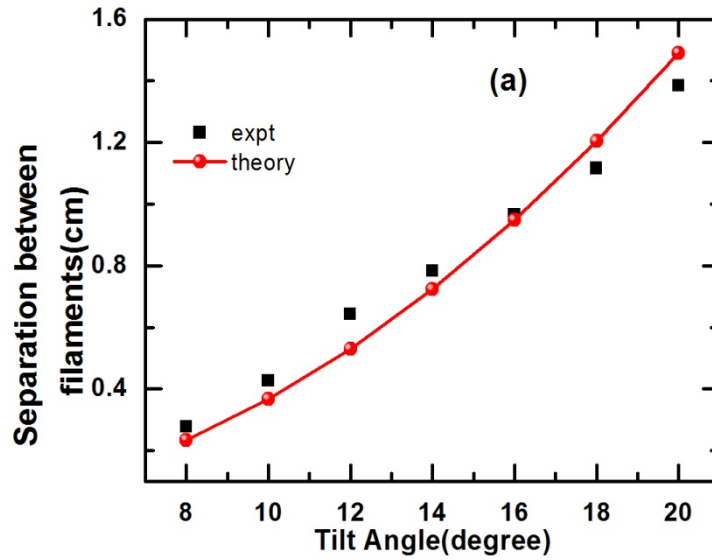


Figure 5.3(a): Comparison of experimentally measured separation between the filaments and the estimated values for different tilt angles under f/6 focusing geometry

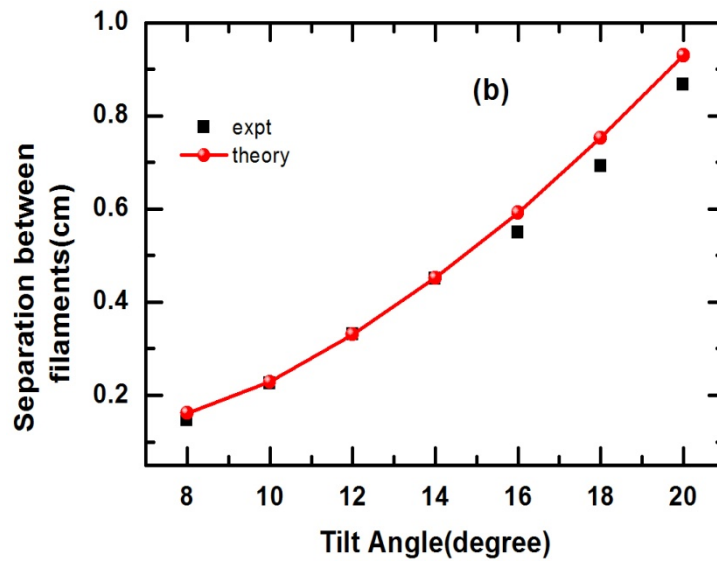


Figure 5.3(b): Comparison of experimentally measured separation between the filaments and the estimated values for different tilt angles under f/7.5 focusing geometry

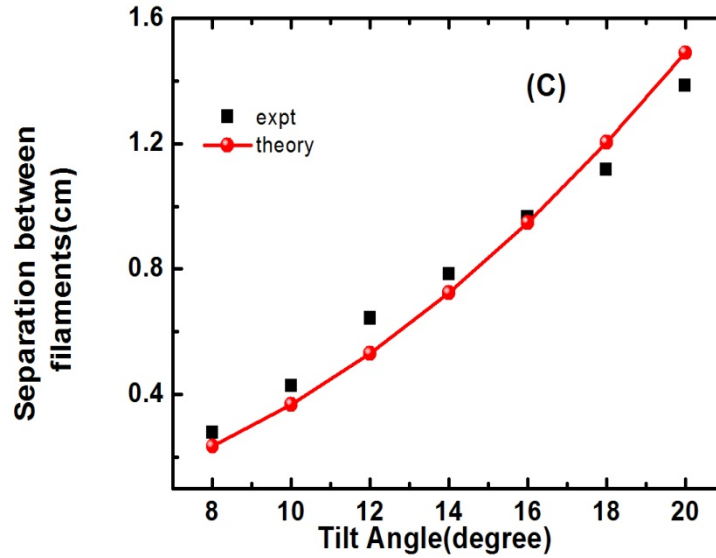


Figure 5.3(c): Comparison of experimentally measured separation between the filaments and the estimated values for different tilt angles under f/12 focusing geometry

At any given lens tilt, the separation between the filaments increased linearly with decreasing NA. At a tilt of 16° the separation between the filaments is ~ 0.4 cm, 0.59 cm and 0.94 cm for f/12 (NA ~ 0.04), f/7.5 (N.A ~ 0.06) and f/6 (NA ~ 0.08) geometry respectively. The separation scaled almost linearly for the NA used in the measurements.

The SCE associated with the filaments illustrated interesting behaviour with increasing tilt of the lens. SCE spectrum with different focal geometry for different tilt angles is shown in figures 5.4 (a) to 5.4.(c). The SCE intensity decreased monotonically with increasing tilt angle. The reduction in the white light continuum emission can be attributed to the distinct separation and shortening of the filaments, which is clearly depicted in Fig 5.2. However, as we moved on to shorter focal lengths (or higher NA), the SCE intensity increased, up to 8° tilt, in the blue region of the spectrum over $550 - 650$ nm.

The shorter the focal length the intense was the SCE in the blue spectral region. Above the tilt of 8° , the spectrum decreased monotonically with increasing tilt angles. Under tight focusing geometry, though two filaments were observed, they had a certain region of overlap ensuring localization of the pulse energy over a continuous distance along the propagation direction.

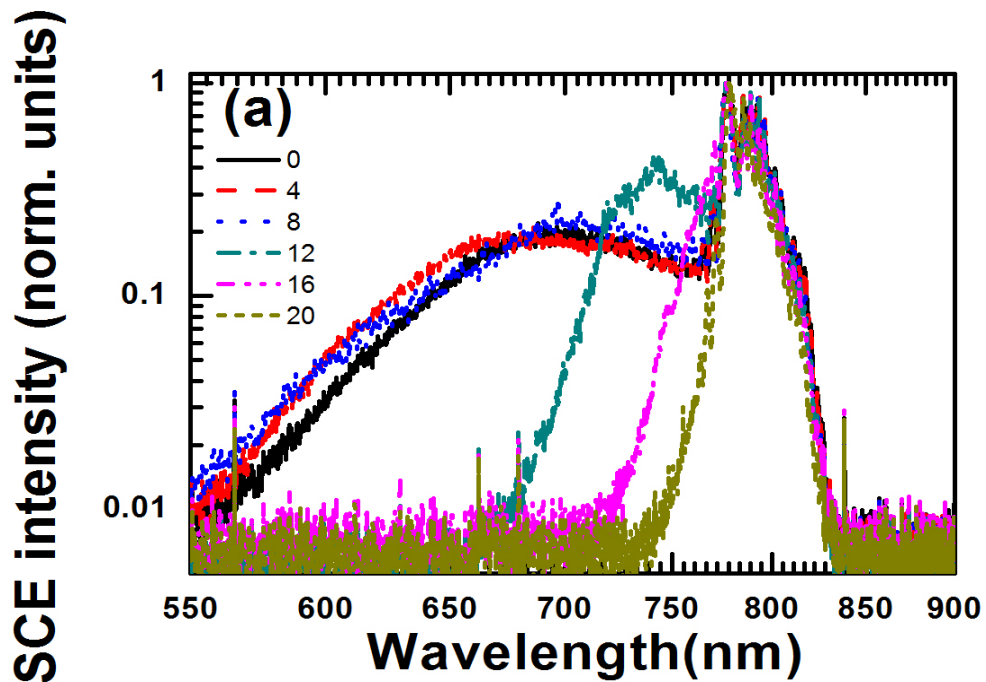


Figure 5.4(a): SCE spectra for different tilt angles under f/6 focusing geometry.

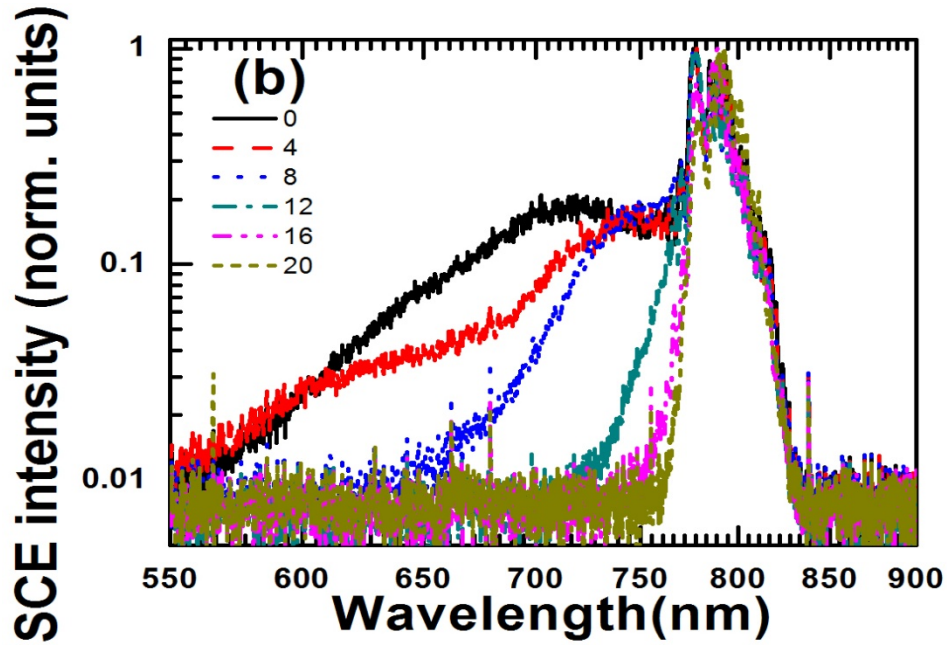


Figure 5.4(b): SCE spectra for different tilt angles under $f/7.5$ focusing geometry.

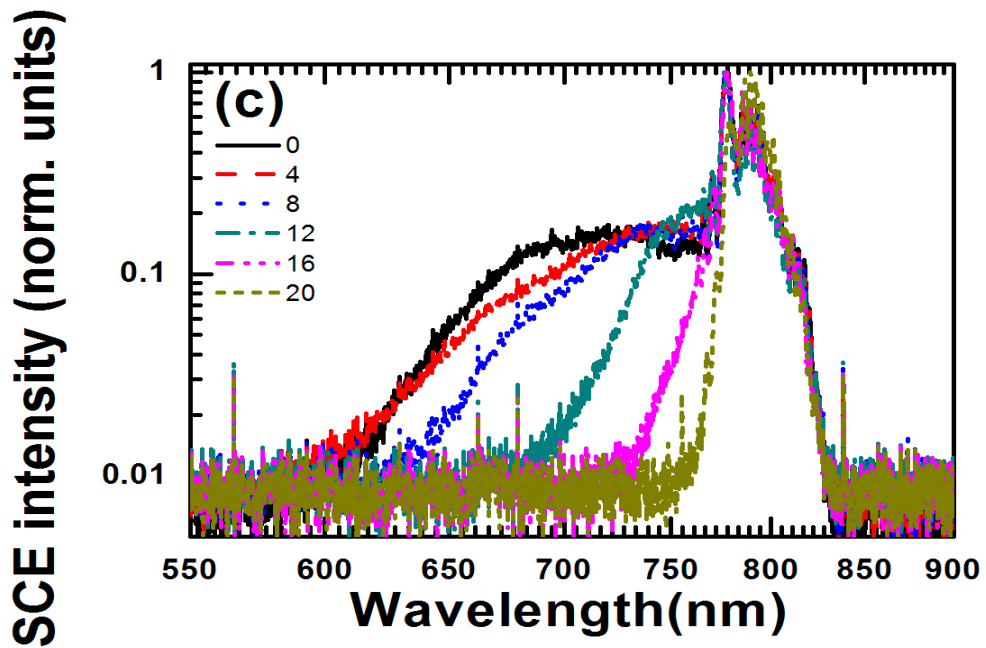


Figure 5.4(c): SCE spectra for different tilt angles under $f/12$ focusing geometry.

5.4 Conclusions

The dominant phenomenon of SCE is decreased monotonically with increased tilt angle of the focusing lens due to the shortening of the filaments. The observed phenomenon was found to be dominant for tight focusing geometries compared to loose focusing geometries. To conclude, a careful design of the astigmatism and geometrical aberration, can be utilized for making brighter SCE sources under tight focusing conditions, by exploiting the phenomenon of filamentation without conventional intensity clamping^{23, 24}.

References

- [1] Couairon, A. and Mysyrowicz, A., “Femtosecond filamentation in transparent media,” *Phys. Rep.* 441, 47-189,(2007).
- [2] Woste, L., Wedekind, C., Wille, H., Rairoux, P., Stein, B., Nikolov, S., Werner, C., Niedermeier, S., Ronneberger, F., Schillinger, H. and Sauerbrey, R., “Femtosecond atmospheric lamp,” *Laser Optoelektron.* 29, 51-53, (1997).
- [3] Rairoux, P., Schillinger, H., Niedermeier, S., Rodriguez, M., Ronneberger, F., Sauerbrey, R., Stein, B., Waite, D., Wedekind, C., Wille, H., Woste, L. and Ziener, C., “Remote sensing of the atmosphere using ultrashort laser pulses,” *Appl. Phys. B* 71, 573–580 (2000).
- [4] Diels, J., C., Bernstein, R., Stahlkopf, K. and Zhao, X., M., “Lightning control with lasers,” *Sci. Am.* 277, 50–55(1997)
- [5] Fischer, R., P., Ting, A., C., Gordon, D., F., Fernsler, R., F., DiComo, D., P. and Sprangle, P., “Conductivity measurements of femtosecond laser plasma filaments,” *IEEE Trans. Plasma Sci.* 35, 1430-1436, (2007).
- [6] Houard, A., D’Amico, C., Liu, Y., Andre, Y., B., Franco, M., Prade, B., Mysyrowicz, A., Salmon, E., Pierlot, P. and Cleon, L., M., “High current permanent discharges in air induced by femtosecond laser filamentation,” *Appl. Phys. Lett.* 90, 171501-171501-3, (2007).
- [7] Alfano R.R., [The Supercontinuum Laser Source: Fundamentals with Updated References], Springer Science+Business Media, Inc., New York, USA, (2006).
- [8] Hauri, C., P., Kornelis, W., Helbing, F., W., Heinrich, A., Couairon, A., Mysyrowicz, A., Biegert, J. and Keller, U., “Generation of intense, carrier-envelope phase-locked few-cycle laser pulses through filamentation,” *Appl. Phys. B* 79, 673–677 (2004).
- [9] Kiran, P., P., Bagchi, S., Krishnan, S., R., Arnold, C., L., Kumar, G., R. and Couairon, A., “Focusing of Ultrashort sub-TW laser pulses in air – Supercontinuum Emission”, *Proc. SPIE* 8173, 81730Q -81730Q-6,(2011).

- [10] Kiran, P., P., Bagchi, S., Krishnan, S., R., Arnold, C., L., Kumar, G., R. and Couairon, A., “Supercontinuum emission from tightly focused femtosecond pulses in air: beyond intensity clamping”, Proc. SPIE 7728, 77281-8,(2010)
- [11] D’Amico, C., Houard, A., Franco, M., Prade, B., Mysyrowicz, A., Couairon, A. and Tikhonchuk, V., T., “Conical forward THz emission from femtosecond-laser-beam filamentation in air,” Phys. Rev. Lett. 98, 235002-235002-4, (2007).
- [12] Nibbering, E., T., J., Curley, P., F., Grillon, G., Prade, B., S., Franco, M., A., Salin, F. and Mysyrowicz, A., “Conical emission from self-guided femtosecond pulses in air”, Opt.Lett. 21, 62-64 (1996).
- [13] Penano, J.R., Sprangle, P., Serafim, P., Hafizi, B. and Ting, A., “Stimulated Raman scattering of intense laser pulses in air”, Phys. Rev. E 68, 056502-056502-16, (2003).
- [14] Chin, S. L., [Femtosecond laser filamentation], Springer Series on Atomic, Optical, and Plasma Physics, 1st ed., (2010).
- [15] Mlejnek, M., Wright, E.M. and Moloney, J.V., “Dynamic spatial replenishment of femtosecond pulses propagating in air”, Opt. Lett. 23, 382–384, (1998).
- [16] Kiran, P., P., Bagchi, S., Krishnan, S., R., Arnold, C., L., Kumar, G., R. and Couairon, A., “Focal dynamics of multiple filaments: Microscopic Imaging and Reconstruction,” Phys. Rev. A 82, 013805 -013805-8,(2010).
- [17] Fibich, G., Eisenmann, S., Ilan, B., and Zigler, A., “Control of multiple filamentation in air,” Opt. Lett. 29,15- 17 (2004)
- [18] Schroeder, H., Liu, J. and Chin, S.L., “From random to controlled small-scale filamentation in water,” Opt. Express 12 (20), 4768-4774 (2004).
- [19] Eisenmann, S., Louzon, E., Katzir, Y., Palchan, T., Zigler, A., Sivan, Y. and Fibich, G., “Control of the filamentation distance and pattern in long-range atmospheric propagation,” Opt. Express 15, 2779-2784 (2007).

- [20] Stelmaszczyk, K., Rohwetter, P., Mejean, G., Yu, J., Salmon, E., Kasparian, J., Ackermann, R., Wolf, J., P. and Wöste, L., “Long-distance remote laser-induced breakdown spectroscopy using filamentation in air,” *Appl. Phys. Lett.* 85, 3977-3979 (2004).
- [21] Kamali, Y., Sun, Q., Daigle, J., F., Azarm, A., Bernhardt, J. and Chin, S. L., “Lens tilting effect on filamentation and filament-induced fluorescence,” *Opt. Commun.* 282, 950–954 (2009).
- [22] Hecht, E., [Optics], Addison Wesley, Fourth edition, 2002.
- [23] Kiran, P., P., Bagchi, S., Krishnan, S., R., Arnold, C., L., Kumar, G. and R., Couairon, A., “Filamentation without intensity clamping,” *Opt. Express* 18, 21504-21510 (2010).
- [24] Sun, X., Xu, S., Zhao, J., Liu, W., Cheng, Y., Xu, Z., Chin, S., L. and Mu, G., “Impressive laser intensity increase at the trailing stage of femtosecond laser filamentation in air”, *Opt. Express* 20, 4790-4795 (2012).

DYNAMICS OF TIGHTLY FOCUSED FEMTOSECOND LASER PULSES IN WATER

6.1.	Introduction
6.2.	Experimental technique
6.3.	Supercontinuum emission (SCE) studies from water
6.4.	Conclusions

Abstract

We present the evolution of plasma dynamics vis-à-vis supercontinuum emission (SCE) resulting from propagation of tightly focused 40 femtosecond (fs) laser pulses propagating in water over a large range of input powers from 6 mW to 1.8W. The effect of linearly polarized (LP) and circularly polarized (CP) light pulses on SCE in different external focal geometries (f/6, f/7.5 and f/10) are discussed. SCE with higher efficiency and a considerable spectral blue shift is observed under tight focusing conditions (f/6) compared to loose focusing conditions of (f/7.5) and (f/10). The effect of temperature on SCE from water is also investigated in this chapter. With higher input powers, the cavitation induced bubbles along the axis of propagation are found to be assisting deeper propagation of pulses and enhancement of SCE

6.1. Introduction

From the initial observation of self-channeling of high-peak power femtosecond (fs) laser pulses in air by Braun et al. [1], propagation of intense fs laser pulses (peak intensities $> 10^{12}$ W/cm²) in different media has been one of the intriguing research areas due to the interest in both fundamental science [2] and technological applications [3-5]. The propagation of intense fs pulses in transparent condensed media or gases is characterized by strong modification of its spatial and temporal profile due to the dynamic interplay between the self-collapse of the laser pulse and the associated spectral broadening due to self-phase modulation (SPM) [6-7]. The spectral manifestation of the spatio-temporal modifications of focused laser beam in a medium results in a broad frequency sweep known as Supercontinuum emission (SCE) extending, typically, from ultraviolet to the near infrared range [6]. SCE associated with filamentation of fs laser pulses occurs when the laser power (P) exceeds critical power for self-focusing (P_{cr}) in the medium [6-7]. Potential applications of this phenomenon include optical pulse compression, [8] fs-LIDAR, and remote sensing [9]. Although the main mechanisms responsible for SCE is believed to be self-focusing followed by SPM, the evolution of SCE under different situations is not understood completely. Different mechanisms generate diverse components of the SCE/white light spectrum at certain positions along the propagation direction of pulse [6]. Self-steepening, space time focusing, plasma generated by multi-photon ionization, four wave mixing are also believed to play a significant role [6].

Despite wide variety of applications, the generation of SCE phenomenon due to filamentation has mainly been associated with long range propagation of intense fs laser beams in a variety of media confined to unfocused or loosely

focused geometries [10-15]. A few recent attempts were directed towards understanding the ultrashort laser pulse filamentation [16-22] and the generated SCE at lower input powers [22,23] with tightly focused beams. While many efforts were made towards achievement of spectrally flat SCE, with large blue shifted spectrum [24 – 28], the extent of blue shift from a medium has been reported to be constant due to the phenomenon of intensity clamping [14]. In view of recent observations of filamentation without intensity clamping [22] (b) interconnection between the spatial and spectral evolution of fs pulses in air under tight focusing conditions, due to complete ionization of the medium [19-22,29] (c) the observation of nonlinear interaction of fs pulses with water using high angle Bessel beams depositing higher energy into the medium [30], and (d) the directional ejection of micro bubbles, we investigated the spectral evolution of SCE from the propagation of tightly focused femtosecond laser pulses in water.

6.2. Experimental technique

A schematic illustration of the experimental setup for generating SCE from water is depicted in figure 6.1(a). Transform limited 40 fs, 800 nm p-polarized laser pulses at a repetition rate of 1 kHz (Coherent; Legend-USP) were focused into an 80 mm-long glass cuvette containing double distilled water. The amplifier was seeded with 15 fs pulses from an oscillator (MICRA, Coherent) having 1 W average power, 80 MHz repetition rate, 60 nm typical FWHM spectral width at 800 nm central wavelength. The input diameter ($1/e^2$) before the focusing element was 10 ± 0.1 mm. BK-7 plano-convex lenses of focal length 60 mm, 75 mm and 100 mm were used to achieve the required focal geometries (numerical aperture (NA) of $f/6=0.083$; $f/7.5=0.066$ and $f/10=0.05$) respectively. For all the focusing geometries, the focus was ensured to be at an identical position within the cuvette.

An attenuator, a combination of a half wave plate (HWP) and a Brewster polarizer (BP), was used to vary the input pulse energy entering the medium. A quarter wave plate (QWP) was employed after the attenuator to change the polarization of the pulse. Part of the SCE generated was collected using a fiber optic coupled spectrometer (USB 4000, Ocean Optics) with a resolution of -1.3 nm. A color CCD camera (SP620U, Ophir-Spiricon) synchronized with a laser pulse was used to image the self-emission and CIB (cavitation induced bubble) from the propagating filament inside water and for estimating the diameter of the energy reservoir surrounding the filament inside the medium. A set of calibrated neutral density filters were placed in front of the spectrometer and CCD camera to avoid saturation of the sensor. The pulse duration of the incident and the transmitted 800 nm pulses were measured using ‘Silhouette’ (Coherent, USA) based on the multi-photon intra-pulse interference phase scan (MIIPS) technique [32]. Appropriate adjustments were made with the laser compressor gratings to ensure that the final pulse duration entering the water cuvette was indeed 40 fs.

SCE spectra were collected for 350 laser shots to reduce the noise from pulse to pulse fluctuations. The experiment was performed for both LP and CP pulses over the power range of 6 mW–1.8 W (energy range of 6 μ J to 1.8mJ per pulse). The power of the incident transmitted 800 nm pulses and the SCE were measured using a power meter (Coherent, PM30). The power entering the medium post Fresnel losses (due to the focusing lens, the entrance face of the cuvette and the cuvette–water interface) was considered as the input power (P_{abs}) for all calculations. We observed that 68–70% of the incident laser power was absorbed by the medium. The efficiency of the SCE (η_{SCE}) is estimated as $P_{\text{SCE}}/P_{\text{abs}}$. A 800 nm filter was used to cut off the transmitted input laser pulses after the cuvette while measuring the efficiency of SCE. The critical power for

self-focusing is calculated from the equation $P_{cr} = 3.77\lambda^2/8\pi n_0 n_2$ where λ is the central wavelength, n_0 and n_2 are the linear and nonlinear refractive indices, respectively. The P_{cr} for water is taken as 4.4 MW [33].

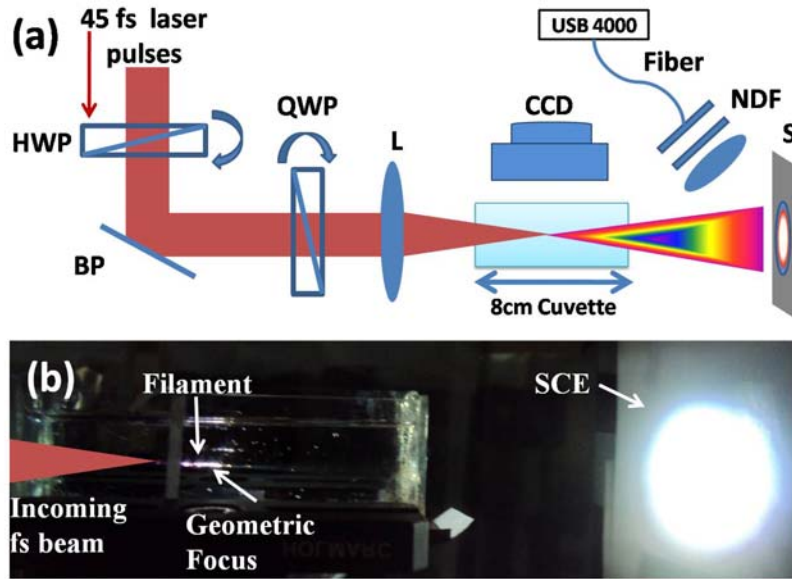


Figure 6.1(a) Schematic experimental setup for investigating SCE from double distilled water using focused fs pulses. HWP-Half Wave Plate, BP- Brewster Polarizer in the reflection mode, QWP-Quarter Wave Plate, L- Lens, C-Cuvette, S-Screen, NDF-Neutral Density Filter and CCD – Camera.

Figure 6.1.(b) Side view of the filament within the cuvette and the SCE generated with $f/6$ focusing geometry at $6929P_{cr}$ for LP pulses.

6.3. Supercontinuum emission (SCE) studies from water

In this section we discuss our results of SCE from a condensed media, water for linearly polarized (LP) and circularly polarized (CP) 40fs pulses in water over a wide range of input powers from 6 mW to 1.8 W corresponding to pulse energies of 6 μ J to 1.8 mJ. The interesting role of cavitation induced bubbles (CIB) in enhancing the SCE with tight focusing geometries and at high input powers where intensity is clamped is also studied. The co-existence of

SCE associated with filamentation and the CIB due to the breakdown of water is observed in water under tight focusing geometries.

6.3.1. SCE spectral studies with linearly polarized fs laser pulses

The femtosecond pulses propagating in water produced SCE with conical coloured rings at low input powers and SCE with predominantly white coloured central portion at high input powers. Figure 6.1(b) shows an image of a typical filament propagating inside water and the associated SCE at an input power of 1.25 W for LP pulses in the $f/6$ focusing geometry. The filamentation is observed to start ahead of the geometrical focus for all the three focusing geometries. The filaments were propagating for over 15–53 mm inside the cuvette corresponding to 74–84 Z_0 , where Z_0 is the Rayleigh range of focusing geometries used in the present study. The onset of filamentation starts from the geometrical focus towards the lens with increase in the input power. Figure 6.2 shows the SCE spectrum recorded at different input powers for LP pulses with $f/7.5$ focusing geometry. The spectra demonstrated broadening towards both sides of the central wavelength. The symmetrical spectral broadening about the incident laser wavelength (800 nm) is ascribed to the Kerr nonlinearity induced SPM. The asymmetric component in the blue spectral region occurs due to processes such as space–time focusing, self-steepening, [34] plasma formation that arise from free electrons generated through multi-photon ionization (MPI) in gases and multi-photon excitation (MPE) in condensed media [6]. In addition to the asymmetric broadening there is a marked dip near 611 nm superimposed on the white light continuum corresponding to an inverse Raman effect due to the –OH stretching bond (3650 cm^{-1}) [25, 26, 35] of water. The Raman dip intensity increased with increasing excitation energy indicating the participation of more water molecules in the process as more of the excitation energy was

converted into Raman modes. The SCE spectrum (figure 6.2) shows a flat response in the 550–750 nm spectral range excluding the inverse Raman dip at 611 nm.

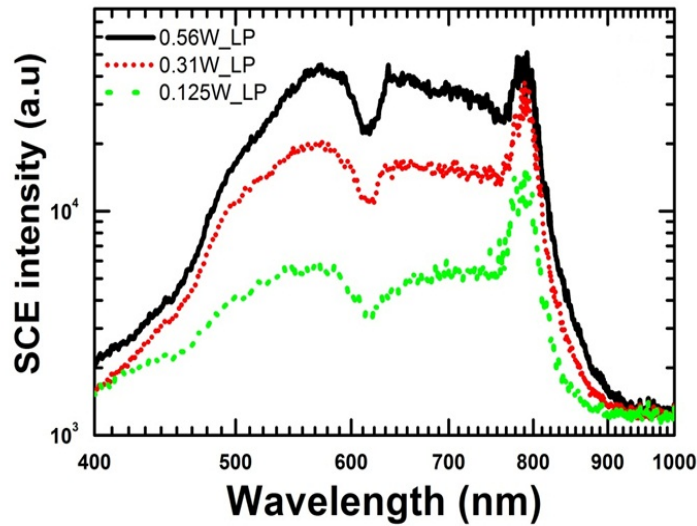


Figure 6.2 SCE spectra with LP pulses obtained in $f/7.5$ focal geometry at an input power of 0.125, 0.31 and 0.56 W. The data is plotted in logarithmic scale for convenient comparison.

6.3.2. Supercontinuum emission studies under different focusing geometries

The SCE spectra for different focal geometries of $f/6$, $f/7.5$ and $f/10$ at an absorbed power of 1.2 W for LP and CP pulses are shown in figure 6.3(a) and 6.3(b) respectively. The spectra illustrate noticeable enhancement in both the symmetric and asymmetric branches of SCE for tight focusing geometry. Tighter focusing in the case of $f/6$ geometry has resulted in increased conversion of incident laser pulse energy into SCE, especially towards the blue side of the spectrum indicating the role of tighter focusing on the evolution of SCE spectrum in terms of increased peak intensity near the focal plane. Along with SCE associated with filamentation, phenomenon of CIB is also observed at very low input powers (300mW) for the $f/6$ focusing geometry whereas in the

case of $f/10$ focusing geometry the co-existence of filamentation and CIB is observed at $\sim 700\text{mW}$ indicating that more laser energy is deposited at the focal plane of the medium with tight focusing geometry.

Figures 6.4 (a), (b) and (c) show the filamentation of fs pulses in water under $f/6$, $f/7.5$ and $f/10$ focusing geometry respectively. We can observe a highly intense and bright filament core under $f/6$ geometry and a less intense diffracted cone of filament in the $f/10$ geometry. This is the clear evidence for the localisation of laser pulse energy in the tight focusing geometry compared to the loose focusing geometry

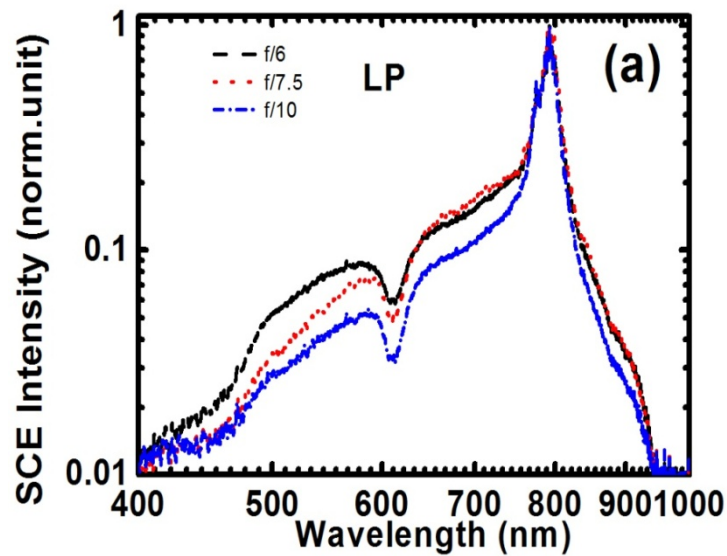


Figure 6.3(a) SCE spectra from water with $f/6$ (black line), $f/7.5$ (red line) and $f/10$ (blue line) focusing geometries at 1.2 W for LP pulses

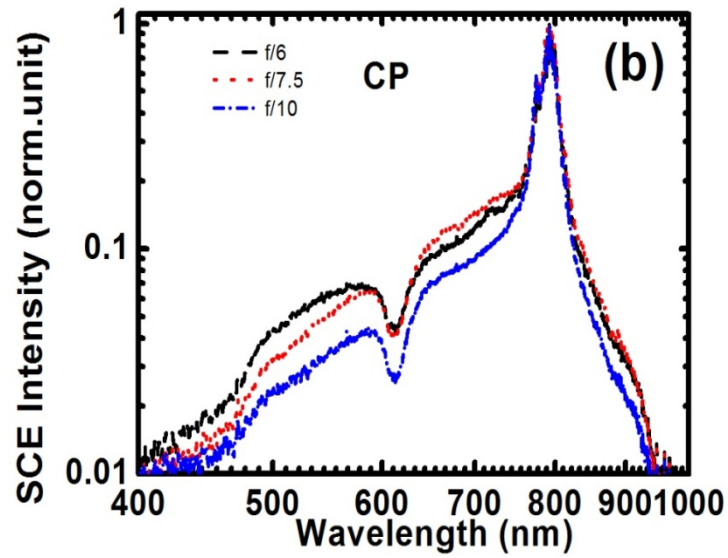


Figure 6.3(b) SCE spectra from water with f/6 (black line) and f/7.5 (red line) and f/10 (blue line) focusing geometries at 1.2 W for CP pulses.

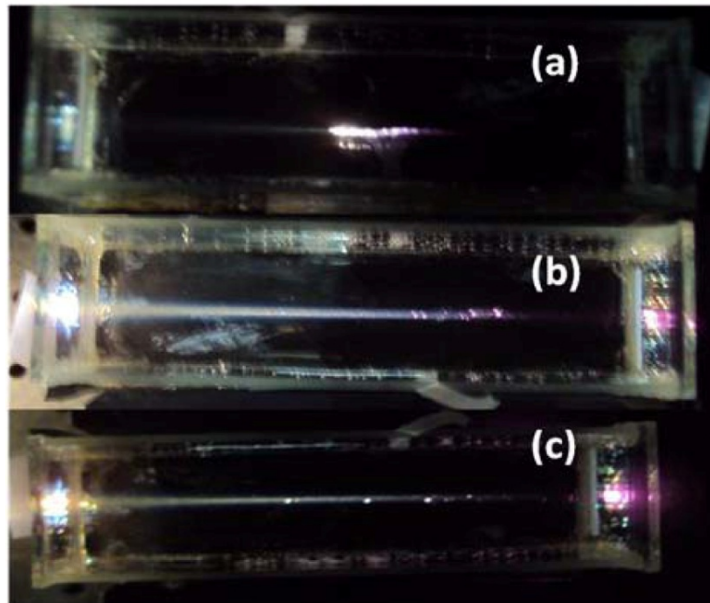


Figure 6.4: Top view of the filament in water (a) for f/6 focusing geometry (b) for f/7.5 and (c) for f/10 focusing geometry

6.3.3. Role of input polarization on the SCE

In this section we discuss our results obtained using linearly and circularly polarized laser beams. The input polarization of the pulse was changed from LP to CP simply by rotating the quarter wave plate. A reduction in the SCE intensity is observed at low input powers as we move from LP to CP pulses for all the three focusing geometries which is in good agreement with earlier reports [35]. However, with increasing input powers the difference in SCE from LP and CP pulses is observed to be negligible due to the increased presence of the CIB along the propagation direction. Figure 6.5 shows a reduction in the intensity of SCE for CP pulses compared to that of LP in the case of f/6 focusing geometry. The same trend is observed in all other geometries.

The main contributing mechanism of SCE is Multi Photon Excitation (MPE) enhanced Self Phase modulation (SPM), four wave mixing processes, and avalanche –ionisation enhanced SPM. Petit et.al have showed that the MPE process is strongly dependent on the input polarisation of the laser. More energy is required for CP light to reach the same number of ions created by LP, and hence MPE is less efficient for CP pulses.

In femto second time scales only non-resonant electronic mechanism is relevant and LP light induces 1.5 times higher Δn than CP pulses [35]. Consequently the onset of self focusing and SCE will be faster for LP pulses. The ratio of 1.5 in the critical power for self-focusing with LP and CP pulses accounts for MPE being less efficient for CP pulses [6]. For a given NA, the ratio of SCE intensities for CP and LP pulses (SCE_{CP}/SCE_{LP}) as a function of wavelength is always less than 1, confirming the reduction of SCE with CP pulses in contrast to LP pulses.

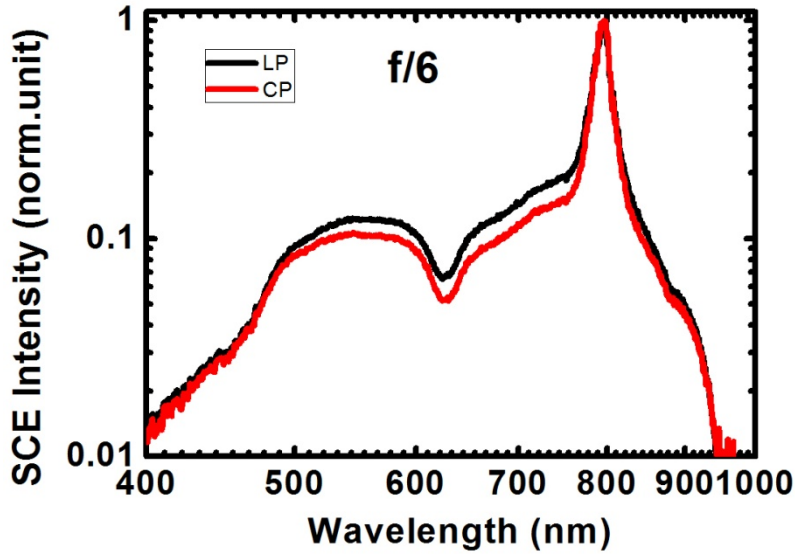


Figure 6.5: Variation of SCE with LP & CP pulses for f/6 focusing geometry in water

6.3.4. Studies on the role of minimum wavelength (λ_{\min}) and intensity clamping on SCE

The blue edge of the SCE spectrum, i.e., the minimum cutoff wavelength (λ_{\min}) or maximum positive frequency shift (ω_{\max}) as a function of the input laser power from the collected SCE spectra, is found to decrease continuously with increasing input power for all the focusing geometries. Figure 6.6a shows the variation of λ_{\min} for both f/6, f/7.5 and f/10 focusing geometries for LP pulses and 6.6 (b) shows the variation of λ_{\min} for LP & CP pulses for f/6 focusing geometry. At lower input powers (<30mW), the λ_{\min} is almost the same for all the focusing geometries and the separation becomes considerable (~100nm) over the 50mW-600 mW input power range. The λ_{\min} was found to be more blue shifted for f/6 focusing geometry compared to f/7.5 and f/10 focusing geometries at input powers >50mW. This clearly demonstrates the presence of higher intensities in the vicinity of interaction region (focal plane) for f/6 focusing geometry and also reveals the blue shift of the SCE

spectra due to the external focusing of the fs pulses inside transparent media. With increasing input powers, λ_{\min} has showed interesting evolution. Under f/6 focusing geometry, λ_{\min} decreased in two rates of P_{abs} before and after 100 mW, while for f/7.5 and f/10 focusing geometries, the transition occurred in three different power regimes of 6 – 50 mW, 100 – 600 mW and beyond 600 mW. A similar blue shift of SCE was observed in the SCE from air using tight focusing conditions [21] though the variation of λ_{\min} observed in water was small compared to that observed in air, because air molecules can be completely ionized without being opaque[20]. Although plasma electron densities of about $7 \times 10^{20} \text{ cm}^{-3}$, which increases with tighter focusing geometry, were observed in numerical simulations (tight focusing geometry of f/3.4 at pulse energies of 4 μ J)[22], the complete ionization of the medium at high input powers without being opaque needs further exploration due to the higher number density (10^{22} cm^{-3} at 1 atmosphere compared to that of 10^{19} cm^{-3} in air) in spite of the optical bandgap and order of MPI being less than that of air. However, λ_{\min} has become constant with increasing input powers above 300 mW, 500mW and 700 mW in f/6, f/7.5 and f/10 focusing geometries respectively, indicating the presence of intensity clamping which is $\sim 1 \text{ TW/cm}^2$ for water. This intensity is sufficient to cause breakdown of water and cause CIB near the focal plane, that is, within the interaction region of laser pulse inside water[36].

The evolution of CIB was studied by capturing the self emission from the wake of fs pulses/filaments propagating in water (figure 6.7). Higher intensity and brighter SCE in the f /6 geometry compared to that of f/7.5 and f/10 geometries clearly indicates the presence of interesting dynamics inside the medium. Moreover, λ_{\min} for f/6 geometry was always more blue shifted compared to other focusing geometries (figure 6.6(a)).

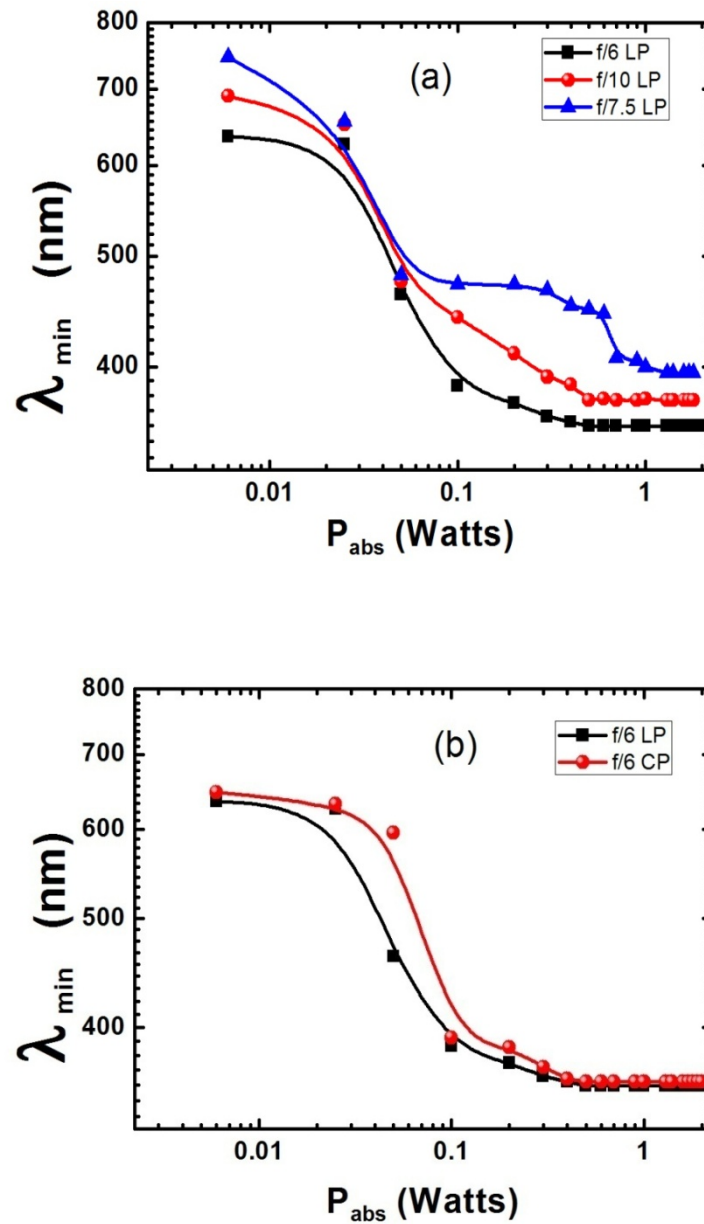


Figure 6.6 Variation of minimum wavelength (λ_{\min}) with absorbed input power P/P_{cr} for f/6, f/7.5 and f/10 focusing geometries for LP pulses. (b) for LP and CP pulses in f/6 focusing geometry.

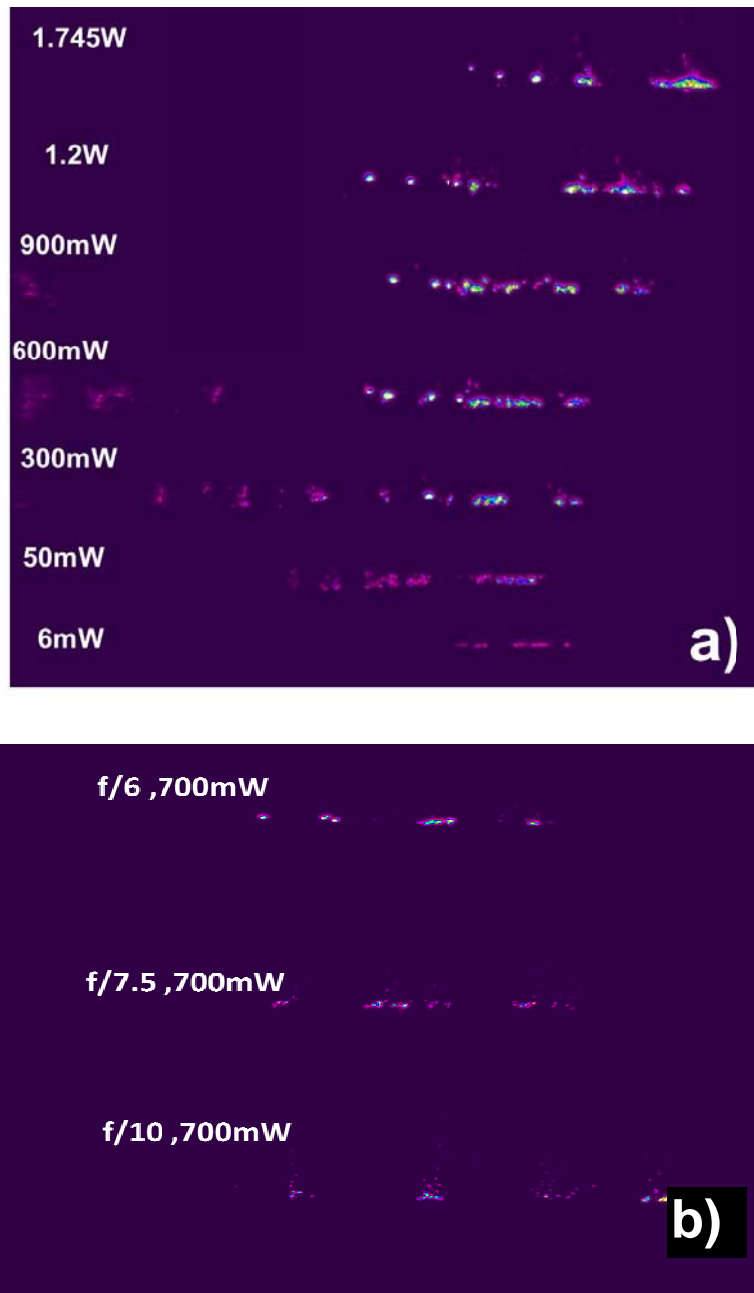


Figure 6.7. Image of the bubbling observed in water during the propagation of 45 fs pulses (a) at different input powers under f/6 focusing geometry. (b) Comparison of the bubbling under f/6, f/7.5 and f/10 focusing geometries for 700mW input power

Notably, the separation of blue shift between the focusing geometries increased with increasing input powers (figure 6.6(a)). This behaviour was more dominant beyond P_{abs} of 100 mW, where the onset of CIB was observed for the focusing geometries used. Figure 6.6 (b) shows the variation of λ_{min} with CP and LP pulses under f/6 focusing geometry.

6.3.5. Efficiency of Supercontinuum emission under different focusing geometries

Figure 6.8 shows the efficiency of the SCE with LP pulses for f /6 ,f/7.5 and f /10 focusing geometries. SCE with an efficiency of ~7% ~9% and ~10% was observed with f/10,f/7.5 and f /6 focusing geometries, respectively. With increasing NA from 0.05 (f/10) to 0.083 (f/6) the efficiency of SCE (η_{SCE}) was observed to increase by 1.5 times indicating higher conversion efficiency. The spectral flatness also increased with increasing numerical aperture (NA) and input powers. However, the flatness reduced slightly with CP pulses compared to that of LP pulses.

At lower input powers, η_{SCE} is observed to be similar (~9%) for all focusing conditions (figure 6.8). With a gradual increase of P_{abs} , an interesting dependence of η_{SCE} on focusing conditions was observed. For f /6 focusing geometry η_{SCE} has remained almost constant, while for f /10 it decreased quite significantly to 6%. The difference in the η_{SCE} has become more obvious above $P_{\text{abs}} \sim 300\text{mW}(30 \mu\text{J})$. Incidentally, the CIB is more obvious around 300 mW. The separation between the CIB at different points along the propagation direction decreased with increasing input power (figure 6.7(a)) and increasing NA (figure 6.7(b)).

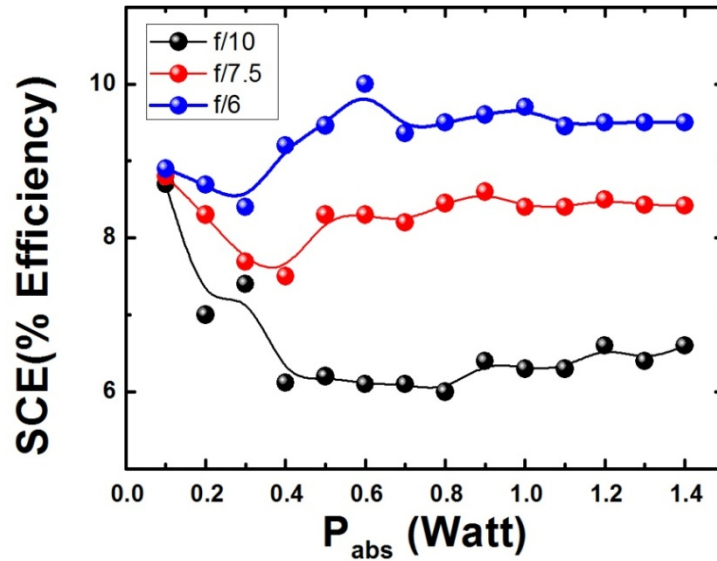


Figure 6.8 Variation of SCE efficiency (%) with P_{abs} for f/6 (blue spheres), f/7.5 (red spheres) and f/10 (black spheres) focusing geometries.

6.3.6. Effect of temperature on SCE

Figure 6.9 shows the SCE spectrum recorded at 1.27 mJ, corresponding to 6400 P_{cr} , with f/6 focusing geometry for different temperatures. The experiment is performed in a similar manner as explained in Section.6.2. In order to investigate the temperature dependence of SCE from water, the temperature of water was varied over 50 degrees from 308 K to 353 K. Part of the SCE generated was collected using a fiber optic coupled spectrometer (USB 4000, Ocean Optics) with a resolution of 1.3 nm. A set of calibrated neutral density filters were placed in front of the spectrometer to avoid the saturation of sensor. SCE spectra were collected for 100 laser shots to reduce the noise from pulse to pulse fluctuations. The magnitude of SCE spectra is enhanced with SCE is enhanced with the decrease in temperature. This enhancement is interpreted by the change in temperature dependence refractive index and the corresponding change in the critical power (P_{cr}) required for the SCE. The

change in refractive index Δn due to a temperature rise ΔT can be expressed by $\Delta n = (dn/dT) \Delta T$ where dn/dT is called the thermo-optic coefficient. In most liquids and solids this is due to a density change (i.e. expansion) with temperature. Since the density decreases in expansion and the nonlinear refractive index is proportional to density, n_2 will decrease. This decrease in n_2 will proportionately increase the critical power for self focusing. We therefore conclude that the SCE is enhanced with the decrease in temperature.

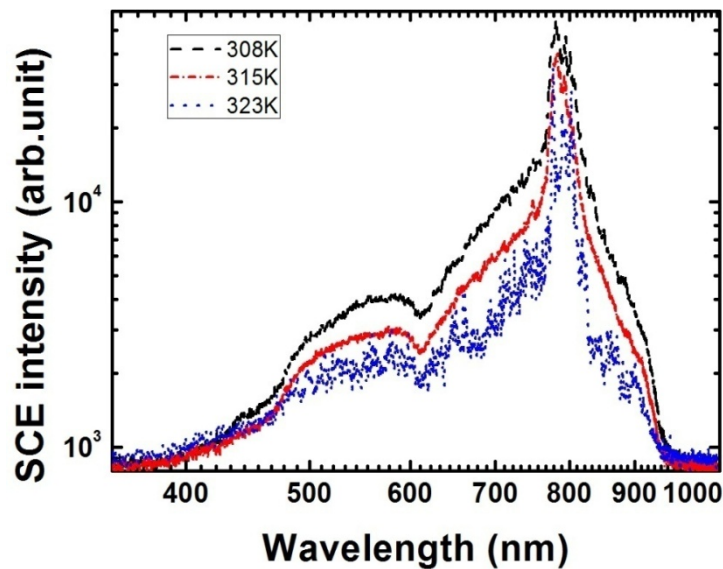


Figure 6.9 SCE spectrum recorded at an input power of 1.27mJ (6400 Pcr) for different temperature in water.

6.3.7. Influence of Cavitation Induced Bubbles (CIB) in SCE

The bubbles filled with gas or vapour can emit light when collapsing violently in a surrounding liquid upon strong excitation. The cavitation bubbles are produced by focused laser light and make a single strong collapse [44]. We believe that the micron-sized CIB [5, 37] along the propagation direction act like tiny spherical lenses for filament propagation by refocusing the diverging laser energy and the trailing edge of the pulse along the propagation axis

overcoming the diffraction. This leads to increasing deposition of laser energy during the propagation of fs pulses and the enhanced SCE in the wake of fs pulses. The observed anomalous increase in the λ_{\min} beyond the clamping intensity seems to originate from the plasma evolution around the focal plane. Moreover, the trailing part of fs pulses was observed to support higher intensities during filamentation [38]. The CIB, due to fs pulses, were observed to live up to few tens of ns with energy-dependent sub-micron to micron diameters [5, 37]. Though the CIB and their interaction is a hydrodynamic phenomenon lasting less than 1 ms which is relatively slow when compared to the ultrafast processes occurring later in the wake of the fs pulse, the laser-produced plasma starts expanding within 20 ps due to electron–ion energy transfer time, effectively inducing a temperature above 200 °C due to the ultrafast phase transitions [39]. The formation of CIB due to fs laser pulses is observed to be a very dynamic process below and above the breakdown threshold of the medium with a typical free electron density of $\sim 3.5 \times 10^{20} \text{ cm}^{-3}$ at the end of the laser pulse [5]. Beyond the threshold energy the CIB progresses as explosive vaporization due to phase explosion with peak focus temperatures $>300 \text{ }^{\circ}\text{C}$ [5]. The phenomenon of CIB in water due to fs pulses is observed to start at intensities higher than TW cm^{-2} [36, 40] and is strongly dependent on the pulse energy, duration and repetition rate [37]. The plasma shielding effect that counters the propagation of laser pulses inside the medium is observed to reduce as the incident pulse duration becomes shorter [36]. We also strongly believe that in the tight focusing geometry, the initial high beam curvature, due to external focusing, leads to a higher degree of ionization of the medium, leading to dynamically interacting CIB acting like a series of spherical lenses which in turn prevent plasma defocusing from playing any significant role in the intensity clamping [5,22]. A similar phenomenon corresponding to

the fully ionized medium with electron density up to $2 \times 10^{19} \text{ cm}^{-3}$ in filamentation in air under similar focusing conditions (NA of 0.11) and in the range of 10^{18} – 10^{19} cm^{-3} for NA of 0.08 [20–22, 39–41] due to the external tight focusing conditions, was recently reported. In condensed media such as water or solids the phenomenon is expected to be totally different due to low ionization thresholds and higher densities.

Many other phenomena such as (i) the propagation of tightly focused fs pulses inside water [30, 31], (ii) ionization, plasma shielding and breakdown phenomena of water at intensities greater than TW cm^{-2} within the filament [36, 40], (iii) the effect of pulse splitting [29] and (iv) interaction of the cavitation bubbles in water [30, 31, 42, 43] with high repetition rate pulses need to be understood completely so as to devise practical high-intensity SCE sources.

6.4. Conclusions

- In this chapter, the effects of external tight focusing conditions on the evolution of SCE resulting from the propagation of 40 fs laser pulses in water is studied in detail.
- A flat SCE with an efficiency of $\sim 6\%$ for f/10 focusing geometry $\sim 8\%$ for f/7.5 and $\sim 10\%$ for f/6 focusing geometry are observed with tightly focused fs pulses.
- The SCE from tight focusing geometry was always higher than the loose focusing geometry for both LP and CP pulses.
- For tighter focusing geometries, however, the minimal cutoff wavelength (λ_{min}) for the SCE got saturated at higher input powers, and CIB along the propagation axis is observed to assist further propagation

of fs pulses, thereby generating enhanced SCE. This makes it possible to stretch the intensity levels of fs pulses inside the medium beyond the clamping value.

- The SCE from water is enhanced with the decrease in temperature. It is explained that the decrease of temperature results in the lower critical power for self focusing due to the increase of the linear and nonlinear refractive index of the water
- Controlled deposition of laser energies around the focal region with tighter focusing conditions is an interesting way of generating enhanced SCE which paves a path for novel intense sources of radiation and several possible practical applications.

References

- [1] Braun A, Korn G, Liu X, Du D, Squier J and Mourou G, "Self-channeling of high-peak-power femtosecond laser pulses in air" *Opt. Lett.* 20, 73-75(1995)
- [2] Belgiorno F, Cacciatori S L, Ortenzi G, Sala V G and Faccio D "Quantum Radiation from Superluminal Refractive-Index Perturbations" *Phys. Rev. Lett.* 104, 140403-140403-4,(2010)
- [3] D'Amico C, Houard A, Akturk S, Liu Y, Le Bloas J, Franco M, Prade B, Couairon A, Tikhonchuk V T and Mysyrowicz "Forward THz radiation emission by femtosecond filamentation in gases: theory and experiment," *New J. Phys.* 10 ,013015(2008)
- [4] T.-J. Wang, C. Marceau, S. Yuan, Y. Chen, Q. Wang, F. Théberge, M. Châteauneuf, J. Dubois, and S. L. Chin "External focusing effect on terahertz emission from a two-color femtosecond laser-induced filament in air", *Laser Phys. Lett.* 8, 57 -61 (2011).
- [5] Vogel A, Linz N, Freidank S and Paltauf G "Femtosecond-laser-induced nanocavitation in water: implications for optical breakdown threshold and cell surgery" *Phys. Rev.Lett.* 100, 038102-038102-4,(2008)
- [6] Couairon A and Mysyrowicz A "Femtosecond laser filamentation in transparent media" *Phys. Rep.* 441, 47-189 (2007)
- [7] Boyd R W, Lukishova S G and Shen Y R" Self-focusing: Past and Present: Fundamentals and Prospects" (New York:Springer) chapter 1(2009)
- [8] Schulz E, Binhammer T, Steingrube D S, Rausch S, Kovacev M and Morgner U "Intense few-cycle laser pulses from self-compression in a self-guiding filament, *Appl. Phys. B* 95, 269 -272 (2009)
- [9] J. Kasparian, M. Rodriguez, G. Méjean, J. Yu, E. Salmon, H. Wille, R. Bourayou, S. Frey, Y.-B. André, A. Mysyrowicz, R. Sauerbrey, J.-P. Wolf, L. Wöste, Kasparian J "White light filaments for atmospheric analysis" *Science* 301, 61-64(2003)

- [10] Eisenmann S, Pukhov A and Zigler A “Fine structure of plasma filaments”, *Phys. Rev. Lett.* 98, 155002 -155002-4,(2007)
- [11] Fibich G and Ilan B “Multiple filamentation of circularly polarized beams” *Phys. Rev. Lett.* 89, 013901-013901-4,(2002)
- [12] M'echain G, Couairon A, Franco M, Prade M and Mysyrowicz A”Organizing multiple femtosecond filamentation in air”, *Phys. Rev. Lett.* 93, 035003-035003-4,(2004)
- [13] Varela O, Zair A, Roman J S, Alonso B, Sola I J, Prieto C and Roso L “Above milli joule supercontinuum generation using polarisation dependent filamentation in atoms and molecules” *Opt. Express* 17, 3630-3639 (2009)
- [14] Liu W, Petit S, Becker A, Akozbek N, Bowden C M and Chin S L “Intensity clamping of a femtosecond laser pulse in condensed media” *Opt. Commun.* 202, 189-197(2002)
- [15] Mizeikis V, Juodkazis S, Balciunas T, Misawa H, Kudryashov S I, Zvorykin V D and Ionin A A” “Optical and ultrasonic signatures of femtosecond pulse filamentation in fused silica”, *J. Appl. Phys.* 105, 123106 (2009)
- [16] Sudrie L, Couairon A, Franco M, Lamouroux B, Prade B, Tzortzakis S and Mysyrowicz A “Femtosecond laser induced damage and filamentary propagation in fused silica” *Phys. Rev. Lett.* 89, 186601-186601-4,(2002)
- [17] Couairon A, Sudrie L, Franco M, Prade B and Mysyrowicz A” Filamentation and damage in fused silica induced by tightly focused femtosecond laser pulses, “ *Phys. Rev. B* 71, 125435-125435-11, (2005)
- [18] Th'eberge F, Liu W, Simard P T, Becker A and Chin S L “Plasma density inside a femtosecond laser filament in air: strong dependence on external focusing” *Phys. Rev. E* 74, 036406-036406-7, (2006)
- [19] Ionin A A, Kudryashov S I, Makarov S V, Seleznev L V and Sinitsyn D V “Multiple filamentation of intense femtosecond laser pulses in air” *JETP Lett.* 90, 423-427 (2009)

- [20] Kiran P P, Bagchi S, Krishnan S R, Arnold C L, Kumar G R and Couairon A "Focal dynamics of multiple filaments: Microscopic imaging and reconstruction" *Phys.Rev. A* 82 , 013805-013805-8,(2010)
- [21] Liu X-L, Lu X, Liu X, Xi T-T, Liu F, Ma J-L and Zhang J "Tightly focused femtosecond laser pulse in air: from filamentation to breakdown. *Opt. Express* 18, 26007-17(2010)
- [22] Kiran P P, Bagchi S, Arnold C L, Krishnan S R, Kumar G R and Couairon A "Filamentation without intensity clamping" *Opt. Express* 18 ,21504-21510 (2010)
- [23] Liu W, Kosareva O, Golubtsov I S, Iwasaki A, Becker A, Kandidov V P and Chin S L "Femtosecond laser pulse filamentation versus optical breakdown in H₂O" *Appl. Phys. B* 76, 215 -229(2003)
- [24] Srinivas N K M N, Harsha S S and Rao D N "Femtosecond supercontinuum generation in a quadratic nonlinear medium (KDP)" *Opt.Express* 13, 3224-3229(2005)
- [25] Moghaddam M R A, Harun S W, Akbari R and Ahmad H " Flatly broadened supercontinuum generation in nonlinear fibers using a mode locked bismuth oxide based erbium doped fiber laser" *Laser Phys. Lett.* 8, 369-375,(2011)
- [26] Buczynski R, Pysz D, Stepień R, Waddie A J, Kujawa I, Kasztelaniec R, Franczyk M and Taghizadeh M R" Supercontinuum generation in photonic crystal fibers with nanoporous core made of soft glass" *Laser Phys. Lett.* 8, 443-448,(2011)
- [27] Dharmadhikari A K, Rajgara F A and Mathur D" Plasma effects and the modulation of white light spectra in the propagation of ultrashort, high-power laser pulses in barium fluoride" *Appl.Phys. B* 82, 575-583,(2006)
- [28] Wang L, Fan Y-X, Yan Z D, Wang H-T and Wang Z-L "Flat-plateau supercontinuum generation in liquid absorptive medium by femtosecond filamentation. *Opt. Lett.* 35, 2925-2927,(2010)
- [29] Papazoglou D G and Tzortzakis S "In-line holography for the characterization of ultrafast laser filamentation in transparent media" *Appl. Phys. Lett.* 93, 041120- 041123 (2008)

- [30] Faccio D, Rubino E, Lotti A, Couairon A, Dubietis A, Tamošauskas G, Papazoglou D G and Tzortzakis S” Emission of correlated photon pairs from superluminal perturbations in dispersive media” *Phys. Rev. A* 85, 033829-033829-6, (2012)
- [31] Faccio D, Tamošauskas G, Rubino E, Darginavičius J, Papazoglou D G, Tzortzakis S, Couairon A and Dubietis A “Cavitation dynamics and directional microbubble ejection induced by intense femtosecond laser pulses in liquids,” *Phys. Rev. E* 86, 036304-06034-6,(2012)
- [32] Xu B, Gunn J M, Cruz J M D, Lozovoy V V and Dantus M “Quantitative investigation of the multiphoton intrapulse interference phase scan method for simultaneous phase measurement and compensation of femtosecond laser pulses,” *J. Opt. Soc. Am. B* 23 , 750-759, (2006)
- [33] Brodeur A and Chin S L “Band-Gap Dependence of the Ultrafast White-Light Continuum., *Phys. Rev. Lett.* 80, 4406 -4409,(1998)
- [34] Gaeta A L “Catastrophic Collapse of Ultrashort Pulses“*Phys. Rev. Lett.* 84, 16 (2000)
- [35] Sandhu A S, Banerjee S and Goswami D “Suppression of supercontinuum generation with circularly polarized light “*Opt. Commun.*181, 101-107(2000)
- [36] Hammer D X, Jansen E D, Frenz M, Noojin G D, Thomas R J, Noack J, Vogel A, Rockwell B A and Welch A J” Shielding properties of laser-induced breakdown in water for pulse durations from 5 ns to 125 fs “*Appl. Opt.* 36, 5630-5640,(1997)
- [37] Tiwari D, Bellouard Y, Dietzel A, Ren M, Rubingh E and Meinders E “Dynamical Observation of Femtosecond-Laser-Induced Bubbles in Water Using a Single Laser Source for Probing and Sensing” *Appl. Phys. Express* 3 ,127101-127101-3,(2010)
- [38] Sun X, Xu S, Zhao J, Liu W, Cheng Y, Xu Z, Chin S L and Mu G “Impressive laser intensity increase at the trailing stage of femtosecond laser filamentation in air“*Opt. Express* 20, 4790-4795,(2012)

- [39] Shaffer C B, Nishimura N, Glezer E N, Kim A M-T and Mazur E” Dynamics of femtosecond laser-induced breakdown in water from femtoseconds to microseconds” *Opt. Express* 3,10196-10124, (2002)
- [40] Geints Yu E and Zemlyanov A A “Characteristics of filaments at high-power femtosecond laser radiation propagation in air and water: II. Numerical simulation “*Atmos. Oceanic Opt.*24, 144-158,(2011)
- [41] Vogel A, Noack J, Nahen K, Theisen D, Busch S, Parlitz U, Hammer D X, Noojin G D, “Rockwell B A and Birngruber R “Influence of Optical Aberrations on Laser-Induced Plasma Formation in Water and their Consequences for Intraocular Photodisruption “*Appl. Phys. B* 68, 271-280(1999)
- [42] Minardi S, Gopal A, Tatarakis M, Couairon A, Tamosaukas G, Piskarskas R, Dubietis A and Trapani P D “Time-resolved refractive index and absorption mapping of light–plasma filaments in water”“*Opt. Lett.*33 ,86-88 (2008)
- [43] Tinne N, Schumacher S, Nuzzo V, Arnold C L, Lubatschowski Hand Ripken T” Interaction dynamics of spatially separated cavitation bubbles in water” *J. Biomed. Opt.*15, 068003-068003-10 (2010)
- [44] I. Akhatov, N.Vakhitova, A.Topolnikov, K. Zakirov, B.Wolfrum, T.Kurz, O. Lindau, R.Mettin, W.Lateurborn” Dynamics of laser induced cavitation bubbles“ *Experimental Thermal and Fluid Science* 26 ,731–737 (2002)

NONLINEAR OPTICAL CHARACTERIZATION OF DNA DOPED RHODAMINE 6G-PVA FILMS USING PICOSECOND PULSES

7.1.	Introduction
7.2.	Experimental Techniques
7.3.	Nonlinear optical measurements- Z-Scan
7.4.	Synthesis of dye doped DNA-PVA film
7.5.	Results and Discussion
7.6.	Conclusion

Abstract

We present our results from the measurements of third-order optical nonlinearity in DNA doped Rhodamine 6G/PVA films achieved through Z-scan measurements using ~2 picosecond (ps) pulses at a wavelength of 800 nm. The films demonstrated negative nonlinear refractive index (n_2) with magnitudes of $(0.065 - 2.89) \times 10^{-14} \text{ cm}^2/\text{W}$ with varying concentration of DNA. Open aperture data demonstrated strong two-photon absorption with a magnitude of ~1.6 cm/GW for films doped with 2 wt% of DNA. These data suggests that DNA is a promising material for photonic applications such as optical switching.

7.1. Introduction

Deoxyribonucleic acid (DNA), a highly nonlinear bio- organic polymer, has been investigated as a photonic material recently with adequate success [1-14]. Biomaterials are interesting due to their remarkable properties which are not easily replicated with conventional organic or inorganic materials in the laboratory. Furthermore, natural biomaterials are a renewable resource and are inherently biodegradable [1]. Two DNA strands organize a DNA double helix through hydrogen bonds between the bases and are stabilized by π - π interactions [2]. DNA in solid-state (thin-film) form has unique combination of optical and electronic properties, which forms the foundation of DNA photonics [3-4]. This potentially viable organic polymer has established various applications in organic light emitting diodes (OLED), organic thin film transistors, polymer electro-optic modulators, polymer lasers etc. [5-6]. OLEDs containing DNA electron blocking layers have been recently reported [7] to exhibit significant enhancement in luminance and luminous efficiency [8]. DNA films produced by treating aqueous solution of DNA with a cationic surfactant such as cetyl trimethyl ammoniumchloride (CTMA) and doped with Sulphorhodamine (SRh) have been reported to exhibit photoluminescence intensity more than an order of magnitude higher than that of SRh in PMMA [10]. Dye doped DNA media have demonstrated amplified spontaneous emission with pulsed laser excitation [11]. Sznitko *et al.* [13] successfully demonstrated amplified spontaneous emission and lasing action in deoxyribonucleic acid blended with cetyltrimethyl-ammonium chloride surfactant and doped with 3-(1,1-dicyanoethenyl)-1phenyl-4,5dihydro-1H-pyrazole organic dye. Hanczyc *et al.* [14] observed remarkable multiphoton absorption properties of DNA intercalating ruthenium complexes such as $[\text{Ru}(\text{phen})_2 \text{ dppz}]$, $[(11,11' \text{- bidppz})(\text{phen}) 4\text{Ru}_2]^{4+}$ and $[11,11' \text{- bipb} (\text{phen})$

4Ru2]4+ in the spectral range of 460 to 1100 nm. Nonlinear optical (NLO) properties of DNA in solution form [15] and in silica films [16] have been investigated recently. Our group recently reported the NLO properties of Rhodamine 6G-PVA solutions doped with DNA where we observed saturable absorption (SA) at lower concentration of DNA and switching behavior at higher concentrations [17]. We expect completely different performance in thin film form and with shorter pulse excitation since the intersystem crossing rates are much slower compared to the pulse duration [18]. Moreover, for any novel nonlinear optical (NLO) material investigated, one needs to apprehend the linear absorption, nonlinear absorption, and nonlinear refractive index magnitudes in various forms such as solutions and thin films to establish their potential in appropriate fields of interest.

7.2 Nonlinear optical measurements- Z-Scan

The Z-scan measurement technique, a simple experimental procedure devised by Sheik–Bahae [19, 22], has been extensively used to characterise the optical nonlinearities of materials. It is a sensitive as well as a single beam technique; comparable to interferometric methods. This method employs the principle of spatial beam distortion for the determination of both sign and magnitude of the refractive and absorptive nonlinear coefficients. The sensitivity of the Z-scan technique is enhanced by the applications of novel extensions such as EZ-scan (eclipsed Z-scan) [23], reflection Z scan, Z scan using top hat beams, dual wavelength (two color) Z scan[24-25] . In EZ Scan, the wings of a circular Gaussian beam are much more sensitive to the far-field beam distortion whereas the dual wavelength (two-color) extension of the standard Z-scan technique has been used to measure the non-degenerate nonlinearities. The dual wavelength extension of Z scan is utilised to study the

time resolved dynamics of the sample by introducing a time delay between the pump and probe. A reflection Z-scan technique was introduced to study the optical nonlinearities of surfaces. The standard experiment uses a Gaussian beam from a laser in tight focus geometry to measure the transmittance of a nonlinear medium through a finite aperture in the far field as a function of the sample position Z, from the focal plane. This technique is called closed aperture Z-Scan in which the transmitted light is sensitive to both nonlinear absorption and nonlinear refraction [19,22] In addition to this, the sample transmittance without an aperture is also measured to extract complementary information about the absorptive nonlinearities of the sample and this mode of measurement is referred to as open aperture z-scan [19].

7.2.1 Nonlinear Absorption

Nonlinear absorption refers to the change in transmittance of a material as a function of intensity or fluence [27] and the Open aperture z-scan technique is used to measure nonlinear absorption in the sample. At low intensities, the light absorbed by a medium shows a linear increase with the incident power, resulting in constant transmittance whereas at high intensities, enhanced absorption of radiation is observed due to multiphoton absorption. The former case, termed as linear absorption can be fully explained by Beer Lamberts law

$$I(z) = I(0) \exp - (\alpha(\omega)z), \quad (7.1)$$

where $I(0)$ is the incident intensity, $\alpha(\omega)$ is the linear absorption coefficient, z is the propagation depth in the absorbing medium and $I(z)$ is the intensity at a depth z . Any deviation from this law is referred to as non linear absorption.

The enhanced absorption of radiation at high intensities due to multiphoton absorption, population redistribution, complicated energy

transitions in complex molecular systems and the generation of free carriers are accompanied by the intense optical fields. These phenomena are manifested optically in a reduced (saturable) or increased (reverse saturable) absorption. Reverse saturable absorption (RSA) is the result of two photon absorption (2PA) or multiphoton absorption (MPA) and excited state absorption (ESA). Two photon absorption (2PA) involves a transition from ground state (1) of a material to a higher lying state (2) by simultaneous absorption of two photons via an intermediate virtual state [29], as schematically shown in figure 7.2

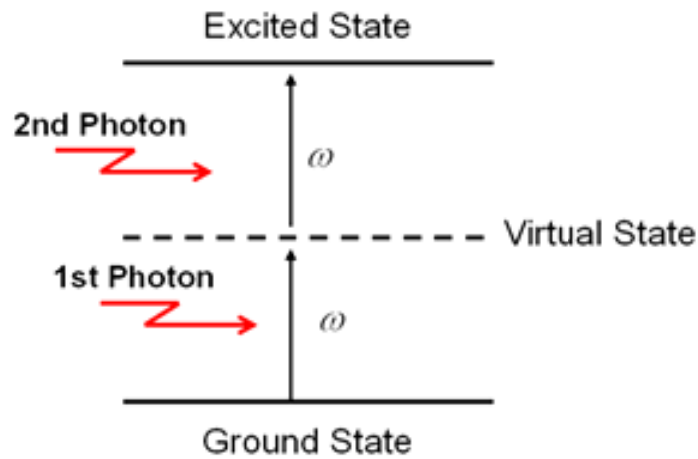


Figure 7.2. Diagrammatic representation of two photon absorption mechanism Picture taken from reference

The nonlinear absorption in this case is proportional to the square of the instantaneous intensity and is given by $\frac{dI}{dz} = -\alpha(I) - \beta I^2$ (7.2)

where α is the linear absorption and β is the two photon absorption coefficient. Multiphoton absorption refers to the simultaneous absorption of n photons from a single beam or multiple beams. The absorption of $(n+1)$ photons from a single optical beam is given by $\frac{dI}{dz} = (-\alpha + \gamma^{(n+1)} I^n) I$ (7.3)

where $\gamma^{(n+1)}$ is the (n+1) photon absorption coefficient.

In organic molecules, transitions are possible to higher energy singlet and triplet manifolds. The excited electrons can rapidly make a transition to higher excited states before it eventually make transitions back to the ground state. There are also a number of higher lying states that may be radiatively coupled to these intermediate states, and for which the energy differences are in near-resonance with the incident photon energy. Therefore, before the photon relaxes to the ground state, it may experience absorption that promotes it to a higher-lying state. This process is called Excited State Absorption (ESA).

When the absorption cross section σ_{12} from the first excited molecular state to the higher state is greater than σ_{01} from ground state to first excited state, more molecules are promoted to the excited state with the increase in the optical excitation energy, thus giving rise to higher absorption. This is called Reverse Saturable Absorption (RSA). When the absorption cross-section from excited state (σ_{12}) is smaller than that from the ground state (σ_{01}), the transmission of the system will be increases with high intensity laser beam. This process is called saturable absorption(SA).

7.2.2 Open Aperture Z-scan to study NLA

Open aperture z-scan technique is employed to measure absorptive nonlinearity in the sample. If nonlinear absorption such as two photon absorption is present, it is manifested in the measurements as a transmission minimum at the focal point.[19].The presence of multi-photon absorption suppresses the peak and enhances the valley, while saturation of absorption produces the opposite effect. The sensitivity of the experiment to refractive nonlinearities is entirely due to the aperture. The removal of the aperture will make the Z-scan sensitive to absorptive nonlinearities alone.

In the low excitation regime, the intensity dependent nonlinear absorption coefficient $\alpha(I)$ can be written in terms of linear absorption coefficient α and 2PA coefficient β as

$$\alpha(I) = \alpha + \beta I \quad (7.4)$$

This modifies the irradiance distribution at the exit surface of the sample as

$$I(z, r, t) = \frac{I(z, r, t)e^{-\alpha z}}{1 + q(z, r, t)} \quad (7.5)$$

where $q(z, r, t) = \beta I(z, r, t)L_{eff}$ (7.5(a))

L_{eff} is the effective length and is given in terms of the length of the sample by the relation $L_{eff} = \frac{(1 - e^{-\alpha L})}{\alpha}$ (7.6)

The total transmitted power $P(z, t)$ is obtained by integrating equation over z and r and is given by

$$P(z, t) = P_I(t)e^{-\alpha z} \frac{\ln(1 + q_0(z, t))}{q_0(z, t)} \quad (7.7)$$

where $P_I(t)$ and $q_0(z, t)$ are given by

$$P_I(t) = \frac{\pi w_0^2 I_0(t)}{2} \quad (7.7(a))$$

$$q(z, r, t) = \frac{\beta I_0(t)L_{eff}z_0^2}{z^2 + z_0^2} \quad (7.7(b))$$

Assuming a spatial and temporal Gaussian profile for laser pulses and utilizing the open aperture Z-scan theory for two photon absorption (2PA)

given by Sheik-Bahae et al. [19] , the equation for 2PA open aperture (OA) normalized power transmittance given by

$$T(z) = \frac{c}{\pi^{1/2} q_0} \int_{-\infty}^{+\infty} \ln(1 + q_0 e^{-\tau^2}) d\tau \quad (7.8)$$

If $|q_0| < 1$, the equation (7.8) can be written as

$$T(z, S = 1) = \sum_{m=0}^{\infty} \frac{(-q_0(z, 0))^m}{(m+1)^{3/2}} \quad (7.9)$$

where m is an integer. Once open aperture Z-scan is performed, the parameter q_0 can be obtained by fitting the experimental results to equation (7.8). Then the nonlinear absorption coefficient can be unambiguously deduced using equation (7.5(a)). The imaginary part of third order susceptibility $\chi^{(3)}$ determines the strength of the nonlinear absorption. The 2PA coefficient is related to $\text{Im} \chi^{(3)}$ by the relation

$$\text{Im}(\chi^{(3)}) = \frac{\epsilon_0 n_0^2 c^2 \beta}{\omega} (m^2 V^{-2}) = \frac{n_0^2 c^2 \beta}{240 \pi^2 \omega} (esu) \quad (7.10)$$

where λ is the excitation wavelength, n_0 is the linear refractive index, ϵ_0 is the permittivity of free space and c the velocity of light in vacuum.

7.2.3 Closed-aperture Z-scan for sign and magnitude of refractive nonlinearity

Closed aperture Z-scan is an example of self-refraction phenomenon or self phase modulation in space. In the absence of nonlinear absorption, a well-defined peak and valley are observed .A sample displaying nonlinear refraction will acts as a lens of variable focal length as it moves along the z axis.

Consider, for instance, a material with a negative nonlinear refraction and of thickness smaller than the diffraction length (also known as Rayleigh length, $z_0 = \frac{\pi\omega_0^2}{\lambda}$) of the focused beam being positioned at various positions along the Z-axis. Z-scan technique is highly sensitive to the profile of the beam and also to the thickness of the sample. Any deviation from Gaussian profile of the beam and also from thin sample approximation will give rise to erroneous results. For ensuring that the beam profile does not vary appreciably inside the sample, the sample thickness should always be kept less than the Rayleigh range.

The sample under consideration is treated as a thin lens of variable focal length due to the change in the refractive index at each position ($n = n_0 + n_2I$). When the sample is far from the focus and closer to the lens, it exhibits negligible nonlinear refraction. At this position the irradiance is quite low and the transmittance characteristics are linear. Hence transmittance through the aperture is fairly constant at this region. As the sample is moved closer to the focus, the increased irradiance induces a negative lens effect which collimates and shifts the waist of the laser beam. This results in the narrowing of beam leading to an increase in the measured transmittance at the aperture. A maximum transmittance through the aperture is obtained when the sample is placed just in front of the focus. As the scan in z direction continues and passes the focal plane, the sample which acts as a negative lens increases the defocusing effect and tend to diverge the beam, resulting in the decrease in transmittance. The maximum transmittance (peak) will drop to a minimum (valley) as the sample is moved further and the beam diverges as a result of negative lensing of the sample. A pre focal transmittance maxima followed by a post focal transmittance minima is the z-scan signature of negative refraction nonlinearity.

It is worthwhile to visualize the various processes taking place in the sample, and its effect on the transmitted beam profile, as we scan the sample across the beam focus. While the input energy measured is kept unchanged, the medium experiences different incident irradiance at different positions, which is decided by the position dependent beam spot size $w(z)$, given by,

$$w^2 = w_0^2 \left(1 + \frac{z^2}{z_0^2} \right) \quad (7.11)$$

Nonlinear refraction in the medium induces a phase distortion in the beam profile that causes a change in the fraction of light passing through the aperture kept at far field. Therefore the aperture transmittance is a function of the sample position z . In this way of describing z -scan, it is assumed that a purely refractive nonlinearity is present and that there are no absorptive nonlinearities such as multiphoton or saturation of absorption in the material.

Non linearity of any order can be measured using this technique, but for simplicity we are considering the cubic nonlinearity, in which refractive index n can be described as

$$n = n_0 + \frac{n_2}{2} |E|^2 \quad \text{or} \quad n = n_0 + \gamma I \quad (7.12)$$

where n_0 is the linear index of refraction, E is the peak electric field (cgs), and I denotes the irradiance (MKS) of the laser beam within the sample. (n_2 , and γ are related through the conversion formula $n_2 = \left(\frac{cn_0}{40\pi} \right) \gamma$ (m^2/W) where c (m/s) is the speed of light in vacuum. The nonlinear refractive index is determined by several physical mechanisms, acting on a broad range of time scales. It is therefore necessary to be explicit about the contributing mechanisms in a

particular experiment. The various contributions to n_2 are $n_2 = n_2$ (electronic) + n_2 (vibrational) + n_2 (electrostriction) + n_2 (thermal). The response times of these various contributions can be estimated from simple arguments. The electronic and vibrational response times can be obtained from the frequencies of optical transitions involving the bound electrons and lattice vibrations; these are 10^{-15} s and 10^{-13} s respectively. The electrostrictive response time is roughly equal to the time required for an acoustic deformation to travel across the diameter of the optical beam which therefore depends on the geometry of the experimental set up, the optics used for creating the beam waist in the laser beam etc. In most experimental conditions using nanosecond pulses, this will be in the range of a few nanoseconds. By suitably choosing the optics and the beam parameters, it is possible to neutralize this effect if one desires so. Thermal diffusion time scales are even longer, and depend on the thermal properties of the medium.

Now let us consider the propagation of an intense laser beam through a material. At high intensities such as at the peak of an ultrashort laser pulse, the refractive index of any medium becomes a function of the incident intensity. Assuming a TEM₀₀ Gaussian beam of beam waist radius w_0 traveling in the +z direction, we can write E as

$$E(z, r, t) = E_0(t) \frac{\omega_0}{\omega(z)} \exp\left(\frac{-r^2}{\omega_z^2} - \frac{ikr^2}{2R_z(z)}\right) e^{-i\phi(z,t)} \quad (7.13)$$

where the radius of curvature, R is defined as $R(z) = z \left(1 + \frac{z_0^2}{z^2}\right)$, z_0 being the Rayleigh range, or depth of focus. $E_0(t)$ denotes the radiation electric field at the focus and contains the temporal envelope of the laser pulse. The $e^{-i\phi(z,t)}$ term

contains all the radially uniform phase variations. For calculating the radial phase variations $\Delta\varphi(r)$ the slowly varying envelope approximation (SVEA) is used and all other phase changes that are uniform in r are ignored.

$L \ll \left(\frac{z_0}{\Delta\varphi(0)} \right)$, where L is the sample length, and the amplitude \sqrt{I} and phase φ of the electric field as a function of z' are now governed in the SVEA by a pair of simple equations

$$\frac{d\varphi}{dz'} = \Delta n(I)K \quad (7.14)$$

$$\frac{d\varphi}{dz'} = -\alpha(I)I \quad (7.15)$$

where z' is the propagation depth in the sample and $\alpha(I)$ in general includes linear and nonlinear absorption terms. In the case of cubic nonlinearity and negligible nonlinear absorption, the above equations (7.14) and equation (7.15) can be solved to get the phase shift $\Delta\varphi$ at the exit of the sample and is given by

$$\Delta\varphi(z, r, t) = \Delta\varphi(z, t) \exp\left[-\frac{-2r^2}{w^2(z)}\right] \quad (7.16)$$

$$\Delta\varphi(z, r, t) = \frac{\Delta\varphi_0(t)}{1 + \frac{z_0^2}{z^2}} \quad (7.17)$$

where $\Delta\varphi_0(t)$ is the on axis phase shift at the focus which is defined as

$$\Delta\varphi_0(t) = k\Delta n_0(t)L_{eff} = \frac{2\pi}{\lambda} n_2 I_0(t)L_{eff} \quad (7.18)$$

where $I_0(t)$ is the on axis irradiance at focus (i.e. at $z=0$).

The electric field at the exit surface of the sample now contains the nonlinear phase change and is expressed as,

$$E_e(z, r, t) = E(z, r, t) e^{\frac{-\alpha l}{2}} e^{i\Delta\varphi(z, r, t)} \quad (7.19)$$

To find out the field at the detector plane, one uses the Gaussian decomposition method (GD method) adopted by Weaire et al [29] For this, the nonlinear phase term is expanded as a Taylor series which modifies E, in equation (7.19) as a sum of infinite number of Gaussian beams. Thus

$$e^{i\Delta\varphi(z, r, t)} = \sum_{m=0}^{\infty} \frac{i\Delta\varphi(z, t)^m}{m!} \exp\left(\frac{-2mr^2}{w^2(z)}\right) \quad (7.20)$$

These Gaussian beams are individually propagated to the aperture plane and then added to get the resultant field, E_α .

$$E_\alpha(r, t) = E(z, r=0, t) \exp\left(\frac{-\alpha d}{2} \sum_{m=0}^{\infty} \frac{i\Delta\varphi(z, t)^m}{m!} \frac{w_{m0}}{w_m} \exp\left(\frac{-r^2}{w^2(z)}\right) - \frac{ikr^2}{2R_m} i\theta_m\right) \quad (7.21)$$

Defining d as the propagation distance in free space from the sample to the aperture plane and $g = 1 + \frac{d}{R(z)}$, the remaining parameters in the equation (7.21) are expressed as

$$g = 1 + \frac{d}{R(z)}; w_{m0}^2 = \frac{w^2}{2m+1}; d_m = \frac{kw_{m0}^2}{2}; \theta_m = \tan^{-1}\left[\frac{d/d_m}{g}\right]; w_{m0}^2 = \frac{w^2}{2m+1}$$

$$w_m^2 = w_{m0}^2 \left[g^2 + \frac{d^2}{d_{m0}^2} \right]; Rm = d \left[1 - \frac{g}{g^2 + \frac{d^2}{d_m^2}} \right]^{-1}$$

The on-axis electric field at the aperture plane can be obtained by putting $r=0$ in equation (7.21). In the limit of small nonlinear phase change ($\Delta\varphi_0 < 1$) only two terms in the sum in equation (7.21) needs to be retained. The normalized z-scan transmittance can be written as

$$T(z, \Delta\varphi_0) = \frac{|E_a(z, r=0, \Delta\varphi_0)|^2}{|E_a(z, r=0, \Delta\varphi_0)|^2} \quad (7.22)$$

$$= \frac{\left| \left(g + \frac{id}{d_0} \right)^{-1} + i\Delta\varphi_0 \left(g + \frac{id}{d_0} \right)^{-1} \right|}{\left| \left(g + \frac{id}{d_0} \right)^{-1} \right|^2} \quad (7.22.(a))$$

The far field condition $d \gg z_0$ can give a geometry-independent normalized transmittance as $T(z, \Delta\varphi_0) = 1 - \frac{4\Delta\varphi_0 x}{(x^2 + 9)(x^2 + 1)}$ (7.23)

where $x = \frac{z}{z_0}$

For a cubic nonlinearity, the peak and valley of the z-scan transmittance can be calculated by solving the equation $\frac{dT(z, \Delta\varphi_0)}{dz} = 0$ (7.24)

Solution to this equation(24) yields the peak valley separation as

$$\Delta z_{p-v} = 1.7 z_0 \quad (7.25)$$

Then the peak valley transmittance change is $\Delta T_{p-v} = 0.406 \Delta\varphi_0$ (7.26)

Numerical calculations show that this relation is accurate to 0.5% for $\Delta\varphi_0 \leq \pi$ For large aperture, this equation is modified within a $\pm 2\%$ accuracy and is given by $\Delta T_{p-v} = 0.406(1-s)^{0.25} |\Delta\varphi_0|$ for $|\Delta\varphi_0| < \pi$ (7.27)

where S is the linear transmittance of the far field aperture. From the closed aperture z-scan fit, $|\Delta\varphi_0|$ can be obtained. Then the nonlinear refractive index n_2 can be determined using equation (7.18) and is given by

$$n_2 \left(\frac{m^2}{W} \right) = \frac{\lambda}{2\pi d_0 L_{eff}} \Delta\varphi_0 \quad (7.28)$$

$$n_2 \left(\frac{m^2}{W} \right) = \frac{\lambda}{2\pi I_0 L_{eff}} \Delta\varphi_0 \quad (7.28)$$

$$n_2 (esu) = \frac{cn_0\lambda}{40\pi 2\pi I_0 L_{eff}} \Delta\varphi_0 \quad (7.29)$$

n_2 is related to $\text{Re}(\chi^{(3)})$ by the relation,

$$\text{Re}(\chi^{(3)}) = \frac{n_0 n_2 (esu)}{3\pi} \quad (7.30)$$

From the real and imaginary part of $(\chi^{(3)})$ the modulus of third order nonlinear susceptibility can be found out.

$$|\chi^{(3)}| = \sqrt{\text{Re}(\chi^{(3)})^2 + \text{Im}(\chi^{(3)})^2} \quad (7.31)$$

The magnitude of $\chi^{(3)}$ is significantly affected by the molecular orientation and it determines the strength of nonlinearity of the material.

7.3 Materials and Methods

We had used DNA powder (SRL, extracted from herring sperm) of appropriate amount in polyvinyl alcohol solution (PVA-Merck) for carrying out the nonlinear optical studies. Since DNA and PVA are water soluble it is very easy to make thin films of DNA-PVA mixture. PVA solution acts as a good matrix for hybridization of functional molecules and has excellent film forming, emulsifying, and adhesive properties. In the DNA-PVA system we have incorporated Rhodamine 6G owing to its high fluorescence quantum yield, low intersystem crossing rate, and little excited state absorption [18]. PVA solutions (8 wt%) were prepared by dissolving appropriate amount of PVA in distilled water at 80°C under continuous stirring for 3 hr. Weighed DNA powder was added to the prepared PVA solution. Rhodamine 6G dye was then added to

technique. Obtained films exhibited good optical transparency in the visible spectral range. The absorption spectra of prepared DNA films were characterized by using UV-VIS NIR spectro-photometer (Jasco V-570). Henceforth, pure Rh6G-PVA films are denoted as Rh6GPVA, DNA 1 wt% doped films are denoted as DNA1, and DNA 2 wt% doped films are denoted as DNA2.

7.4 Experimental Technique

NLO measurements were performed by Z –scan on DNA1, DNA2 films with thickness of ~ 100 μm . The Z-scan measurements [19] were performed using ~ 2 ps, 800 nm pulses with a repetition rate of 1 kHz from an amplified Ti:sapphire system (Legend, Coherent). The amplifier was seeded with ~ 15 fs pulses from the oscillator (Coherent, Micra). The beam waist ($2\omega_0$) at focal plane was estimated to be ~ 60 μm ($\text{FW1}/e^2\text{M}$) with a corresponding Rayleigh range (Z_r) of 3.5 ± 0.4 mm ensuring the validity of thin sample approximation. The input beam was spatially filtered to obtain a pure Gaussian profile in the far field. Z-scan studies [19,20,21] were performed by focusing the 3-mm diameter input beam using a 200 mm focal length convex lens into the sample in the psec domain. The sample was placed on a high resolution translation stage and the detector (Si photodiode, SM1PD2A, Thorlabs) output was connected to a lock-in amplifier. Both the stage and the lock-in amplifier were controlled by a computer program. Closed aperture scans were performed at intensities where the contribution from the higher order nonlinear effects is negligible and the value of $\Delta\phi$ estimated in all the cases was $< \pi$. The experiments were repeated more than once and the best data were used for obtaining the nonlinear optical coefficients from the best fits. Schematic of the experiment is shown in figure 7.1

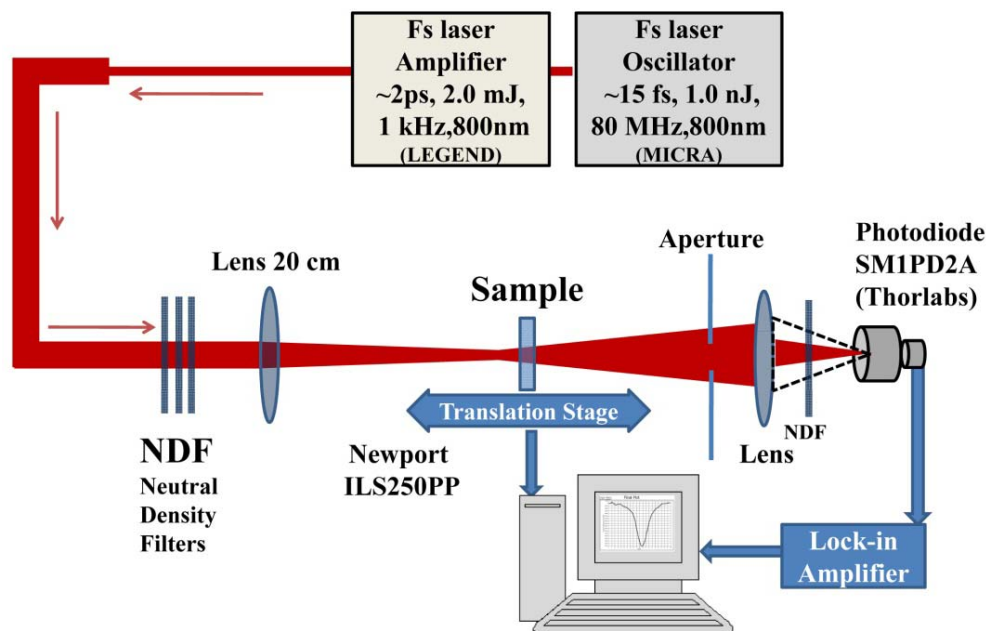


Figure7. 1: Schematic for Nonlinear Optical Measurements using Z-Scan technique.

7.5 Results and Discussion

Figure7.3 illustrates the linear absorption spectra of DNA1 film and Rh6GPVA film. Figure 7.3(a) shows the presence absorption peak near 260 nm which is the characteristic of DNA. The peak is due to $\pi-\pi^*$ (where π represents bonding orbitals and π^* represents anti-bonding orbitals) transition of the electrons of C = C bond in DNA bases [10]. The prominent absorption peak of Rh6G, near 532nm, is evident from Figure7. 3(b).

Z-scan studies were performed by focusing the input beam using an achromatic doublet ($f = 200$ mm) for ps excitation. The peak intensities used in experiments were in the 100-150 GW/cm^2 . All the studies were performed with thin films of thickness ~ 100 micrometer providing $\sim 80\%$ linear transmission at

800nm. We maintained similar intensity levels to ensure identical experimental conditions for all the samples.

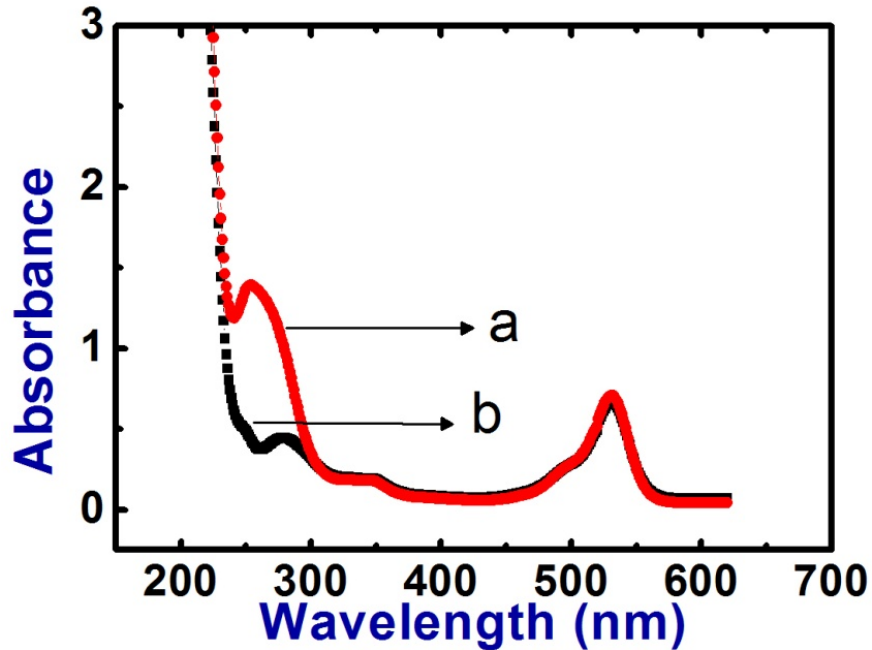


Figure7. 3 Absorption spectra and (a) Rh6G - DNA-PVA film
(b) Rh6G-PVA film

7.5.1 Two photon absorption with 800nm, 2ps pulses

Figures 7.4 (a) to (d) show the open aperture data (open circles) of DNA doped Rh6GPVA thin films DNA1 and DNA2 recorded at 800 nm with 2 ps pulses and input peak intensities in the range of 100-130 GW/cm^2 . The presence of valley in normalized transmittance in open aperture (OA) scans indicates strong reverse saturable absorption (RSA) at these peak intensities beyond which the sample was damaged which was indicated by the discoloration of solutions.

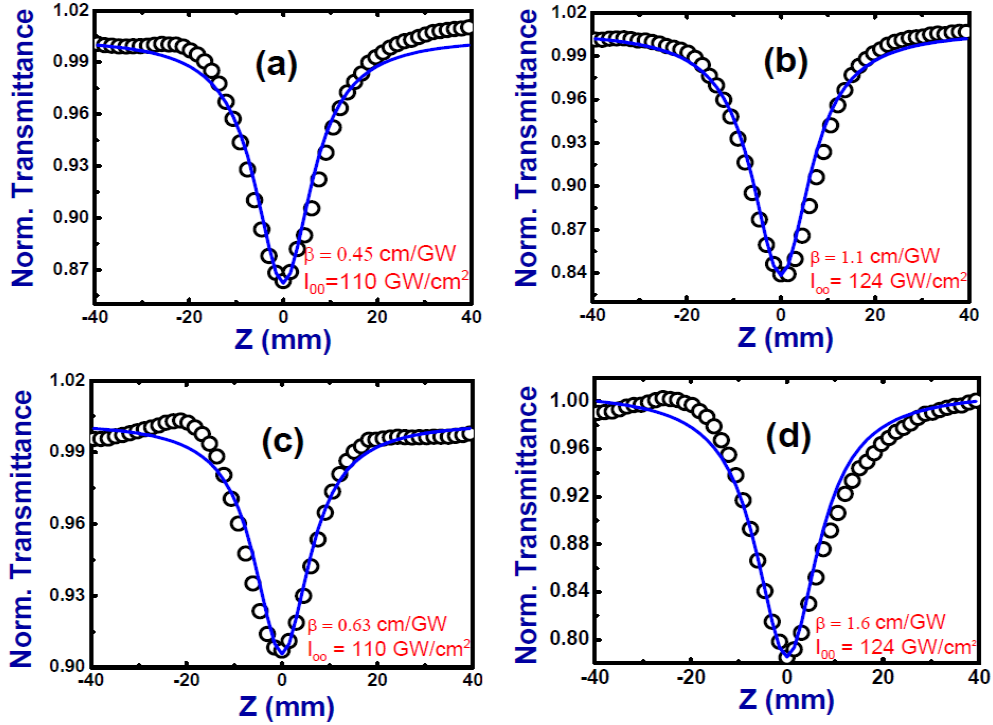


Figure 7. 4 Open aperture Z scan curves for (a) DNA1, 110 GW/cm² (b) DNA1, 124 GW/cm² (c) DNA2, 110 GW/cm² and (d) DNA2, 124 GW/cm². Open circles indicate the experimental data while the solid (blue) lines indicate theoretical fits

We have observed strong reverse saturable absorption (RSA) kind of behaviour in the intensity range mentioned above. For higher peak intensities the sample was damaged and indicated by the discoloration of the film. Obtained experimental data were fitted using equations

$$T_{OA}(2PA) = \frac{1}{\pi^{1/2} q_0} \int_{-\infty}^{+\infty} \ln \left(1 + q_0(z, 0) e^{-\tau^2} \right) d\tau \quad (7.32)$$

for two-photon absorption (2PA, β)

$$T_{OA}(3PA) = \frac{1}{\pi^{1/2} p_0} \int_{-\infty}^{+\infty} \ln \left\{ \left[1 + p_0^2 e^{-2\tau^2} \right]^{1/2} + \left[p_0 e^{-\tau^2} \right] \right\} d\tau \quad (7.33)$$

for three-photon absorption (3PA, γ)

where $q_0 = \beta L_{eff} I_{00}$, $p_0 = 2\gamma L_{eff}' I_{00}^2$, β =2PA coefficient, γ =3PA coefficient, L_{eff} and L_{eff}' is the effective path length in sample of length L for 2PA and 3PA respectively. I_{00} is the peak intensity at the focus.

We found the best fit was obtained with the transmission equation for two-photon absorption (2PA). The blue solid line in the figures (7.5.a) to (7.5.d) represent the theoretical fit with equation for two photon absorption (7.32) and the solid red line with equation for three photon absorption (7.33). It is evident that 2PA is the dominant mechanism for the observed RSA kind of behaviour. 3PA fits are also shown in the figures (7.5.a) to (7.5.d) for comparison and undoubtedly the fits are off from the experimental data.

Sample	Power (mW)	I_{00} (GW / cm ²)	$\beta \times 10^{-9}$ (cm / W)
Rh6GPVA	4mW	110.44	0.26
DNA1	4mW	110.44	0.45
	4.5mW	124.25	1.10
DNA2	4mW	110.44	0.63
	4.5mW	124.25	1.61

Table: 7.1 Nonlinear absorption properties with open aperture Z- scans:

The fits from Figure 7.4(a) (110 GW/cm²) provided a 2PA coefficient of 0.45 cm/GW and Figure 7.4(b) (124 GW/cm²) provided 2PA coefficient of 1.10 cm/GW for DNA1. The magnitude of β for DNA2 retrieved from the fits was 0.635 cm/GW for 110 GW/cm² and 1.61 cm/GW for 124 GW/cm². The magnitude of β in Rh6GPVA film was < 0.25 cm/GW.

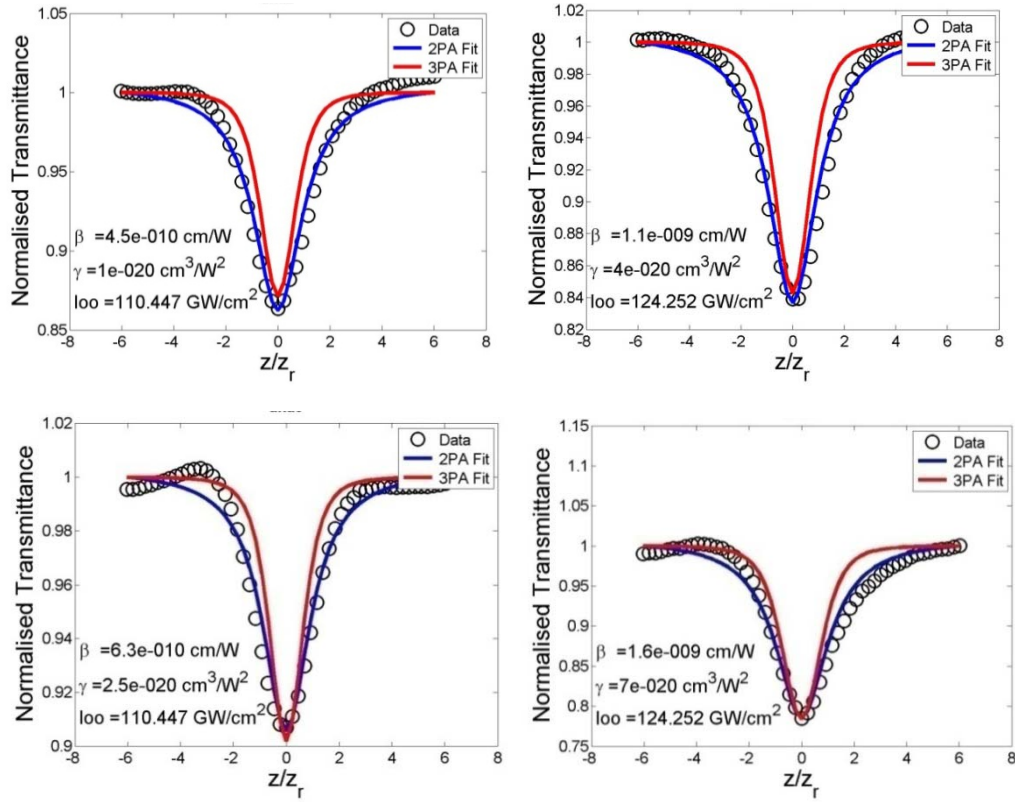


Figure 7.5 Open apertures Z scan curves for DNA 1 and DNA 2 obtained with 800nm, 2 ps pulses. Open circles experimental data while the blue solid line represents theoretical fits with two photon absorption. Red solid lines represent the fit with three photon absorption. Top two figures refer to DNA 1, bottom two figures refer to DNA 2

7.5.2 Nonlinear refraction properties with closed aperture Z- scans

Figure 7.6 illustrate the typical closed aperture Z-scan curve obtained for DNA1, DNA2, and R6GPVA, respectively, recorded with a peak intensity of $\sim 110 \text{ GW/cm}^2$. These curves represent normalized data obtained after division of closed aperture data with the open aperture data to eliminate the contribution of nonlinear absorption. The curves were obtained at low peak intensities to avoid contributions to the nonlinearity that are not electronic in origin. It is apparent that both DNA1 and DNA2 show negative nonlinearity as

indicated by the peak-valley structure. The closed aperture data, T_{CA} , were fitted to the equation

$$T_{CA} = 1 - \frac{4\Delta\varphi_0 \left(\frac{z}{z_0} \right)}{\left[1 + \left(\frac{z}{z_0} \right)^2 \right] \left[9 + \left(\frac{z}{z_0} \right)^2 \right]} \quad (7.34)$$

where $\Delta\varphi_0$ is the phase change. We have evaluated the non linear refractive

index using $n_2(\text{cm}^2\text{W}^{-1}) = \frac{|\Delta\varphi_0|\lambda}{2\pi I_{00} L_{eff}}$ (7.35)

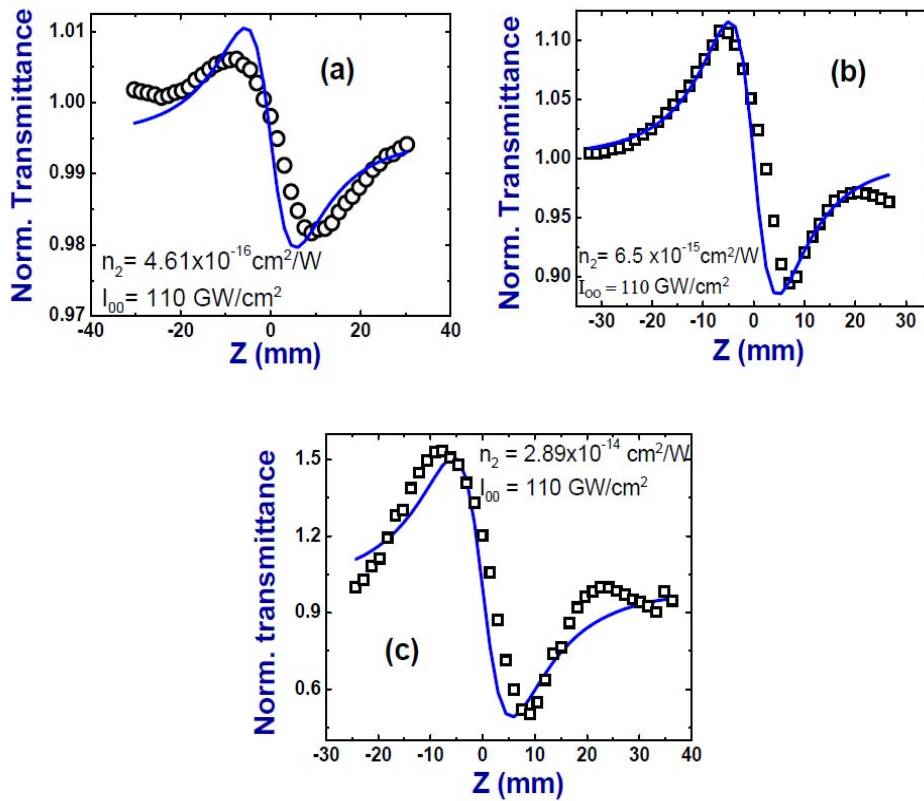


Figure 7.6 Closed aperture Z-scan curves for (a) R6GPVA film (b) DNA1 film and (c) DNA2 film. Circles/squares represent the data while the solid (blue) lines indicate theoretical fits

The observed phase change ($\Delta\phi_0$) was less than π ($\Delta\phi_0=0.51$ for DNA 1 and 2.51 for DNA 2 respectively.). The magnitude of n_2 was $\sim 4.61 \times 10^{-16} \text{ cm}^2\text{W}^{-1}$ for Rh6G doped PVA film. The magnitude of n_2 for DNA1 was $\sim 6.5 \times 10^{-15} \text{ cm}^2\text{W}^{-1}$ while for that of DNA2 was $\sim 2.89 \times 10^{-14} \text{ cm}^2\text{W}^{-1}$. Both the magnitudes were higher than that of n_2 recorded in Rh6GPVA. Enhancement in n_2 can be attributed to increase of charge transfer, which takes place in the system and is due to the presence of many highly polarizable conjugated π electrons of DNA [17]. Moreover, the interactions due to intercalation into base pair stack at the core of double helix and/or insertion into the minor groove of DNA are documented to have strong impact on the optical characteristics. The magnitudes of n_2 ($10^{-14} \text{ cm}^2\text{W}^{-1}$) obtained here are at least one order higher than those obtained in solution form ($10^{-14} \text{ cm}^2\text{W}^{-1}$) using femtosecond pulses [15]. The magnitudes of 2PA coefficient obtained (1.61 cm/GW) are again higher than those obtained (0.2 cm/GW) in solutions [15]. Krupka et al. [26] obtained purely electronic, fast NLO susceptibility in a DNA–CTMA complex thin film with a third-order nonlinear optical susceptibility magnitude of 10^{-14} e.s.u. In our case the magnitudes of $\chi^{(3)}$ were estimated to be 8.45×10^{-13} e.s.u. for DNA1 and 2.72×10^{-12} e.s.u. for DNA2, respectively.

Sample	I_{00} (GW/cm ²)	$n_2 \times 10^{-14}$ (cm ² /W)
Rh6GPVA	110	- 0.46
DNA1	110	- 0.65
DNA2	110	- 2.89

Table 7.2. Nonlinear refraction properties with closed aperture Zscan

7.6 Conclusions

- We studied the NLO properties of thin films of Rhodamine 6G, doped with DNA, obtained using ps pulses.
- The addition of DNA enhanced the NLO properties of thin films. We identified that the films demonstrated negative n_2 with a highest magnitude of $2.89 \times 10^{-14} \text{ cm}^2/\text{W}$ for DNA2 films.
- Open aperture data demonstrated strong 2PA with a highest magnitude of $\sim 1.6 \text{ cm/GW}$, again for DNA2 films.
- We conclude that PVA is a good matrix for fluorescent dyes incorporated into the double helix of DNA molecule enabling them suitable for practical applications in optical devices.

References

- [1] P. N. Prasad, "Introduction to Bio-Photonics," Wiley, New York, 2003.
- [2] N. Kitazawa, S. Miyagawa, K. Date, W. Aroonjaeng, M. Aono and Y. Watanabe, "Optical Properties of Dye-Doped Deoxyribonucleic Acid Films," *Journal of Materials Science*, 44, 4999-5003, (2009).
- [3] A. J. Steckl, "DNA—A New Material for Photonics?" *Nature Photonics*, 1, 3-5,(2007)
- [4] J. G. Grote, E. M. Heckman, D. Diggs, J. A. Hagen, P. Yaney, A. J. Steckl, G. S. He, Q. Zheng, P. N. Prasad, J. Zetts and F. K. Hopkins, "DNA-Based Materials for Electro-Optic Applications," *Proceedings of SPIE*, 5934, 38-43 ,(2007)
- [5] A. J. Steckl, H. Spaeth, H. You, E. Gomez and J. Grote, "DNA as an Optical Material," *Optics and Photonics News*, 22, 34-39,(2011).
- [6] A. J. Steckl, A. Hagen, Z. Yu, R. A. Jones, W. Li, D. Han, D. Y. Kim and H. Spaeth, "Challenges and Opportunities for Biophotonic Devices in the Liquid State and the Solid State," *IEEE Nanotechnology Conference*, 1, 159-161,(2006).
- [7] J. A. Hagen, W. Li and A. J. Steckl and J. G. Grote, "Enhanced Emission Efficiency in Organic Light-Emitting Diodes Using Deoxyribonucleic Acid Complex as an Electron Blocking Layer," *Applied Physics Letters*, 88, 171109-171109-4, (2006)
- [8] Z. Yu, W. Li, J. A. Hagen, Y. Zhou, D. Klotzkin, J. G. Grote and A. J. Steckl, "Photoluminescence and Lasing from Deoxyribonucleic Acid (DNA) Thin Films Doped with Sulforhodamine," *Applied Optics*, 46, 1507-1513,(2007).
- [9] Y. Kawabe, L. Wang, S. Horinouchi and N. Ogata, "Amplified Spontaneous Emission from Fluorescent-Dye-Doped DNA—Surfactant Complex Films," *Advanced Materials*, 12, 1281-1283,(2000).

- [10] J. Grote, D. Y. Zang, F. Ouchen, G. Subramanyam, P. Yaney, C. Bartsch, E. Heckman and R. Naik, “Progress of DNA Photonics,” *Proceedings of SPIE*, 7765, (2010)
- [11] N. Balan, M. Hari and V. P. N. Nampoori, “Selective Mode Excitation in Dye-Doped DNA Polyvinyl Alcohol Thin Film,” *Applied Optics*, 48, 3521-3525,(2009)
- [12] B. Sahraoui, M. Pranaitis, D. Gindre, J. Niziol and V. Kazukauskas, “Opportunities of Deoxyribonucleic Acid Complexes Composites for Nonlinear Optical Applications,” *Journal of Applied Physics*, 110,083117- 083117-4,(2011)
- [13] L. Sznitko, J. Mysliwicz, P. Karpinski, K. Palewska, K. Parafiniuk, S. Bartkiewicz, I. Rau, F. Kajzar and A. Mi- niewicz, “Biopolymer Based System Doped with Non- Linear Optical Dye as a Medium for Amplified Sponta-neous Emission and Lasing,” *Applied Physics Letters*, 99,031107-031107-3, (2011)
- [14] P. Hanczyc, B. Norden and M. Samoc, “Two-Photon Absorption of Metal-Organic DNA-Probes,” *Dalton Transactions*, 41, 3123-3125,(2012).
- [15] M. Samoc, A. Samoc and J. G. Grote, “Complex Nonlin-ear Refractive Index of DNA,” *Chemical Physics Letters*, 431, 132-134,(2006).
- [16] B. Sahraoui, M. Pranaitis, K. Iliopoulos, M. Mihaly, A. F. Comanescu, M. Moldoveanu, I. Rau and V. Kazukauskas, “Enhancement of Linear and Nonlinear Optical Properties of Deoxyribonucleic Acid-Silica Thin Films Doped with Rhodamine,” *Applied Physics Letters*, 99, 2011,
- [17] B. Nithyaja, H. Misha, P. Radhakrishnan and V. P. N. Nampoori, “Effect of Deoxyribonucleic Acid on Nonlinear Optical Properties of Rhodamine 6G-Polyvinyl Alcohol Solution,” *Journal of Applied Physics*, 109,021330-021330-4, 2011.

- [18] C. V. Bindhu, S. S. Harilal, V. P. N. Nampoori and C. P. G. Vallabhan, "Studies of Nonlinear Absorption and Aggregation in Aqueous Solutions of Rhodamine 6G Using Transient Thermal Lens Technique," *Journal of Physics D: Applied Physics*, 32, 407-411,(1999)
- [19] M. Sheik-Bahae, A. A. Said, T. H. Wei, D. J. Hagan and E. W. Van Stryland, "Sensitive Measurement of Optical Nonlinearities Using a Single Beam," *IEEE Journal of Quantum Electronics*, 26, 760-769,(1999).
- [20] S. Venugopal Rao, P.T. Anusha, T. S. Prashant, D. Swain, S. P. Tewari, "Ultrafast Nonlinear Optical and Optical Limiting Properties of Phthalocyanine Thin Films Studied Using Z-Scan" *Mater. Sci. Appl. 2*: 299- 306,(2011).
- [21] P.T. Anusha, P. Silviya Reeta, L. Giribabu, Surya P. Tewari, S. Venugopal Rao," Picosecond nonlinear optical studies of unsymmetrical alkyl and alkoxy phthalocyanines" *Mater. Lett.* 64,1915-1917,(2010).
- [22] M. Sheik-Bahae, A. A. Said, and E. W. Van Stryland, "High-sensitivity, single-beam n_2 measurements," *Opt.Lett.* 14, 955–957, (1989).
- [23] T Xia, D J Hagan, M S Bahae and E W Van Stryland *Opt. Lett.*" Eclipsing Z-scan measurement of $\lambda/10 < \sup > 4 < /sup >$ wave-front distortion" 19 , 317-319,(1994)
- [24] M S Bahae, J. Wang, R De Salvo, DJ Hagan and E W Van Stryland, *Opt. Lett.*" Measurement of nondegenerate nonlinearities using a two-color Z scan"17,258-260,(1992)
- [25] H Ma and C B de Araujo. "Two-color Z-scan technique with enhanced sensitivity " *Appl. Phys. Lett.* 66, 1581-1583,(1995)
- [26] O. Krupka, A. El-Ghayoury, I. Rau, B. Sahraoui, J.G.Grote, F. Kajzar, "NLO properties of functionalized DNA thin films," *Thin Solid Films* 516,8932-8936,(2008).

- [27] Richard L Sutherland; “Handbook of nonlinear optics”, CRC press (2003)

- [28] M.Casalino,” Near-Infrared Sub-Bandgap All Silicon Photodetectors:A Review”, International Journal of Optics and Applications 2,1-16,(2012).

- [29] D. Weaire, B. S. Wherrett, D. A. B. Miller, and S. D. Smith, “Effect of low-power nonlinear refraction on laser-beam propagation in InSb,” Opt. Lett. 4, 331–333 (1979).

Chapter - 8

CONCLUSIONS AND FUTURE PERSPECTIVES

- | | |
|-----|---------------------|
| 8.1 | Conclusions |
| 8.2 | Future Perspectives |

Abstract

This chapter summarizes the results obtained in this thesis. Future implications and directions are discussed in brief.

8.1 Conclusions

We have presented the detailed , systematic and experimental study of filamentation in air and water under tight focusing regime and the nonlinear optical characterization of Rh6G doped -DNA-PVA matrix. This chapter summarizes the result of our studies on filamentation and characteristics of fs pulses in air, effect of lens tilt on Supercontinuum Emission, dynamics of fs pulses in water and the nonlinear studies of Dye- DNA system, highlighting our contributions. A brief outlook on future directions of the studies are also presented.

We have performed the experiments on filamentation and associated SCE in air for different input power and polarization, under three different geometries. The intensity of SCE spectrum using the tight focusing geometry is more compared to the loose focusing geometry indicating the conversion of laser energy to the SCE spectrum is more for tight focusing geometry. It is also noticed that the SCE spectrum is suppressed as we change the polarization from LP to CP. The most exciting feature of SCE spectrum is that, contrary to the earlier observation of a limit in the spectral extent of the SCE spectrum, the blue edge of the spectrum i.e., the minimum cutoff wavelength (λ_{\min}) as a function of the P/P_{cr} is found to decrease continuously for tight focusing geometries .This is an indication of the transition to a regime where we are able to go for an intensity beyond the clamping value. In the tight focusing geometry, the initial high beam curvature attributed to external focusing, leads to complete ionization of the medium which in turn prevents the plasma defocusing to play an important role in the intensity clamping.

As an effort to characterize the filaments and to estimate the filament intensity we have performed an analysis of filament length, width and intensity

under different input powers, polarization states and different geometries. It is found out that, for a given focusing geometry, the filament length and width increased with increasing input peak power. However, at higher NA, the length and width were observed to saturate. Breakup of a single filament into multiple filaments and fusion along the propagation direction were observed with higher NA and for CP pulses. Filament intensity inside a single filament is estimated from the self-emission and was found to be of the order of 10^{12} W/cm².

The motivation of pursuing the lens tilting studies in the filamentation was to control the dominant phenomenon of multiple filamentation over long distances. However, no report to date has ever dealt with the effect of lens tilting on the filament properties under a tight focusing geometry. We have investigated the role of focusing lens tilting on filamentation characteristics and Supercontinuum emission (SCE) for both tight and loose focusing geometries. Our results confirm that the filament splitting and SCE suppression is dominant at large angle of tilt and the SCE suppression is attributed due to shortening of filaments. Astigmatism is the reason for the splitting of filaments.

In spite of voluminous literature available on the generation and application of SCE in water, a more detailed scrutiny in this exciting field of research led us to investigate in more detail the following aspects of SCE in water: a) The interesting role of cavitation induced bubbles (CIB) in SCE b) The role of input Polarization on the SCE c) The role of minimum wavelength (λ_{\min}) and intensity clamping on SCE d) Effect of temperature on SCE

To understand the evolution of CIB, self emission from the wake of fs pulses/filaments propagating in water was captured. The studies on SCE from water were performed under three different focusing geometries such as

f/6, f/7.5 and f/10. Higher intensity and brighter SCE in the f/6 geometry compared to that of f/7.5 and f/10 geometry clearly reveals the presence of interesting dynamics inside the medium. λ_{\min} for f/6 geometry was always blue shifted compared to other geometries and the separation of blue shift between the focusing geometries increased with increasing input powers. This behaviour is predominant with the onset of cavitation bubble. These micron-sized CIB along the propagation direction acts like tiny spherical lenses for filament propagation and refocus the diverging laser energy and the trailing edge of the pulse along the propagation axis overcoming diffraction. This leads to increasing deposition of laser energy during the propagation of fs pulses and the enhanced SCE in the wake of fs pulses. The reduction in SCE intensity is observed at lower inputs, in agreement with the earlier results. However, with increasing input powers the difference in SCE from LP and CP pulses is observed to be negligible due to the increased presence of the CIB along the propagation direction. Under f/6 focusing geometry, the λ_{\min} decreased in two rates of absorbed power, while for f/7.5 and f/10 focusing geometries, the transition occurred in three different power regimes. The variation of λ_{\min} observed in water was small compared to that observed in air, because air molecules can be completely ionized without being opaque. It is observed that the SCE is enhanced when the temperature is decreased. This enhancement is interpreted by the change in temperature dependent refractive index and the corresponding change in the critical power (P_{cr}) required for the SCE.

The third-order optical nonlinearity in DNA doped Rh6G-PVA films was characterized by Z-scan measurements using ~2 picosecond (ps) pulses at a wavelength of 800 nm. The films demonstrated negative nonlinear refractive index (n_2) with magnitudes of $(0.065-2.89) \times 10^{-14}$ cm²/W for varying

concentrations of DNA. The addition of DNA enhanced the NLO properties of thin films. Open aperture data demonstrated strong two-photon absorption with a nonlinear absorption coefficient of ~ 1.6 cm/GW for films doped with 2 wt % of DNA. These data suggest that DNA is a promising material for applications such as optical switching. We conclude that PVA is a good matrix for fluorescent dyes to be incorporated into the double helix of DNA molecule enabling them to be suitable for practical applications in optical devices.

8.2 Future Perspectives

There is tremendous scope for the present work, both in theoretical and experimental aspects. In the present thesis, we addressed filamentation in air and water under tight focusing geometry from the experimental point of view. Attempts can be done to model the experimental results; even though modelling of these experimental results are pretty difficult due to the presence of complicated nonlinear optical processes occurring in this phenomenon.

In this work, the filament intensity inside a single filament is estimated from the self-emission. However, the same method may not be extended to estimate the filament intensity in the presence of multiple filaments, as the effects like break up and fusion of the propagating filaments indicate varying intensity along the direction of propagation. One can attempt to address the challenging scenario of filament intensity measurements in the presence of multiple filaments.

We presented our results on the effect of temperature on SCE from water. This part of the work can be elaborated to find out the efficiency of SCE with the variation of temperature. One can also study the variation of refractive index of water with the change in temperature.

Nonlinear optical characterization of the DNA doped Rh6G-PVA matrix is an area which can be extended to evaluate the nonlinearities at different wavelengths in the visible/near-IR spectral regions. Attempts can be made to find out the ultrafast response of this material using ps/fs pump probe spectroscopy.